1972

Application of holographic methods to vibration measurement of turbine discs.

Walter J. Pastorius
University of Windsor

Recommended Citation
Pastorius, Walter J., "Application of holographic methods to vibration measurement of turbine discs." (1972). *Electronic Theses and Dissertations.* Paper 1197.

APPLICATION OF HOLOGRAPHIC METHODS
TO VIBRATION MEASUREMENT
OF TURBINE DISCS

A Thesis

Submitted to the Faculty of Graduate Studies Through the

Department of Mechanical Engineering in Partial Fulfillment

of the Requirements for the Degree of

Doctor of Philosophy at the

University of Windsor

by

Walter J. Pastorius

Windsor, Ontario

1972

ABSTRACT

A study is made of the vibration of simulated gas turbine discs. Both theoretical and experimental results are given.

Holographic interferometry is used for experimental analysis. The design and construction of a low cost holographic facility is described Various holographic techniques are compared, including time average analysis in both real and non-real time, stroboscopic analysis and ruby laser methods.

Theoretical results are calculated by the finite element method. A circular sector element with sixteen degrees of freedom is predominantly used. Various approaches are employed utilizing different segments of the disc with various boundary conditions to obtain results in the optimum manner.

Three disc profiles are studied. Profiles selected are : constant thickness, linear taper, and constant centrifugal stress. Good agreement between theory and experiment for both natural frequencies and deflected mode shapes is found.

ACKNOWLEDGEMENT

I would like to express my sincere thanks to my advisor, Dr. Z. Reif for his encouragement and guidance during this investigation.

The assistance and understanding of my wife, Barbara, and son, Curtis, are deeply appreciated.

The financial support of the National Research Council of Canada in the form of Grants A3360 and A7439 and a Postgraduate Scholarship made this research possible.

In addition, I would like to express my gratitude to the Central Research Shop and Mr. B. Gordon of the Electronics Research and Design Shop of the University of Windsor for assistance in fabricating the experimental equipment. Thanks are also due to Mr. W. Gibson of Wright-Patterson AFB for information regarding the sector element.

TABLE OF CONTENTS

APPENDIX

LIST OF FIGURES

Figure Page

LIST OF TABLES

NOMENCLATURE

a	object length
D	bulk modulus
$D(x)$	total derivative of x
$\mathcal{F}$	sensitivity factor
$\{F\}$	load vector
f	frequency
f_e	experimental frequency
f_t	theoretical frequency
H_{ij}	Hermitian polynomials
h	cantilever plate thickness
$I(x,y)$	intensity of holographic reconstruction
$I_{st}(x,y)$	intensity of holographic reconstruction of static object
J_o	zero order Bessel function
$[K]$	stiffness matrix
$[M]$	mass matrix
$M(x,y)$	local vibratory amplitude
m	number of diametral nodes
N	fringe order
$N(x,y)$	local fringe order
n	number of circular nodes
m/n	mode identification
P	load
p	recording film fringe frequency
r	radius

r_i	element inner radius
r_0	element outer radius
r_1	disc inner radius
r_2	disc outer radius
t	thickness
t_1	disc inner thickness
t_2	disc outer thickness
w	transverse deflection
w_{ij}	transverse slope
Z	object to hologram distance
Δ	non-dimensional deflection
δ	deflection
$\{\delta\}$	deflection vector
λ	wavelength of light
Ω	non-dimensional frequency
ω	circular frequency of vibration
ω_r	disc rotational frequency
ρ	material mass density
Φ_r	angle between object and reference beam at recording plane
Φ	angular position
Φ_1	lower element angle
Φ_2	higher element angle
Φ_e	$\Phi_2-\Phi_1$
∇	stress

θ_1	angle between direction of propagation of light incident on the object and displacement vector
θ_2	angle between axis of observation and displacement vector
ν	Poissons ratio

1. INTRODUCTION

1.1 SUBJECT OF INVESTIGATION

This study investigates the vibrational characteristics of gas turbine discs. A theoretical and experimental study is described aimed at determining natural frequencies and modal shapes of discs. The theoretical study is based on finite element procedures in which a circular sector element is predominantly used. Results are verified by experimental studies using holographic interferometric techniques. These techniques are shown to be very effective in vibration measurement and are simple and easy to use once initially installed.

It is intended that this work serve as a guide for the establishment of a holographic interferometric system, particularly if funds are limited. Also,a finite element method of analyzing vibration of objects of circular boundaries is described which allows use of a few degrees of freedom with accuracy equivalent to an analysis with many degrees of freedom.

1.2 SIGNIFIGANCE OF DISC VIBRATION

Gas turbine design, particularly in the case of aircraft engines, is a highly complex procedure. The designer is faced with high temperature gradients, large steady state stresses, and a broad spectrum of possible vibratory forcing functions. Sources of these functions are aerodynamic fluctuations, gearbox vibrations, partial admission and many others. Thus, each component must be carefully analyzed to determine its vibratory characteristics. Parts must be optimized for minimum weight, but reliability must not be jeapordized since failure of any one component often leads to catastrophic engine failure.

The axial flow engine is most popular for aircraft use owing to its small profile. The discs in an axial flow machine rotate at speeds of ten to fifty thousand rpm, creating large centrifugal stresses. Smaller but signifigant stresses are caused by torsional and gas bending forces exerted from the blades. When a resonant vibration is superimposed on these essentially steady state stresses, the life of the disc may be signifigantly reduced. Thus, a knowledge of the disc vibratory phenomenon is required. Several solutions to the vibratory characteristics of uniform thickness discs have been found. The purpose of the present study is to determine the applicability of finite element techniques to the rapid determination of natural frequencies and mode shapes of discs of arbitrary profile.

1.3 FINITE ELEMENT METHOD

Due to the complexity of the design procedure and the cost of prototype construction, automatic component analysis has become an important design tool. The advance of analysis techniques has been greatly enhanced by the availability of large, high speed computers. Before computer based analysis can become a reality, a problem of complex continua must be reduced to a finite number of degrees of freedom. This discretization was first performed by the process of finite differences.

Recently, a more general form of discretization, the finite element procedure, has become known. It is based on the dissection of the continua into finite blocks or elements with finite degrees of freedom. The influence coefficients of each block with respect to its neighbours are formed into matrix equations which describe the approximate properties of the continua. The solution of the equations is generally based on matrix algebra.

The present study illustrates the application of finite element techniques to the turbine disc problem. Emphasis is placed on elements with curved boundaries which best approximate the geometries involved.

1.4 HOLOGRAPHIC TECHNIQUE

The recently developed three-dimensional imaging technique of holography has found many applications. It has advanced interferometry from optically flat models to include engineering components of arbitrary shape. Holographic interferometry provides an elegant method of displacement analysis over the full object field with a sensitivity of approximately one half the wavelength of light. It is applicable to static, transient, and vibratory displacements.

The experimental aspect of the project involves the construction of a holographic system and the application of the technique to the disc vibration problem. The constraints placed on the system at the design stage are versatility and low cost.

1.5 SCOPE

The study is split into two parts. One is concerned with the finite element method, the other with the holographic technique. The application of the finite element method begins with an analysis of rectangular cantilever plates for static and dynamic cases. This initial investigation is undertaken both for familiarization with the technique and to check the various inversion and eigenanalysis routines to be used in the disc analysis. In applications to discs, elements with circular arc boundaries are emphasized because of their exceptional modelling effectiveness. The elasticity matrices for the disc are checked by applying theoretical static loads and comparing results to those given by various authors for cases of uniform thickness and linear radial taper. Dynamic results are then obtained for discs of uniform thickness, linear taper and constant centrifugal stress profile.

The holographic system design is discussed in detail. Initial static and dynamic studies are carried out on cantilever plates and compared to the results developed by finite element analysis. The technique is then applied to simulated discs of various profiles and compared to the finite element theory.

2. LITERATURE REVIEW

2.1 THEORETICAL DISC VIBRATION ANALYSIS

Disc vibration in the fundamental umbrella mode has been studied using a Rayleigh Ritz method by Biezeno and Grammel (1) and Timoshenko (2). While Rayleigh's method is simple, even for discs for arbitrary profile, only the fundamental frequency is readily found. The result of Rayleigh's method is an upper bound on the fundamental frequency.

A Myklestad approach for arbitrary profile discs has been used by Ehrich (3). This technique provides results for the general case, but requires successive iterations to determine each natural frequency. If a large number of frequencies is desired, the technique requires a great deal of computation.

Blech (4) has used a collocation method for analysis of arbitrary profile discs. He found an optimum degree of the polynomial deflection approximation for each mode desired.

The receptance functions and frequency equations for flat circular plates with various boundary conditions have been given by McLeod and Bishop (5). This Monograph is limited to lower order modes of plates of uniform thickness.

For the particular case of a disc of lenticular profile, Harris (6) has shown that an exact solution to the natural frequencies of free vibrations may be found. Unfortunately, this profile is seldom found in practice.

The effect of rotation on disc vibration has been investigated by Eversman and Dodson (7). Their study is limited to uniform thickness discs.

Recently, several works on disc design utilizing a frequency constraint have appeared. DeSilva (8) has illustrated the design problem of achieving minimum disc weight while maintaining certain dimensions and tolerance limits. The constraint that the lowest disc natural frequency must exceed a given value completes the problem. The frequency is calculated by iterative solution of the differential equations of vibration using the Mykelsford-Holzer method. Olhoff (9) has considered a similar problem. He attempted to obtain the maximum fundamental natural frequency for a given disc volume and diameter. Olhoff uses a Rayleigh-Ritz solution to determine the lowest frequency. He has reported increases in the fundamental frequency of up to 544%.

Another technique of vibration prediction is that of finite element analysis. The following section provides a brief review of the history of the method.

2.2 FINITE ELEMENT TECHNIQUE

The finite element technique basically involves the dissection of a continuum into a number of pieces or elements, connected at a finite number of points or nodes. The influence of forces and deflections on each element are prepared and manipulated in matrix form to approximate the behaviour of the continuum. Several authors have provided general, basic works on the technique (10) (11) (12) (13). A theoretical analysis of the method has been given by Oliveira (14). Analysis of the reasons and requirements for convergence has been done (15) (16). Dunne (17) has analyzed the requirements for the assumed element displacement function.

In the realm of vibration analysis, a controversy has arisen over the form of the mass or inertia matrix formulation. Initial studies utilized lumped mass forms. Further work suggested that a mass matrix derived on the assumption of distributed mass was superior, although much more difficult to prepare. Several comparisons of the two approaches have been given (18) (19). A distributed or equivalent mass matrix may be formulated on the basis of complimentary energy (20) or Rayleigh -Ritz principles (21). Extension to transient analysis is also possible. (22).

Original finite element studies considered rectangular elements. General objects however can not be easily modelled by such elements. Thus, elements of triangular shape have been developed.(23) (24).

Triangular elements, however, are not suited for modelling curved boundaries. Consequently, several elements representing surfaces of revolution have been developed (25) (26). For more general boundaries, elements with general curvature on the edges are available (27). For circular boundary problems, elements are available as sectors of circular arcs (28).

2.3 EXPERIMENTAL TECHNIQUES OF VIBRATION ANALYSIS

Accelerometers have found broad usage in experimental analysis. The accelerometer utilizes piezoelectric, inductive or resistive principles to convert vibration into an electrical signal. Unfortunately, all of these devices and their lead wires may affect the vibration, particularly if the mass of the accelerometer is within several orders of magnitude of the object mass. Similarly, attatchment of an LVDT or velocity probe to an object may affect its vibration. A strain gage may be mounted on the object. Although the gage is of very low mass, it still requires lead wires. Often, strain gages must be mounted away from the point of maximum stress to avoid gauge fatigue failures, necessitating calibration procedures.

Capacitive or magnetic transducers may be used as non-contacting displacement detectors . However, these devices require careful calibration for high resolution measurements. They must be set at small distances from the object. Optical tracking devices may be used for vibration detection although the cost is generally high for high resolution devices.

Another non-contacting technique has been developed using the coherent speckle pattern produced from a laser reflection (29). The laser is also the basis of diffractographic vibration analysis (30). The technique utilizes the diffraction of light from an aperture formed between the object and a fixed reference. This last technique has the unique capability of producing vibration amplitude information along a continuous line.

All of the above methods, except for the diffractographic technique, give information about vibration at a point. To obtain a picture about the vibration of a body, large numbers of sensors or scanning techniques must be used. To avoid this problem, several full field techniques have been developed.

One of the earliest full field techniques is the Chladni pattern. A fine sand is sprinkled on the object and is thrown off by the vibration at every point except the nodes. Other methods of nodal determination are based on moire methods (31) and optical techniques (32). All of these techniques give no information about frequency or amplitude of vibration.

For very large amplitude vibration, a stroboscope may be used to determine amplitude and frequency of vibration. This technique has been used to analyze soft rubber models (33) although only qualitative data is basically given.

In laboratory studies photoelastic models may be used although Poissons ratio may introduce modelling uncertainties. Interferometric techniques are applicable if optically flat models are available. For larger amplitude vibration, projected fringes may be used as a non-contacting vibration detector (34).

An experimental analysis of actual hardware disc vibration has been done by French (35). He studied the vibration of stationary discs using Chladni patterns as a preliminary step to experimental rotating tests. In the rotating tests, capacitive gages were used as stationary detectors. Strain gages with slip rings were employed as vibration detectors on the disc itself.

In another series of experiments, Tobias and Arnold (36) studied static and rotating disc vibration. They encountered non-linear effects in the vibration at maximum amplitudes of 10^{-3} diameters.

Holographic interferometry has proven a very useful tool for vibration analysis. It provides full field, non-contacting amplitude information at a sensitivity of approximately the wavelength of light. It is frequency independant and can yield frequency information if stroboscopic illumination is used. The current study outlines the application of holographic techniques to the vibration of discs. A review of the development of holographic interferometry follows.

2.4 HOLOGRAPHIC INTERFEROMETRIC DISPLACEMENT ANALYSIS

2.4.1 HOLOGRAPHY

Standard photography involves the recording of the amplitude distribution of light reflected from or created by an object. The light from the object must be focused on an image plane by either a lens or a pinhole. A two dimensional image of the object is then stored on a photosensitive material. No information about light phase is recorded.

Holography, or wavefront reconstruction, stores both amplitude and phase information regarding the light from the object. The recorded image, or hologram, bears no resemblance to the object. Rather, it consists of a series of blobs, specks and whorls. The creation of an intelligible image from the hologram is known as the reconstruction process.

The holographic technique was first conceived in 1947 by Dennis Gabor of the Imperial College of Science and Technology in London (37)(38) At the time of this discovery, Gabor was attempting to increase resolution in electron microscopy. He and later researchers in this field were seriously hampered experimentally by lack of a sufficiently intense source of coherent light.

The Gabor-type hologram is a photograph of the Fresnel diffraction pattern from an object. This recorded pattern is then reconstructed by passing a beam of coherent light through the hologram. Unfortunately, phase information is lost in this type of hologram. The technique is only suitable for transparent objects with small opaque areas. Also, an extraneous image is formed which is superimposed on the desired image along with an intermodulation distortion component.

The discovery of the laser in 1960 provided Leith and Upatnieks (39) of the University of Michigan with a highly coherent source. They developed the two beam technique shown in Fig. 1 which produces separate high quality images, even of continuous tone objects. The object is illuminated with collimated coherent light. It's Fresnel diffraction pattern falls on the hologram recording plane. This object beam interferes optically with the reference beam deviated by the prism. Thus phase information regarding the light from the object is retained and recorded by the photosensitive medium at the recording plane.

The simplest method of reconstructing the hologram is shown in Fig. 2. The straight through portion of the incident beam, shown as the zero order, provides the same reconstruction as the earlier Gabor-type holograms. The fine interference pattern recorded by the hologram acts as a diffraction grating which produces a pair of first-order off-axis diffracted waves. One of these creates a real image which may be seen by placing a screen beyond the hologram at its focal point. The other, termed the virtual image, appears on the opposite side of the zeroth order.

Both real and virtual images are of good quality. They are separated from each other and the intermodulation term. Both images are seen to be hanging in space at the same distance from the hologram as the object was from the hologram during the recording process. To maintain good quality images, the hologram must be clean, free from dust and scratches, and if on a flexible backing, must be placed in an index matching fluid to minimize film thickness variation effects.

Extension of the two-beam technique to diffusely illuminated and three dimensional objects was again pioneered by Leith and Upatnieks (40). They placed a diffusing element, such as opal glass, between the source and object in the system shown in Fig. 1. Although the diffuser destroys the coherence of the object beam, it does so in a time-invariant way so that the requirement for coherent illumination is met.

On reconstruction the hologram behaves much as the non-diffuse illumination hologram described above, producing both real and virtual images. However, both images now become visible to the naked eye as images of transparencies illuminated by a reconstructed diffuser. The virtual image may be seen by looking through the hologram as a window and the real image appears suspended in front of the hologram. The hologram no longer retains the Fresnel diffraction pattern of the object but rather appears as in Fig. 3 . The regular structure is due only to dust particles and other light scatterers in the reference beam. This "noise" does not affect the reconstructed image in any way.

Also, under diffuse illumination, each part of the object illuminates all parts of the hologram. The hologram may be broken or cut, but each piece will retain the entire image as long as it is large enough to provide a signifigant reconstructing aperture.

By a similar argument, portions of the hologram may be damaged or removed by dust particles, scratches or fingerprints without affecting the reconstructed images.

The concept of diffuse illumination holography leads directly to the holographic recording of the three- dimensional objects. The basic technique is illustrated in Fig. 4 . Coherent monochromatic light is reflected by the object to the recording plane to provide the object beam. The reference beam is produced by reflecting a portion of the incident light beam to the recording plane with a mirror.

The reconstruction process for a hologram of three-dimensional objects is shown in Fig. 5 . The hologram is illuminated by a beam of monochromatic light. Both real and vitrual images may be seen by the naked eye. The virtual image is observed by looking through the hologram as if it were a window and appears hanging in space behind the hologram. It appears exactly as the original object and retains both depth of field and parallax or three-dimensionality. It may be photographed by imaging with a lens, but the lens must be stopped down to provide sufficient depth of field if the entire image is to be kept in sharp focus. The real image is formed in front of the hologram and may be photographed by placing a photographic plate at the hologram focal position. In this case, the hologram reconstruction is difficult to focus since the real image also has depth of field. The real image appears to be pseudoscopic, that is, it is reversed from front to rear.

Holography of three-dimensional objects immediately found many uses, including novel forms of photography and true three-dimensional images displays which may exist in colour (41) as well as black and white. It has been used for transient analysis of aerosol particle distributions (42). In this case a hologram of the particles was taken using a short high intensity pulse from a ruby laser. This "stop action" three-dimensional hologram was then analyzed at leisure since it stored a true three- dimensional image of the particles.

The hologram has also been suggested as a medium for data storage.

It is particularly interesting for this application since scratches, fingerprints and so on which would destroy a portion of the image of a normal photograph do not degrade the holographic image. An added attraction to holography for image or data storage is that a number of images may be stored on a single hologram by rotating the hologram between each exposure in a technique known as multiplexing.

Holography is able to store phase objects as well as continuous tone objects (43) . It thus has applications in microscopy, accoustical work and aerodynamic flow visualization.

An object to be recorded holographically need not be directly accessible. It may be holographed by fibre optics (44), mirrors or other image conducting elements.

2.4.2. HOLOGRAPHIC INTERFEROMETRY - STATIC ANALYSIS

Classical interferometry is an exceptionally elegant technique of out of plane displacement analysis. Its advantages include high sensitivity (better than half a wavelength of light) and the determination of the entire surface displacement at one time. Disadvantages of classical interferometry are that it can only be applied to optically flat models, requires careful optical alignment and demands a stable bench isolated from environmental perturbations. It has not been used a great deal for engineering studies as optically flat objects are seldom encountered. It has however been useful in plastic model studies similar to photoelasticity (45).

Holography has served to eliminate the most severe limitation on interferometry - that of optically flat models. Indeed, holographic interferometry is applicable to almost any surface or volume since it involves differential rather than absolute (classical) interferometry.

The first work in holographic interferometry appears to have been done by Herman (46) who was studing flow visualization in gas dynamics, and by Burch (47). Explanations of holographic interferometry were given by Collier (48) based on Moire theory and by Stetson and Powell (49), who showed the interferometric fringes were the same as those found by many early holographers in static holograms which were caused by insufficient environmental isolation. Further work was done by Heflinger (50) who illustrated the possibility of using a pulsed ruby laser for differential interferometry.

Analysis of fringe positions for general motions of the object have been given by Stetson and Powell (51), Haines and Hilderbrand (52) and Vienot (53). A review of the equations involved is given by Brown, Grant and Stroke (54). The inverse problem of determining a general unknown motion from the interferometric fringes generated by the motion has been considered by Sollid (55).

Holographic interferometry exists in two modes: real time and non-real time. Non-real time or double exposure holographic interferometry is available to any experimenter who has a holographic recording apparatus. The system is set up as for conventional holography, but only one half of the exposure required for the optimum reconstruction is used. Loads or strains are then applied or varied and the second half of the exposure taken. Precautions must be taken to insure that the only movement of components in the system between exposures is the object displacement. When this double-exposure hologram is processed and reconstructed, two images are formed corresponding to the undeformed and deformed objects. If these two images nearly coincide, interference fringes will be superimposed on the reconstruction at points where the optical path length has changed one wavelength. The disadvantages of double exposure holographic interferometry are that one holographic plate is consumed for each data point and results are not available in real time. Results, however, are stored permanently on the hologram and are impervious to fingerprints, scratches or even fracturing of the hologram.

The alternative technique is real-time or live-fringe holographic interferometry. In this case, the full exposure is taken and the hologram processed. It is then returned to its initial position within a fraction of a wavelength of light. Reconstruction is carried out with the reference beam. The virtual image is exactly superimposed on the object, which is illuminated by the object beam. When the object is viewed through the hologram and loads or strains applied, interference fringes are formed between the reconstructed image and the deformed object. Results are thus obtained in real time, and may be stored by photographing the image-object interferogram. In the real time mode, the virtual image may be considered a master "object" and the object the comparison object. Disadvantages of real-time interferometry are that a specially designed plateholder is required for exact repositioning of the hologram (or a liquid gate may be used to process the plate in place). Also, processing of the plate must be undertaken with great caution to minimize image distortion due to inevitable changes in emulsion dimensions.

Numerous applications for such a method of full field deflection analysis can be envisioned. Butters (56) and Jeffers (57) have used it to study deflections in transducer diaphrams. Grant and Brown (58) have a non-destructive test unit based on holographic interferometry for determination of de-bonds and other flaws in automotive tires and sandwich structure panels up to five feet square. Plate deflection is another obvious area of investigation and has been studied by several people, such as Boone (59), Wilson et al (60) and Hageniers (61).

The sensitivity of the method is often too high for measuring large deflections. Leadbetter and Allen (62) overcame this problem when studying the prebuckling behaviour of cylinders by using differential interferometry and incremental loads. Varner (63) illustrated a hologram-moire technique of decreasing the sensitivity of holographic interferometry using multiple wavelengths.

The technique is also suitable for measurement of torsion (64) and of in-plane surface strain (65). A hologram of a master part may be made and its reconstruction compared interferometrically to a test object if the object beam strikes the object at high incidence angles in order to minimize effects of surface finish. This technique has been applied to inspection of cylinder bores by Ennos (66) (67) (68).

Holographic interferometry has greatly simplified the separation of principal stresses in photoelasticity. In the past, this type of study required optically flat models to determine isopachic fringe trajectories for combination with isochromatic data (69). Holographic interferometry has relaxed this restriction allowing isopachic data to be taken from photoelastic materials. It is often possible to obtain a single holographic image containing both isochromatic and isopachic data sets, although quantitative interpretation of the results may be extremely tedious (70) (71).

In many cases of analysis of plates, the experimenter is interested in stresses rather than deflections. Several methods for determination of bending moments from holographic interferograms have been suggested (72) (73) but all suffer from lack of accuracy or do not yield full-field bending moment information.

2.4.3. HOLOGRAPHIC INTERFEROMETRY - VIBRATION ANALYSIS

An object which undergoes simple harmonic motion spends most of its time near the peak values of displacement. Thus, a hologram taken of an object vibrating under the conditions of simple harmonic motion contains two reasonably well defined images of the object near the peak vibratory excursions. On reconstruction, these two images will interfere in a similar manner to that described for double exposure holography. This phenomenon was presented experimentally and theoretically by Powell and Stetson (49) (74) (75). Theory shows that the holographic interferogram reconstruction for the case of vibratory object motion may be represented as the static object reconstruction locally modulated by a zero order Bessel function whose argument is a function of the wavelength of light, the recording geometry and the vibratory amplitude. Interferograms of vibrating objects show nodes and fixed boundaries as bright areas, and vibrating regions contain dark bands or fringes. As fringe order increases, fringe contrast decreases. Osterberg (76) provided an analysis of the parallel case of an object vibrating in an interferometer. Since this type of interferogram represents an average exposure of the object during the vibratory time domain, it is commonly refered to as a time average interferogram.

Further work by Powell and Stetson (51) (77) showed that vibratory information could be obtained in real time. In this case, a slight angular mismatch was introduced to the system after processing the plate. At object resonances, nodal lines appear as the original set of fringes introduced by the mismatch, but antinodal area fringes are washed out due to the time-averaging effect.

The validity of the zero-order Bessel function theory was demonstrated by Wall (78), and Lurie and Zambuto (79) in a series of experiments. Wall also suggested a multiplexing technique for altering fringe visibility.

Further work by Stetson (80) included a description of fringe localization for various forms of motion. Depending on the type of motion involved in the interferogram, the interferometric fringes may occur on the object surface or at some point removed from the surface, in which case photographing the fringes may present difficulties due to depth of field requirements.

The necessity of pure simple harmonic motion to produce the optimum fringe contrast has been discussed by Wall (81) and Powell (82) who showed that a drift of the vibratory mean position greater than one half an optical wavelength would seriously decrease fringe contrast. Powell at the same time discussed a fringe theory for an object vibrating at up to three different frequencies simultaneously. Further work on objects vibrating at more than one frequency (both rationally and irrationally related) has been carried out both experimentally and theoretically by Wilson and Strope (83) (84).

The case of an object vibrating at one frequency with a superimposed constant velocity has been studied by Lurie (85) and Zambuto (86) who compared the results of time-average interferograms of harmonic motion, constant velocity and the two combined not only with theory but also with results obtained by means of a Twyman - Green interferometer with accuracy of ± 0.04 λ. An extension to constant acceleration motion has been given theoretically by Vikram and Sirohi (87).

Monahan and Bromley (88) have shown that the error involved in interpreting amplitude in a holographic time-average interferogram may be less than 1.6% for a fringe order of four provided that the fringe pattern is analyzed on a microdensitometer with a fringe order resolution of ±0.05 fringe.

The technique has been applied to several problems where full-field amplitude determination is required. Waddell and Kennedy (89) have studied plates and curved beams. Accoustic transducers have been observed by Monahan and Bromley (88) and Grant and Von Winkle (90). The latter paper is of particular interest since some of the tests described were carried out with the transducer under water.

Other studies have included turbine blades (91), discs (92) and combined blade - disc systems (93). Long slender cantilever beams were studied by Aprahamian and Evensen (94) at frequencies up to 99kHz.

Time average interferometry possesses two disadvantages. The primary problem is that results are not available until the hologram is processed and reconstructed. Also, fringe contrast is determined by a zero-order Bessel function. As a result, fringe contrast decreases as vibratory amplitude increases. The former disadvantage may be overcome by real-time or live fringe techniques. Unfortunately, fringe contrast is poorer in real-time analysis than in time average work. The solution to these problems is real-time stroboscopic methods. Fringe contrast is good provided that the duration of illumination is short with respect to the period of vibration. Several methods of synchronizing the laser pulse with the vibratory motion have been suggested. Archbold and Ennos (68) (95) passed the laser beam through a hole in the shaft of an air turbine. A synchronized sinusoidal waveform is obtained from the reflection of polarized light from a polaroid mounted on the end of the shaft as detected by a photocell. Frequency stability with this system often requires an additional magnetic "lock-in" system.

A second method, suggested by Shajenko and Johnson (96) involves the use of a Pockels cell (basically a high speed optical shutter) triggered from the same source as the vibratory exciter. A similar and novel method was developed by Aleksoff (97) who was studying resonances in ADP crystals. ADP is a birefringent material, so Aleksoff passed the reference beam through the crystal so that it was phase modulated by the object.

Rotary disc strobes have been suggested in several forms. Synch motors have been used with modifications to their capacitors (98) (99). In this case the motor is driven from the same source as the vibration exciter. Alternately, a stabilized DC motor may be used to drive the disc (92), which also provides the sine wave for the vibration exciter.

Other modulation methods are possible, such as an acousto-optic device (100) or the use of a repetitively pulsed laser. The latter is generally far more advantageous in terms of laser power. Pulse width must be kept small with respect to the vibratory period in order to minimize fringe smearing (101). Shortest pulse widths (less than 1μ sec.) are available from solid state lasers, but their use in holography is limited to non-real-time (102) (103).

Fryer (104) developed a method of using a rotating disc as a shutter to store a complete vibratory cycle on one plate. In this case the disc, with a slot in it, is rotated in front of the hologram plate in synchronism with the object vibration. If an observer scans across the hologram, the whole cycle of vibration may be seen.

An extension of live stroboscopic holographic interferometry to rotating discs has been reported by Waddell and Kennedy (105) (106), in which a Pockels cell is triggered from a magnetic probe near the disc.

Extreme care must be taken to avoid any axial or radial motion of the disc as it rotates. Also, since very short ($<30\mu$ sec.) pulses must be used, reconstructions are extremely dim, even with the most powerful continuous output, visible wavelength lasers.

Unless stroboscopic illumination is used, the frequency of an unknown oscillation is not provided by the hologram, nor is the phase of vibration available. This difficulty may be overcome by using a known initial fringe pattern and stroboscopic illumination (107).

3. FINITE ELEMENT IMPLEMENTATION

3.1 INTRODUCTION

Statically, the finite element method involves the derivation of the matrix equation :

$$\{F\}=[K]\{\delta\} \tag{1}$$

The solution is obtained by application of boundary conditions to equation (1) and inversion of the matrix equations to solve for deflections as a function of applied forces. For vibration analysis, inertia forces, calculated by D'Alembert's principle, must be included. In the case of free vibration, the governing equation is

$$\left([K]-\omega^2[M]\right)\{\delta\}=0 \tag{2}$$

The solution of equation (2) consists of determining the eigenvalues (relating to the natural frequencies) and eigenvectors (deflection profiles).

3.2 SECTOR ELEMENT

The selection of elements for a given problem is mainly determined by the object boundaries. For accurate results, the element should be able to model object boundaries very closely. The element should be compatible with each of its neighbours.

The annular sector element of Gibson (28) was selected for the present study. Element geometry is shown in Fig. 6. First order Hermite (oscullatory) interpolation polynomials are used for the element deflection profile. A plot of these oscullatory polynomials is shown in Fig. 7.

Element corners are taken as nodes. Each node has four degrees of freedom : the transverse deflection, w ; radial and tangential slopes, $w_{,r}$, $w_{,\theta}$; and nodal twist, $w_{,r\theta}$. Thus, each element has a total of sixteen degrees of freedom. The element is assumed to be isotropic and of constant thickness.

3.3. PROGRAMMING CONSIDERATIONS

3.3.1 ELEMENT SUBROUTINE

The program for finite element analysis is written in FORTRAN for an IBM 360/50 computer. Initial effort was directed at preparing a subroutine to set up the stiffness and mass matrices. Required integrations are done in the routine. The subroutine differs slightly in construction from that of ref. 28. Gibson's suggestion of using polynomial rather than trigonometric interpolation functions in the tangential direction was followed. This produces a simpler program with no signifigant loss of accuracy. The subroutine produces both stiffness and mass matrices for a given element geometry. The output matrices consist only of the lower triangle stored row wise. Both matrices are symmetric. The mass matrix is consistent.

3.3.2 STATIC ANALYSIS

Accuracy of the stiffness matrix was checked using a static problem. The geometry chosen is shown in the sketch of Table A.1 . This problem was selected since analytical solutions for a number of cases are available (108) for comparison.

Since only axi-symmetric loading was used, a single radial strip of elements wasrequired. Individual element geometry is automatically calculated for the cases of constant thickness, linear taper or constant stress. The variable correlation technique (Appendix E) is used to assemble element stiffness matrices into the overall matrix. The variable correlation table is generated in a subroutine.

The overall matrix is inverted using the IBM Scientific Subroutine MINV. This is a standard Gauss-Jordan inversion routine. The inverted stiffness matrix is multiplied by the load vector and the resulting deflections and slopes are printed.

Execution time on the 360/50 is several seconds for a ten degree of freedom model. A flowchart of the static analysis program is given in Fig. 8.

3.3.3 DYNAMIC ANALYSIS PROGRAM

The dynamic analysis program may be found in Appendix F and is flowcharted in Fig. 9. Extensive use of named COMMON areas increases the program efficiency. The entire disc need not be studied. Rather a partial segment is analyzed in most cases.

Individual element geometry is set up in subroutine GEO. Any combination of numbers of radial and tangential elements can be used. Element thickness is generated automatically for constant thickness, linear taper or constant stress disc profiles. Element thickness is taken as the mean radial thickness.

The correlation table (Appendix E) is generated in subroutine VCT. Five different types of table may be generated, as dictated by the input variable MCODE. The cases are :

MCODE = 1 The outer radial edges of the element group chosen are antinodes. No symmetry is implied. Resultant modes include both the no diametral node case, and the modes with diametral modes which are compatible with the segment angle chosen.

MCODE = 2 One outer radial edge of the element group chosen is an antinode, the other is a node. When applied to a group of elements which subtend 90°, this case provides natural frequencies of modes with a odd number of diametral nodes.

MCODE = 3 The outer radial edges of the element group chosen are both antinodes. No symmetry is implied. When applied to a group of elements which subtend 90°, this case provides natural frequencies of the modes with no diametral nodes as well as modes with even numbers of nodal diameters.

MCODE = 4 The outer radial edges of the element group chosen are nodes. Also, deflections along the edges are equal. Resultant frequencies are modes with no diametral nodes and modes with an even number of nodal diameters in each element segment. For a small segment angle, the latter modes are very high in frequency relative to the former and are not generally found.

MCODE = 5 The outer radial edges of the element group chosen are nodes. The edge deflections are equal in magnitude but opposite in sign. Resulting frequencies correspond to modes with an odd number of nodal diameters in each segment. Most of the lower frequency results found correspond to the case of one nodal diameter per segment. The segment angle selected governs the resultant number of nodal diameters. The angle must therefore be evenly divisible into 360°.

The overall stiffness and mass matrices are assembled from the element matrices in subroutine ASSEM. The two are assembled simultaneously. Negative values from the correlation table are acceptable.

Since both stiffness and mass matrices are symmetric, eigenanalysis may be done by IBM Scientific Subroutine NROOT. This routine is based on the method found in Cooley and Lohnes (109).

The results of the eigenanalysis are the eigenvalues (squares of the natural circular frequencies) and corresponding eigenvectors (deflection profiles).

To aid in identifying a given mode, a small profile routine DEFN is also available. This routine provides an array plot of the deflection shape of each element.

Execution time on the 360/50 is 48.5 seconds for 16 degrees of freedom and 2.5 minutes for 36 degrees of freedom. A major portion of execution time is spent determining deflection profiles. For example, a 24 degree of freedom problem executes in 1 minute 6 seconds and requires a further 29 seconds for computation of profiles.

4. HOLOGRAPHIC ANALYSIS SYSTEM

4.1 SITE FOR HOLOGRAPHIC SYSTEM

In order to minimize requirements for isolation of the optical table for holography, it is desireable to have a site with low levels of structural vibration. This generally means a basement room, preferably one in a low traffic area. Unfortunately, such a site was not available. Rather, a small second floor laboratory directly connected to a darkroom was chosen. The room had a separate air supply which could be shut off for environmental stabilization. The room could be darkened fully for periods when holographic film was uncovered.

4.2. MECHANICAL STABILITY

The interference pattern formed on the hologram between the object and the reference beams must be well defined for brilliant reconstructions. Any movement of the fringe pattern during the exposure will decrease image brightness rather than sharpness, since reconstruction is caused by diffraction by this pattern. A common cause of interference pattern movement is mechanical motion of one or more optical components causing a change of path length in either the object or reference beams. The requirements for mechanical stability of the components have been given by Rogers (110). Basically, components must be stable to be better than $\lambda/8$.

To achieve this stability requires isolation of components from floor-borne oscillations. Thus an optical bench was constructed from a four foot square cast iron machinery base donated by the Ford Motor Company. This table weighs approximately 2500 pounds and is reinforced on its underside by a transverse web for high flexural rigidity.

The upper surface has five slots cut in an inverted " T " shape for clamping fixtures to the table top. A flat table is convenient for holography, although some 3-D frames (93) have been used.

A preliminary survey of the second floor laboratory floor vibrations indicated a predominant 30 cps motion (due to nearby rotating electrical equipment) and numerous random signals of lower frequency. The latter terms were traced to such various sources as people walking through nearby halls and laboratories.

An initial low cost isolation system based on 18" square styrofoam layers interleaved with plastic "bubble" packing material proved succesful for several days until the plastic"bubbles" collapsed due to air leakage. In an effort to avoid an expensive air-cylinder isolation system, a second system was sought.

An alternative was found in AEON hollow rubber springs, distributed by Go-Tract Systems. These springs are designed to replace both springs and shock absorbers in heavy-duty vehicular suspension systems. One spring (model 535/65) was placed under each corner of the table on top of eight inches of 18"x18" styrofoam pads supported by two rows of concrete blocks, Fig. 10 . The load from the spring is distributed over the styrofoam by an 18" square piece of $\frac{1}{2}$" steel plate. This support system has a vertical natural frequency of about 2.5 Hz . Isolation from building-borne vibration is further enhanced by the relatively large hysteretic damping in the rubber springs. Table stability was checked with a long-leg Michelsen interferometer (111) which essentially covered the full width and breadth of the surface. The interferometric fringes were found to be stable to better than $\lambda/8$. Total cost of this isolation system was under $100.

Optical elements on the table must be held rigidly in place. Some elements are therefore bolted directly to the table surface. Other components, such as mirrors, and lenses require frequent adjustment in position. Thus, heavy component mounts are fabricated from 6" lengths of 3½ inch diameter steel stock, Fig. 11 . Total weight of each mount is approximately 20 pounds. The surface of the table is in a rough, as-cast condition, causing the mounts to rock. Thus, the base of each is relieved to create a three-point support. Optical elements are mounted on 0.50" steel or aluminum shafts which drop into holes in the centre of each mount. A transverse locking screw holds the shaft. A second locking ring on each shaft rides on the mount to allow rotary adjustment once component height is fixed.

Another problem area is the change of optical path length owing to air currents. If a live fringe hologram is observed under normal conditions, several fringes wander back and forth throughout the object field. This problem is solved by shutting off the air supply to the room during a test. Power amplifiers and fan-cooled equipment are kept as far away from the table as possible. Baffles are placed between them and the table. These simple precautions are sufficient to eliminate optical path length differences due to air currents. Before holograms are made, room temperature is allowed to stabilize for at least 30 minutes after shutting off the air supply. This is important since one interferometric fringe represents a path length difference of approximately 12 μin., while steel has a thermal coefficient of expansion of 6 μ in/in/ °F.

4.3. OPTICAL COMPONENTS

4.3.1. LASER

Selection of the laser is an important part of the recording system design. Lasers of various types are available from $100 to almost any cost. However, the range of types is signifigantly reduced when the requirements for holographic recording are applied.

The laser must have an axial coherence length greater than the largest depth of field (or object/reference beam path difference) to be recorded. It should operate in the fundamental transverse emmission mode (i.e. the output should be uniphase across its diameter). Power output should be high enough to allow suitably short recording times, bearing in mind that price increases drastically with power. Both power and mode content should be stable with respect to time. The laser should be reliable with a relatively long tube life. The output wavelength should be in the visible range to correspond to the spectral sensitivity range of ultra fine grain films.

The Spectra Physics Model 120 Helium-Neon gas laser was selected. This laser provides a guaranteed minimum of 5 milliwatts of optical power at 6328Å. It requires essentially no adjustment for power and operates only in the TEM_{00} mode with a coherence length of about 1 metre. This laser has power quite acceptable for holography. Its only drawback may be the price of approximately $1100. Since the purchase of this laser several similar models have been produced by various manufacturers which may be more cost effective.

4.3.2. SPATIAL FILTER

The laser beam must be expanded by lenses to cover the entire object and the holographic plate. Microscope objectives are quite suitable for this purpose, particularly if a set from 5x to 60x is available to provide a range of beam sizes. Filtering of the beam, to remove the effects of dust spots, etc. may be accomplished by placing a small pinhole at the focus of the lens. Although pinhole size is a function of lens focal length, laser beam diameter and wavelength, it has been found that a 25.0μm pinhole is useable with 10x to 60x lenses. Since the pinhole must be placed exactly at the objective focus, a three axis positioning mechanism is required. This positioning device, known as a lens-pinhole spatial filter, is available as a unit, complete with lenses and pinholes, from many optical component suppliers. The Gaertner Scientific model is perhaps the least expensive. Since any reflection of the laser beam, or passage through any disruptive medium, will distort the beam, it is desireable to have the spatial filter as the last element before the object or plate in the optical path to obtain the maximum benefit of its filtering properties.

4.3.3. BEAMSPLITTER

It is often desireable to split the object and reference beams into two discrete components using a beamsplitter. Splitters are available in various ratios of output beams, from 50/50 to 1/49, and of various materials with internal losses (absorption) from almost nothing to 75% or more of the input beam. It was found that for the current study, a glass microscope slide was most suitable. The air-glass surface reflects 4% of the beam and losses are very small. The reflection from the glass-air surface is blocked by proper positioning of the spatial filter.

Another method of splitting the beam is to reflect the laser beam from a back surface mirror to provide multiple reflections. The brightest reflection and one beside it are selected by an iris and passed through a single spatial filter. Although this is a simple system, it is often difficult to adjust the spatial filter and the intensity ratio of the object and reference beams is fixed.

4.3.4. MIRRORS

It is generally necessary to reflect the laser beam several times on the table. To avoid multiple reflections, front surface mirrors must be used. These must be flat (generally $\lambda/8$) over the area used. For an undiverged laser beam, this is a very small area. It is also desireable to have one larger mirror (say 3" dia.) for reflecting the reference beam. If it is necessary to conserve light, dielectric mirrors are most efficient but very expensive. Signifigantly cheaper silver or aluminum mirrors have been found acceptable. These mirrors are easily mounted on a rigid frame.

4.3.5. SHUTTER

A leaf shutter is adequate in most cases. It should be mounted close to the laser to minimize stray reflections. The shutter should be constructed so that it creates minimal vibration when tripped. It should be mounted on rubber or otherwise to avoid transmitting vibration to the table.

Speeds from $\frac{1}{100}$ to one second should be available, as well as a "B" or preferably a "T" setting. A long release cable is desireable to avoid transmitting vibration to the table and to allow the operator to be sufficiently far away from the table that his breathing will not cause signifigant air turbulence during exposures.

4.3.6. RECORDING MEDIUM

For ease in processing and low cost, the recording medium selected was photographic film. A primary consideration in selection of a film is that it must be able to resolve the fine interference pattern between the object and reference beams. Rogers (110) has stated this

$$p = \frac{\sin \Phi_r}{\lambda} \qquad (3)$$

[illegible] object and reference beams at the [illegible]

For example, if $\lambda = 6328$ Å and $\Phi_r = 15°$ the resolution required is 412 l /mm . This resolution criterion is really a gross oversimplification. Films do not have a resolution "limit" but rather should be classified by their modulation transfer function (MTF). The MTF is an indicator of the film contrast capability at various line frequencies. However, resolution limit is a much simpler concept and is generally sufficient for holography.

A second but equally important consideration is that the emulsion must be suitably sensitive to the laser wavelength. Higher sensitivity decreases exposure time, which relaxes stability requirements of the system . Generally, an exposure to produce an average diffuse density of 0.6 is required. Sensitivity is particularly important using He-Ne or ruby lasers since their output is in the far visible red (6328 and 6943 Å respectively) . At these wavelengths, most films are signifigantly less sensitive than their nominal rating. Unfortunately high resolution (high MTF at high spatial frequencies) and high sensitivity to light are properties which run in opposite directions.

Although films such as Kodak Tri-X Pan have been used for low angle holography (112), much higher resolution is required for reflection holography. Table 1 presents data on numerous films used by the author. This data has been obtained from the manufacturers and from available literature (113) (114) (115) (116).

For real time analysis, a rigid film plane is required. Thus, glass plates are a necessity. Early holographers were limited by availability to 649-F plates. Unfortunately 649-F is one of the least sensitive emulsions, requiring long exposure times (approximately 16 seconds for the system layout of Fig. 12). The Agfa- Gevaert Scientia plates are a signifigant improvement and Ilford He-Ne 1 is even faster. The He-Ne 1 sensitivity of 5 ergs per cm^2. is acheived with resolution similar to 649-F. Exposure time with He-Ne 1 is less than a second.

Glass plates are generally most available in the 4"x5" size. Even on standard flatness plates, the cost of each plate is about $1.50. For double exposure or time average interferometry a rigid emulsion plane is not required. Thus, less expensive plastic base films are suitable. Agfa-Gevaert 14C70 film in 9x12 cm. format has proven very satisfactory. It is more sensitive than He-Ne 1 and the decreased resolution is generally acceptable . Cost of each 14C70 hologram is about 50¢.

In many cases, even 9x12 cm. film is larger than required. Often 24x36 mm. is large enough. In this case, Agfa-Gevaert 10E75 in 35mm. format is very convenient. Required exposure is about 2 seconds. The longer exposure is acceptable in general, particularly when offset by handling convenience. This film is available in bulk at a price of pennies per frame. Agfa 10E75 in 35mm. was used for the major portion of the current work, both for interferograms and for system testing purposes.

4.3.7. PLATEHOLDER

The method of holding the holographic recording medium is very important. The emulsion plane must be held stable in position to better than $\lambda/8$. Techniques used for holding the emulsion depend on the type of film in use.

For small aperture holograms, the film on a plastic base may be loaded into a 35mm. camera which has the lens removed. This method is particularly attractive when many holograms must be made, since processing of 35mm. film in daylight tanks is very convenient. The film should be advanced several minutes before the exposure is made to minimize any problems due to film creep. Larger holograms, (4x5" and larger) may be conveniently made by loading the film into cut film holders. The holders may then be clamped to a rigid frame. Both of these methods provide support for the film and protect it from air currents which could cause motion. The backs in both cases are designed to minimize reflections. Cut film holders are equipped with a dark slide which aids in handling.

A second requirement is added for live fringe holography : the operator must be able to replace the processed hologram (which must be on a glass plate) to within a fraction of a wavelength of its position during exposure.such that the holographic reconstruction is exactly superimposed on the object. Although various exotic plateholders with micrometer adjustments are available for this purpose, the author has found the plateholder shown in Fig. 13 quite adequate. The plate is forced against three pins and held in place by three springs. After processing, the plate is remounted in exactly the same manner. Slight finger pressure is then applied to exactly align the hologram.

4.3.8. SPECIMEN SURFACE PREPARATION

The only requirement on surface preparation for holographic studies is that the surface be diffusely reflecting. It must not produce glare which would affect the hologram, making fringes difficult to see. This is often a problem with machined surfaces. A coat of light coloured (white or non-gloss aluminum) paint is generally sufficient to reduce glare and to make a dark surface sufficiently reflective. When it is desired to produce holograms from low power lasers, or when maximum back reflection of light from the object is desired, a coating of "Scotchlite" or " Codit " may be useful (65). The surface under study need not be flat, indeed, it may be any surface which is accessible to the laser beam.

4.3.9. SPECIMEN FIXTURE

The theoretical fixed or en castre boundary condition is seldom found in practice, even though one goes to great lengths to approach this condition. The mounting fixture for cantilever plates is shown in Fig. 14 . It consists of a 14"x14"x1" base plate, a rear block, 12"x6"x2" fixed to the base plate by 14-½" socket head screws, and a removeable front block, 12"x3"x2", bolted both to the base plate and the rear bearing block. All mating surfaces, including the jaws, are surface ground. All bolts must be thoroughly tightened on assembly or else discrepancies in frequencies up to 4% were found. A tower-pulley system is available to apply dead weight loads to the system. Total weight of the mounting fixture is 135 pounds. All components are fabricated from steel.

The discs require careful mounting as well. To assist the realization of a fixed boundary condition at the inner radius, the discs are machined from solid six inch diameter round stock, leaving an integral shaft approximately one inch long on either disc face. Both ends of the shaft are mounted in split bearing supports of $4\frac{1}{2}$"x2"x1" steel as shown in Fig. 15 . Each cap is held in place by four $\frac{1}{4}$" cap screws. All support pieces are painted flat black to minimize unwanted reflections.

4.3.10. OBJECT VIBRATION EXCITATION

Several methods were used to excite object vibrations. An 8 inch audio speaker was often used for this purpose. The speaker is housed in a perspex reflex chamber. The signal generator output drives the speaker by way of a 36 watt audio amplifier in the frequency range of 30Hz. to 15 kHz . Vibratory amplitudes under audio excitation are generally sufficiently large for holographic purposes, although sound levels up to 130 dbA are required, causing some operator discomfort.

Piezoelectric extension crystals are also very suitable for vibration excitation. The optimum position for the crystal is tangential, near the outer circumference. The crystals were installed with Locktite Minute Bond Adhesive 312. Excitation for the crystal is derived from a $60V_{rms}$ amplifier driven from a signal generator.

For a given amount of energy input to an elastic system, vibratory amplitude is limited by damping, which may be highly frequency dependant. If an object resonance is highly damped, a great deal of energy must be applied to the object. Thus, an alternative method of excitation is by means of an electrodynamic shaker with a frequency range of 50Hz to 20 kHz . The shaker is driven by a current amplifier capable of supplying 1 amp into 240 Ω . The shaker moving mass is forced against a free edge of the object and excitation applied. Unfortunately, this object-exciter contact affects both the natural frequencies and mode shapes of the object in some cases. The effect in frequency is generally less than four percent, but mode shapes are seriously altered.

Non-contacting magnetic vibration excitation is also suitable. In this case a Bruel and Kjaer magnetic transducer, type MM0002 is used. Again, input from the transducer is derived from a 60 V_{rms} amplifier driven from the signal generator. The transducer is placed near the object and its magnetic field provides vibration excitation.

In the case of magnetic objects, this type of excitation adds no mass to the object. Non-magnetic objects require a small disc of magnetic material glued to the surface nearest the transducer for proper coupling. Frequency of the magnetic transducer is up to 2 kHz.

In most cases, excitation was supplied from a Bruel and Kjaer 1025 vibration exciter. This instrument provides a pure sine wave output from 5Hz to 10kHz. In the range above 10kHz., a Hewlett Packard 200CD oscillator was used. Amplifiers were run well below their maximum rated power levels to minimize distortion. It is necessary that the vibratory waveform be as close to a perfect sinusoid as possible. Any departure from this waveform will result in a signifigant loss of fringe contrast.

4.3.11. OPTICAL COMPONENT LAYOUT

For initial studies, a relatively simple layout was used, as sketched in Fig. 12 . This system uses a minimum of elements, providing the least chance for unwanted component vibration. A single spatial filter diverges the laser beam to cover both the reference beam mirror and the object. The major drawback of this simple arrangement is that it is very difficult to adjust the beam balance (reference beam intensity/object beam intensity). The required beam balance for recording is 5/1. However, this may not be the best value for live fringe analysis. It is often desireable to alter the beam balance on reconstruction for optimal fringe contrast.

Thus, the layout sketched in Fig. 16 . and shown in Fig. 17 is more desireable for live fringe analysis. In this system neutral density or polarizing filters may be used before the individual spatial filters to alter beam balance. Filters may not be used after the spatial filters between exposure and reconstruction unless they are optically flat and homogeneous over the field used. Otherwise, fringes are introduced due to path length differences through the filters. A microscope slide serves as the beamsplitter. Care must be taken that the total path lengths of the object and reference beams differ by less than the coherence length of the laser used.

4.3.12. HOLOGRAM RECORDING SEQUENCE

The chronological sequence of the hologram recording process given here is complete. Various steps are not required for each hologram if no major changes to the component geometry are made. Room air supply is turned off and all electronic components required, including the laser, switched on 30 minutes prior to a test. This allows the air in the room to reach a thermal equilibrium. The object is rigidly clamped in the fixture after appropriate surface preparation as described above. A check of the beam balance at the recording plane is made using a sensitive photographic light meter and a frosted glass. Object illumination is checked for uniformity. (A Pentax Spotmeter with an acceptance angle of only one degree is useful for this purpose.) All optical mounts should be checked for tightness.

The appropriate film is selected and loaded into a holder. Shutter speed, if under one second, is set using a photocell and oscilloscope or digital timer. It has been found that the time markings on inexpensive or large diameter shutters are not only unreliable but also rather non-repeatable. For an initial setup, the proper exposure is determined by trial and error.

The room is darkened and the film holder opened. The operator then moves away from the table and waits several minutes. This waiting period allows air currents to settle out and allows the plate to cool to room temperature after being in contact with the operators hands. The shutter is then released gently and the exposure taken.

4.3.13. HOLOGRAM PROCESSING

In general, holograms are best processed according to film manufacturers recommendations. These were followed in the present study. Processing is carried out as close to 68°F. as possible. All washes must also be kept at 68°F. Constant temperature processing is important to minimize emulsion shrinkage and recording media non-linearities. Both factors will degrade the reconstructed image and may produce undesireable higher order images (117) (118). After washing, the holograms are dipped in Kodak Photo-Flow solution to prevent water spotting. Drying is done in still air to minimize emulsion distortion due to drying stresses. For real time interferometry, the plate dries in about one hour.

Holograms processed as above are " amplitude " holograms in the sense that the interference pattern in the emulsion is stored as amplitude or darkness information. Such holograms are not very efficient optically. Diffraction efficiency is defined as the percentage of reconstructing light diffracted by the hologram into the reconstructed image. The maximum theoretical diffraction efficiency of an amplitude hologram is 4%. Actual values are generally about 2% (119).

The diffraction efficiency can be increased by converting the original pattern to one of surface relief or phase change. Efficiencies up to 100% have been reported for these holograms (120). The process is commonly known as bleaching since the conversion of silver in the original pattern to height or density variations results in a clear almost colourless plate.

A number of bleaching procedures have been reported. Efficiencies up to 10% have been found for Agfa-Gevaert 10E75 plates (116). Values of 40% are possible for 8E70 (121) . An experimental comparison of bleached and unbleached holograms has been prepared by Leonard (119).

Two bleaching processes were examined. The first, recommended by Agfa-Gevaert (122), was a potassium bichromate bleach. Results were acceptable but great care was taken because of the toxic nature of the bleach. The second bleach was based on Kodak Chromium Intensifier (123). Results again were acceptable but the holograms were not stable. After several hours of exposure to room light, the bleached holograms deteriorated in quality.

Bleaching presents several disadvantages. The hologram must be exposed longer to provide a high pre-bleaching density. Processing takes longer since several extra steps are required. Each extra step also provides a greater chance for unwanted emulsion shifting to occur due to thermal gradients. The chemicals used are often toxic and the resulting hologram is often unstable. Bleaching increases noise and decreases resolution.

The advantage of bleaching lies in the brighter reconstructed images which it produces. However it was found that even a 1 mw laser provided reconstruction from unbleached holograms of excellent visibility. Reconstructions were readily photographed. Thus, it was found that the disadvantages of bleaching outweighed the advantages and bleaching was discontinued.

In some cases it may be desired to optimize the recording process, particularly if the laser light is of low power. Techniques for carrying out the optimization have been given by Kaspar and Lamberts (124) Biedermann (125) and Leonard and Smirl (119).

4.3.14. HOLOGRAM RECONSTRUCTION

The reconstructing process is highly dependant on the type of hologram recorded. Double exposure and time-average holograms should be reconstructed by a wavefront which is identical to the recording reference beam. However, it was found that, for the system used, any divergent laser wavefront could be used for reconstruction without introducing signifigant abberations. Either the real or virtual image may be viewed although the virtual is usually the sharpest image. Although reconstruction with non-coherent sources is possible, it was found that coherent sources produced the sharpest, brightest images.

An alternative method of reconstruction uses convergent light. In this case, the laser beam was diverged with a small lens, then made convergent by a Sun 85-210 mm. photographic zoom lens. This lens provided a good quality convergent wave of variable focal length. When the hologram is placed in this wavefront, the reconstructed image comes to a focus behind the hologram. It may be observed by placing a frosted glass or screen at this focal plane.

A hologram for live fringe interferometry must be reconstructed by the same reference beam as used during its exposure. It is replaced in the plateholder and placed firmly against the positioning pins. The object is illuminated by the original object beam. Generally a few fringes are seen at this stage. Slight finger pressure on the plate moves it to exactly its original position, resulting in a fringe free state. If required, filters may be placed in the object or reference beam so that the optimum fringe contrast is seen when the object is loaded.

4.3.15. PHOTOGRAPHING THE INTERFEROGRAM

It is often desireable to obtain a photographic record of the interferogram for storage or interpretation purposes. Both double exposure and live holographic interferograms may be easily photographed using standard photographic techniques. A 35mm. SLR camera with a 35 or 50mm. lens was found convenient for this purpose. The camera is placed directly behind the hologram and focussed on the image. An aperture of f/4 was found to produce sufficient depth of field while not introducing speckle on the image. Speckle is a common problem in coherent imaging systems when small apertures are used. A behind the lens exposure meter may be useful, but optimum exposure is best determined by trial and error.

A number of films were tested. The film must have sufficient speed at 6328Å to acheive reasonable speeds. Kodak Panatomic-X (ASA 32) and Kodak 2475 Record Film (ASA $\simeq$ 1200) produced best results. Panatomic-X produced images of good contrast but the speed of 2475 is often convenient. Processing was carried out under manufacturers recommended conditions. Prints were made on Kodabromide F-4 paper processed in full strength Dektol for maximum contrast. For colour transparencies, Kodak Hi-Speed Ektachrome was found most useful.

Excellent prints of time average interferograms may also be obtained on Polaroid film. In this case, the hologram is reconstructed with converging light as described under "Hologram Reconstruction". A Polaroid filmpack is placed at the focal point and exposed. A Polaroid back for a bellows camera proved useful for this purpose. Since this is a single step imaging process, without any lenses between the hologram and the recording plane, little scattering or abberation results.

4.3.16 EXPERIMENTAL PROCEDURE

For each object, an initial live fringe hologram was made. An appropriate vibration exciter was placed behind the object and an initial survey of the object response taken. It was found that the speaker provided best excitation in the audio range while the piezoelectric crystals were excellent above 10kHz. Both of these exciters caused minimum undesireable effects on the vibration.

Excitation frequency was adjusted until a resonance was indicated by formation of live interferometric fringes. Frequency of excitation was determined by a digital counter. Live time average fringes generally are of low contrast. Thus, if a photograph of the interferogram was desired, the resonance was set up and a time average hologram made. In this case a piezoelectric crystal, accelerometer, or the increase in object noise level was used to set the level of excitation for the number of fringes desired. The resulting time average interferogram may be studied at leisure or easily photographed. The crystals used were Vernitron PZT-4 models. The accelerometers used were Bruel and Kjaer type 4336. The sound transducer was a Bruel and Kjaer 1 inch condenser microphone, FET cathode follower and 2606 Measuring Amplifier. Output levels for each transducer were determined during the live fringe test. When calibrating the transducer in this mode, one must remember that double exposure interferometry is twice as sensitive as the live case.

It was found that the piezoelectric crystals or sound level detectors were most desireable for auxillary resonance determination. The accelerometers, although of 0.07 oz. weight, influenced resonant frequencies up to 7% and in some cases influenced the mode shapes.

4.3.17 FRINGE INTERPRETATION

The initial task in converting an interferogram to deflection information lies in determination of the fringe order at the points in question. This is a reasonably simple procedure in time average analysis since all nodal or zero deflection lines appear as bright lines in the interferogram. This is the zero fringe. Fringe order at any point may be determined by counting the fringes from the zero order to the point in question. At an antinode, the order is maximum and decreases from there to the next zero.

Conversion of fringe order to amplitude for the case of simple harmonic motion is governed by a Bessel function equation given by Powell and Stetson (75) as:

$$I(x,y)=J_0\left[(2\pi/\lambda)(\cos\theta_1+\cos\theta_2)M(x,y)\right]I_{st}(x,y) \qquad (4)$$

Each fringe occurs at a zero of the Bessel function (where the argument takes on values of 4.77, 10.9, 17.2, ...). Typically $\theta_1=\theta_2=11^\circ$ (see Fig. 4) and Fig. 18 presents a plot of fringe order against amplitude. Also plotted is the result of an equivalent static linear approximation in which fringe order is related to amplitude in the closed form (49)

$$M(x,y)=\frac{N(x,y)\ \lambda}{\cos\theta_1+\cos\theta_2} \qquad (5)$$

For higher order fringes, the error in the linear approximation is small. The term $\cos\theta_1+\cos\theta_2$ controls the sensitivity. However, Fig. 19 shows that in the range of angles normally used, the change of sensitivity is small.

Fig. 20 is a plot of equation 4. It shows the half order or bright fringes are shifted toward the zero amplitude axis. It also shows that fringe contrast decreases rapidly as fringe order increases.

Equation 4 indicates that all points on a given fringe must be vibrating at the same amplitude. Thus, each fringe represents an iso-amplitude. If velocity or acceleration data is required, a chart such as Fig. 21 or the equations for simple harmonic motion may be used. These equations indicate that each fringe is also aniso-velocity and an iso-acceleration.

5 RESULTS AND DISCUSSION

5.1 STATIC THEORETICAL ANALYSIS

Results of the static analysis are given in Table 2. Convergence of cases 1 and 2 (uniform thickness) occurs at two degrees of freedom. These results agree exactly with the analytical results of Timoshenko (108). Case 3 (uniform thickness corresponding to the experimental disc) converges at six degrees of freedom. Cases 4 and 5 converge at ten degrees of freedom. These linear taper cases agree with the results of Timoshenko (108). These are the special cases of linear taper projected to zero thickness at zero radius. Case 5 is a particularly severe taper, but still shows good convergence. Cases 6 and 7 (the experimental discs of linear taper and constant stress) show convergence at 12 degrees of freedom.

A further set of runs varied the element included angle from 10 to 360 degrees for the geometry of case 1. The variation in deflection was less than 1.2 %. Thus it may be seen that the accuracy of the stiffness matrix is unaffected by the element included angle for axisymmetric cases. In all cases convergence is relatively rapid. Results agree well with analytical solutions where available. The stiffness matrix is therefore considered acceptable.

5.2 THEORETICAL VIBRATION ANALYSIS

5.2.1 INTRDUCTION

Dynamic analysis was caried out for cases 3,6 and 7 since these correspond to the experimental discs. These cases are referred to as constant thickness, linear taper and constant stress, respectively.

A number of initial calculations were carried out in order to determine the optimum configuration of elements for the problem. It was found that a segment of the disc, with appropriate boundary conditions, provided a much more economical analysis than the entire disc It also became apparent that the number of elements selected in the tangential direction for a given segment did not affect the resulting eigenvalues. A run with four radial elements and four tangential elements produced the same eigenvalues (within 0.8%) for a given mode as a run with four radial elements and one set of tangential elements.

This effect was used for further economy in the program. All runs were made with a single radial strip of elements.The element segment included angle for a given run was taken as :

$$\phi_e = \frac{180^\circ}{m} \tag{6}$$

where m is the number of diametral nodes desired.

The correlation table was set up under MCODE=5. For the special case of no diametral nodes (m=0), MCODE=4 was used and element included angle arbitrarily chosen as 30°.

Table 3 shows a typical convergence check for an increasing number of radial elements. Under MCODE = 4 or 5, the individual element is reduced to two effective degrees of freedom. The sector element, when used in this fashion, is fully conforming. Thus, the discretization error should decrease as the number of elements increases. Numerical or computational error is seen to become signifigant at 9 elements for this case. Eigenanalysis was done with single precision numbers. The computational error may be further reduced, if required, by double precision eigenanalysis or use of a more precise eigenanalysis subroutine. Decreased error is accomplished at the expense of larger core requirements and longer computation time. If necessary, extrapolation may also be used to obtain more precise eigenvalues. These procedures were not found necessary in the present study.

5.2.2 THEORETICAL FREQUENCY RESULTS

Results for the predicted natural frequencies of the discs studied are presented in graphical form in Figs. 22, 23, and 24. Disc natural frequencies are seen to increase with both number of nodal diameters and number of nodal circles. These results were obtained with 8 to 12 radial element strips, depending on disc geometry. The constant thickness disc was analyzed with eight elements, the linear taper with 10 or 12 and the constant stress with 12. These numbers were selected as optimum from convergence checks on each profile for one case of no diametral nodes.

Natural frequencies for the linear taper and constant stress disc are reasonably similar. This is expected since the two profiles are relatively alike in geometry.

5.2.3. EFFECT OF POISSONS RATIO ON THEORETICAL FREQUENCIES

The constant thickness disc was also analyzed for Poisson's ratios of 0 and 0.5. Results are plotted in Fig. 22. Where nodal circles exist, a decrease in Poissons ratio to 0 decreases natural frequencies while an increase in Poissons ratio to 0.5 increases natural frequencies. For no nodal circles, the effect is reversed for $m > 2$. Up to 60 kHz, the the effect of changing Poissons ratio to 0 or 0.5 from 0.333 is generally less than 15 %.

5.2.4. THEORETICAL RADIAL PROFILE OF DEFLECTIONS

Theoretical normalized radial profiles of deflection for $n=0,1$ and 2 are shown in Figs. 25, 26 and 27 respectively for the constant stress disc. This disc was chosen since it represents the most severe case of thickness change. For no circular nodes, the deflection at a given radius decreases as the number of diametral nodes increases. This is attributed to the stiffening effect of diametral nodes, since the circumference is stretched an increasing amount as the number of diametral nodes increases. For $n = 1$ and 2, this stiffening effect again reduces normalized amplitudes. It also moves the position of the antinodes further from the fixture. The same trends were found for the other discs analyzed.

5.2.5. THEORETICAL TANGENTIAL PROFILE OF DEFLECTION

The normalized outer circumference deflection profile for the constant stress disc for $3 \geq m \geq 0$ is shown in Fig. 28. For no diametral nodes, the normalized deflection has a constant value of 1.0. This corresponds to the umbrella modes where deflection is axi-symmetric and independant of angular position. For $m \geq$, 1 the profile appears sinusoidal in form. To further investigate this effect, the angular position was normalized by dividing by the number of diametral nodes. These results were plotted in Fig. 29. The profile is independant of the number of diametral nodes and appears as a single line. A sinusoid is also plotted in Fig. 29 and is seen as identical to the theoretical deflection curve. This effect was found to be true for all three discs studied.

The normalized tangential profile of deflection at any radius other than the outer circumference may be found by multiplying the normalized curve by the local radius value of the normalized radial profile of deflections.

5.3 EXPERIMENTAL ANALYSIS

5.3.1 FREQUENCY RESULTS

Natural frequencies for the three discs were obtained by live fringe holographic interferometry. This technique allowed rapid determination of frequencies and mode shapes. Natural frequencies for all modes experimentally found are plotted with the theoretical curves of Figs. 22 to 24. Agreement with theory is generally good with almost all cases being within 10% particularly for the constant thickness and linear taper discs. The results for the constant stress disc are also seen to be in agreement to better than 10% except for the higher order modes ($m > 8$ or $n > 3$). Agreement for higher order modes should be obtainable by using more degrees of freedom provided that computational errors can be suppressed.

Sources of differences between experimental and theoretical frequencies are material anisotropies, machining errors in profile, variations in Poissons ratio, Youngs modulus and density.

5.3.2. DEFLECTION PROFILE RESULTS

Deflection profile results are presented here for the constant stress disc. This was selected since it is the most severe profile studied. Results for the other discs are very similar. Deflection profiles were experimentally determined from double exposure holographic time average interferograms. Photographs of the interferograms may be found in Figs. 30 to 35. Both theoretical and experimental frequencies are given beside each mode.as well as the percentage difference between the two. Modes are identified as m/n (number of nodal diameters/number of nodal circles.)

In Fig. 30, two frequencies are shown for the 1/0 mode. One has a vertical node, the other has a horizontal node. Both frequencies differ signifigantly from the theoretical value. This behaviour was found for all discs. It is attributed to the fact that this mode exerts a net bending moment at the disc shaft. The support structure is not able to restrain this couple and the result is that the inner fixed boundary condition is not obtained. All higher modes ($m \geqslant 2$) are reactionless, that is they produce a net force and moment of zero at the shaft. This is illustrated for the 2/0 mode of Fig. 30 where one support structure has been removed but the frequency and mode shape are as expected.

For higher modes, some distortion of the nodal lines from the expected symmetric result is seen, particulaly in Fig. 33 for modes 3/2 and 5/2 and in Fig. 34 for modes 4/3 and 6/3. This is attributed to slight anisotropies in the disc properties. The last two interferograms of Fig. 35 (at 43.8 and 51.0 kHz) appear to be complex modes. These result when two or more modes have nearly the same frequency and are excited simultaneously.

Fringe order information was taken from the interferograms and converted to deflection from equation (4). Results for the tangential profile of deflection were normalized and added to Fig. 29. Agreement between the theoretical and experimental points is excellent. This verifies the theoretical result that the tangential profile is very close to a sine wave. In the radial direction, the theoretical profiles of Figs. 25 to 27 were replotted for each value of m in Figs. 36 to 44. Experimentally determined profiles are also plotted on these figures.

For $m = 0$ and 1, Figs. 36 and 37, only the cases of no diametral circles could be excited. Agreement for this mode in both cases is found within 4%. For $m = 2$, Fig. 38, both the zero and one circular node cases were excited. Again, the experimental and theoretical results agree within 4%. For higher order modes $8 \geqslant m \geqslant 3$, (Figs. 39 to 44), experimental results for the no circular node case ($n = 0$) is better than 4%. For $n > 0$, agreement becomes less exact. Antinodal deflections differ by as much as 19%. Positions of nodes and antinodes differ up to 6.4%. Antinodal deflections differ by greater than the maximum possible experimental error (Appendix B). However, the general shape is the same and positions of nodes and antinodes agree well. An increase of number of degrees of freedom should bring higher order theoretical antinodal deflections into closer agreement with the experiment, at an increase in computational time and cost as well as the increased possibility of computational error. A further source of difference is the slight asymmettry of some of the higher order mode shapes indicating the existance of imperfections of disc material, machined shape and perhaps fixing. For most purposes, a designer is concerned with natural frequencies and not deflection profiles so a difference in normalized deflections of 19% would be quite acceptable.

6. RECOMMENDATIONS FOR FURTHER WORK

6.1 EXPERIMENTAL PROCEDURES

Extension of the technique to rotating objects would be very useful. This would require carefull mounting of the disc and a higher power stroboscopic laser. Axial and radial runout on the disc, at least when rotating, should be less than $\lambda/2$ to prevent formation of fringes due to disc motion. The disc should be carefully balanced to minimize unwanted vibration. For a 2500 rpm rotational speed, a strobe pulse of approximately 30μsec. is required. Even if a 50 mw. c.w. laser is used, power after the strobe is so low that the reconstruction may not be visible. A far better approach would be the use of a strobed burst argon laser with much greater power. At present, only one model of this laser is available on the market at a cost of over $10,000. Should such a technique be succesful, experimental analysis of rotating discs would be greatly simplified.

6.2 FINITE ELEMENT ANALYSIS

1. The sector element should be expanded to allow in-plane strains to be analyzed. The element could then be used for analysis of rotating discs.

2. The addition of further element types to include the effects of a blade ring and blades would allow analysis of more realistic cases.

3. The addition of full field stress calculations would allow an analysis of the severity of each mode. This would also require determination of the material hysteretic damping constants (which are usually frequency dependant) and an analysis of aerodynamic damping.

4. Extension of the sector element to include effects of linear radial taper in thickness would result in faster convergence for disc profiles of arbitrary shape.

7 CONCLUSIONS

1. Holographic interferometry provides an excellent tool for full field vibration analysis. Establishment of a holographic facility is relatively simple. Once installed, it is inexpensive and easy to use.

2. Live fringe time average holographic interferometric analysis allows determination of object natural frequencies in real time. No mass need be added to the object. Modal information is readily obtained from the interferogram.

3. Double exposure time average holographic interferometry provides high quality images which are suitable for determination of full field amplitude data. Resolution is better than one optical wavelength and accuracy can be better than a few per cent.

4. Curvature of the object surface does not affect holographic interferometric results. Frequency response of the technique is virtually unlimited.

5. The sixteen degree of freedom sector element rapidly converges to the deflection of an arbitrary profile disc under axi-symmetric static loading.

6. The sixteen degree of freedom sector element provides an excellent tool for analysis of the natural frequencies and mode shapes of discs of arbitrary profile.

7. Proper combination of boundary conditions and the segment angle for a given mode set can signifigantly reduce the number of degrees of freedom required to solve for natural frequencies and mode shapes without a loss of accuracy.

8. Disc natural frequencies increase as either the number of diametral or circular nodes increase.

9. Disc natural frequencies are altered slightly as Poisson's ratio is varied from 0 to 0.5.

10. Theoretically predicted radial profiles of deflection are in agreement with experimental values provided sufficient degrees of freedom are allowed.

11. The tangential profile of deflection for a disc vibrating with one or more diametral nodes can be closely approximated by a sinusoidal curve.

BIBLIOGRAPHY

1. Biezeno, C. and Grammel R., Engineering Dynamics, Vol. III Steam Turbines, Blackie and Son, London and Glascow, 1954.
2. Timoshenko, S., Vibration Problems in Engineering, D. Van Nostrand Co., Princeton, N.J., 3rd edition, 1959.
3. Ehrich, F., "A Matrix Solution For the Vibration Modes of Non-uniform Discs", A.S.M.E. Journal of Applied Mechanics, March, 1965, p. 109-115.
4. Blech, J., "Computer Analysis of Flexural Vibrations of a Rotating Disc with an Arbitrary Profile", A.S.M.E. Paper 65-WA/GTP-8
5. McLeod, A. and R. Bishop, "The Forced Vibration of Circular Flat Plates", Mechanical Engineering Science Monograph No.1, March 1965.
6. Harris, G., "The Normal Modes of a Circular Plate of Variable Thickness", Quart. Journal of Mechanics and Applied Mathematics, Vol. 21, 1968, pp.321-327.
7. Eversman, W. and R. Dodson, "Free Vibrations of a Centrally Clamped Spinning Circular Disc", A.I.A.A. Journal, Vol.7, pp. 2010-12.
8. de Silva, B., "Minimum Weight Design of Discs Using a Frequency Constraint", A.S.M.E. Journal of Engineering for Industry, Vol. 91, Nov. 1969, pp. 1091-1099.
9. Olhoff, N., "Optimal Design of Vibrating Circular Plates", Int. Journal of Solids and Structures, Vol. 6, 1970, pp. 139-156.
10. Melosh, R., "Basis for Derivation of Matrices for the Direct Stiffness Method", A.I.A.A. Journal, Vol. 1, 1963, pp. 1631-1637.

11. Argyris, J., "Continua and Discontinua", Matrix Methods in Structural Mechanics, Wright-Patterson A.F.B., Ohio, 1965, pp. 11-189.

12. Zienkiewicz, O. and Y. Cheung, The Finite Element Method in Structural and Continuum Mechanics, Revised First Impression, McGraw-Hill, London, 1968.

13. Holland, I. and K. Bell, Finite Element Methods in Stress Analysis, TAPIR-Technical University of Norway, Trondheim, 1969.

14. Oliveira, E., "Theoretical Foundations of the Finite Element Method", Int. Journal Solids and Structures, Vol.4, 1968, pp. 929-952.

15. Tong, P. and T. Pian, "The Convergence of the Finite Element Method in Solving Linear Elastic Problems", Int. Journal of Solids and Structures, Vol. 3, 1967, pp. 865-879.

16. McLay, R., "On Certain Approximations in the Finite Element Method", A.S.M.E. paper 70-WA/APM-34.

17. Dunne, P., "Complete Polynomial Displacement Fields for the Finite Element Method", Aero. Journal of the Royal Aero. Society, Vol.72, 1968, pp. 245-246.

18. Leckie, F. and G. Lindberg, "The Effect of Lumped Parameters on Beam Frequencies", Aero. Quarterly, Vol. 14, 1963, p.224-240.

19. Tolani, S. and R. Rocke, "A Strain Energy Comparison of Discrete Modelling for Vibrating Continuous Systems", A.S.M.E. Paper 71-Vibr-5.

20. Melosh, R. and T. Lang, "Modified Potential Energy Mass Representation for Frequency Prediction", Matrix Methods in Structural Mechanics, Wright-Patterson A.F.B., Ohio, 1965, p.445-455.

21. Archer, J., "Consistent Mass Matrix for Distributed Mass Systems", A.S.C.E., Journal of the Structural Division, ST4, 1963, p. 161-178.

22. Klein, S., and R. Sylvester, "The Linear Elastic Dynamic Analysis of Shells of Revolution by the Matrix Displacement Method", Matrix Methods in Structural Mechanics, Wright-Patterson A.F.B., Ohio, 1965, p. 299-328.

23. Cowper, G. et al., "Static and Dynamic Applications of a High Precision Triangular Plate Bending Element", A.I.A.A. Journal, Vol. 7, 1969, p. 1957-1965.

24. Olson, M. and G. Lindberg, "Free Vibrations and Random Response of an Integrally Stiffened Panel", N.R.C. Aero. Report LR-544.

25. Percy, J. et al., "Application of Matrix Displacement Method to Linear Elastic Analysis of Shells of Revolution", A.I.A.A. Journal, Vol. 3, 1965, p. 2138-2145.

26. Webster, J., "Free Vibrations of Shells of Revolution Using Ring Finite Elements", Int. Journal of Mechanical Science, Vol.9 1967, p. 559-570.

27. Ergatoudis, I., et al., "Curved Isoparametric Quadrilateral Elements for Finite Element Analysis", Int. Journal of Solids and Structures, Vol. 4, 1968, p. 31-42.

28. Gibson, W., "Finite Element Analysis of Flat Plates in Polar Co-ordinates", Case Western Reserve School of Engineering, Division of Solid Mechanics, Structures and Mechanical Design, Report#34.

29. Groh, G., "Engineering Uses of Laser Produced Speckle Patterns", Symposium on the Engineering Uses of Holography, Strathclyde 1968, p. 483-494.

30. Pastorius, W., T. Pryor and W. North, "Application of Diffractographic Techniques to Vibration Analysis", accepted for publication, Experimental Mechanics.

31. Hargall, C. and R. Niven, "Visualization of Nodes and Antinodes in Vibrating Flat Plates", Experimental Mechanics, Vol. 8, 1968, p. 225.

32. Theocaris, P., "Optical Nodal Pattern Analysis", Experimental Mechanics, Vol. 7, 1967, p. 237.

33. Stargarter, H., "Dynamic Models of Vibrating Rotor Stages", A.S.M.E. paper 66-WA/GT-8.

34. Spicer, P., and B. Wastrasiewicz, "Vibration Analysis by Projected Fringes", Optica Acta, Vol. 15, 1968, p. 521-522.

35. French, R., "Aircraft Gas Turbine Rotating Compressor Disc Vibration", A.S.M.E. paper 65-WA/GTP-11.

36. Tobias, S. and R. Arnold, "Influence of Dynamical Imperfections on the Vibration of Rotating Discs", Proc. Inst. Mechanical Engineers, Vol. 171, 1957, p. 669-690.

37. Gabor, D., "A New Microscopic Principle", Nature, Vol. 161, 1948, p. 777-778.

38. Gabor, D., "Microscopy by Reconstructed Wavefronts", Proc. Royal Society (London), Vol. A197, 1949, p. 454-487.

39. Leith, E. and J. Upatnieks, "Wavefront Reconstruction with Continuous Tone Objects", J. Optical Society of America, Vol. 53, Dec. 1963, p. 1377-1381.

40. Leith, E. and J. Upatnieks, Wavefront Reconstruction with Diffused Illumination and Three-Dimensional Objects", J. Optical Society of America, Vol.54, Nov. 1964, p. 1295-1301.

41. Leith, E., "Applications of Holography", S.A.E. paper 680014.

42. Fourney, M., "Aerosol Size and Velocity Determination Via Holography", Review of Scientific Instruments, Vol 40, 1969, p. 205-213.

43. Gabor, D., "Reconstruction of Phase Objects by Holography", Nature, Vol. 208, Dec. 1965, p. 1159-1162.

44. Hsu, T. and R. Moyer, "Application of Fibe Optics in Holography", Applied Optics, Vol. 10, Mar. 1971, p. 669-670.

45. Frocht, M., "Isopachic Stress Patterns", J. Applied Physics, Vol. 10, 1939, p. 248-257.

46. Horman, M., "An Application of Wavefront Reconstruction to Interferometry", Applied Optics, Vol. 4, 1965, p. 333-336.

47. Burch, J., "The Applications of Lasers in Production Engineering", The Production Engineer, Vol. 44, 1965, p. 431-449.

48. Collier, R., "Application of Moire Techniques to Holography", Applied Physics Letters, Vol. 7, 1965, p. 223-225.

49. Stetson, K. and R. Powell, "Hologram Interferometry", J. Optical Society of America, Vol. 55, 1965, p. 1570A.

50. Heflinger, L. et. al., "Holographic Interferometry ", J. Applied Physics, Vol. 37, 1966, p. 642-649.

51. Stetson, K. and R. Powell, "Hologram Interferometry", J. Optical Society of America, Vol. 56, 1966, p. 1161-1166.

52. Haines, K. and B. Hildebrand, "Surface Deformation Measurement Using the Wavefront Reconstruction Technique",Applied Optics, Vol. 5, 1966,p. 595-602.

53. Vienot, J. et. al., "Surface Displacement Fringe Analysis", Symp. Engineering Uses of Holography, Strathclyde, 1968, p. 133-150.

54. Brown, G. et. al., "Theory of Holographic Interferometry", J. Accous. Society of America, Vol. 45, 1969, p. 1166-1179.

55. Sollid, J., "Holographic Interferometry Applied toMeasurements of Small Static Displacements of Diffusely Reflecting Surfaces", Applied Optics,Vol. 8, 1969, p. 1587-1595.

56. Butters, J., "Application of Holography to Instrument Diaphram Deformation and Associated Topics", Symposium on the Engineering Uses of Holography, Strathclyde, 1968, p. 151-169.

57. Jeffers, L., "Investigation of a Diaphram-Type Pressure Transducer Using Holographic Interferometry", Electro-Optical Systems Design Conference, 1969, p. 115-119.

58. Grant, R. and G. Brown, "Holographic N.D.T. in the Automotive Industry", S.A.E. paper 690051.

59. Boone, P., "Application of Hologram Interferometry to Plate Deformation and Translation Measurement", Optica Acta, Vol. 16, 1969, p. 555-567.

60. Wilson, A., et. al., "Holographic and Analytic Study of a Semiclamped Rectangular Plate Supported by Struts", Presented at 1970 Spring Meeting of Society for Experimental Stress Analysis, paper #1650.

61. Hageniers, O.,"A Theoretical and Experimental Investigation of Deflections and Bending Moments in Cantilever Plates : With Application to Helical Gear Design", Ph.D. Thesis, Dept. Mechanical Engineering, University of Windsor, Windsor, Ont.

62. Leadbetter, I. and T. Allen, "Holographic Examination of the Pre-Buckling Behaviour of Axially Loaded Cylinders", Symp. Engineering Uses of Holography, Strathclyde, 1968, p.185-195.

63. Varner, J., "Desensitized Hologram Interferometry", Applied Optics, Vol. 9, 1970, p. 2098-2100.

64. Wilson, A., "Holographically Observed Torsion in a Cylindrical Shaft", Applied Optics, Vol. 9, 1970, p.2093-2097.

65. Ennos, A., "Measurement of In-Plane Surface Strain by Hologram Interferometry", J. Scientific Instruments, Series2, Vol. 1, 1968, p. 731-734.

66. Ennos, A., "Holography and Its Applications", Contemp. Physics, Vol. 8, 1967, p. 153-170.

67. Ennos, E., "Holographic Techniques in Engineering Metrology", Proc. Inst. Mechanical Engineers, 1968.

68. Archbold, E. and A. Ennos, "Techniques of Hologram Interferometry for Engineering Inspection and Vibration Analysis", Symp. on the Engineering Uses of Holography, Strathclyde, 1968, p. 381-396.

69. Nisida, M. and H. Saito, "A New Interferometric Method of Two Dimensional Stress Analysis", Experimental Mechanics, Vol. 4, 1964, p. 366-376.

70. Fourney, M., "Application of Holography to Photoelasticity", Society for Experimental Stress Analysis Paper 1218.

71. der Hovanesian, J. et. al., "A New Experimental Stress Optic Method: Stress-Holo-Interferometry", Society for Experimental Stress Paper 1282.

72. der Hovanesian, J. and J. Varner, "Methods for Determining the Bending Moments in Normally Loaded Thin Plates by Hologram Interferometry", Symp. on the Engineering Uses of Holography, Strathclyde, 1968, p. 173-184.

73. Stetson, K., "Moire Methods for Determining Bending Moments from Hologram Interferometry", Optics Technology, 1970, p. 80-84.

74. Powell, R. and K. Stetson, "Interferometric Vibration Analysis of Three dimensional Objects by Wavefront Reconstruction", J. Optical Society of America, Vol. 55, 1965, p. 612A.

75. Powell, R. and K. Stetson, "Interferometric Vibration Analysis by Wavefront Reconstruction", J. Optical Society of America, Vol. 55, 1965, p. 1593-1598.

76. Osterberg, H., "An Interferometric Method of Studying the Vibrations of an Oscillating Quartz Plate", J. Optical Society America, Vol. 22, 1932, p. 19-35.

77. Stetson, K. and R. Powell, "Interferometric Holographic Evaluation and Real Time Vibration Analysis of Diffuse Objects", J. Optical Society of America, Vol. 55, 1965, p. 1694-5.

78. Wall, M., "The Form of Holographic Fringes", Symposium on the Engineering Uses of Holography, Strathclyde, 1968, p. 355-380.

79. Lurie, M. and M. Zambuto, "A Verification of Holographic Measurement of Vibration," Applied Optics, Vol. 7, 1968, p.2323-2325.

80. Stetson, K., "Vibration Measurement by Holography", Symp. on Engineering Uses of Holography, Strathclyde, 1968, p.307-331.

81. Wall, M., "Recording High-Order Holographic Vibration Fringes", Optics Technology, 1969, p. 266-269.

82. Powell, R., "The Measurement of Vibration by Holography", Symp. on Engineering Uses of Holography, Strathclyde, 1968, p.333-345.

83. Wilson, A., "Characteristic Functions for Time-Average Holography", J. Optical Society of America, Vol. 60, 1970, p. 1068-1071.

84. Wilson, A. and D. Strope, "Time-Average Holographic Interferometry of a Circular Plate Vibrating Simultaneously in Two Rationally Related Modes", J. Optical Society of America, Vol. 60, 1970, p. 1162-1165.

85. Lurie, M., "Verification of Holographic Measurement of Three Types of Motion", Symp. on Engineering Uses of Holography, Strathclyde, 1968, p. 397-399.

86. Zambuto, M. and M. Lurie, "Holographic Measurement of General Forms of Motion", Applied Optics, Vol. 9, 1970, p. 2066-2072.

87. Vikram, C. and R. Sirohi , "Holographic Images of Objects Moving With Constant Acceleration", Applied Optics, Vol. 10, 1971, p. 672-673.

88. Monahan, M. and K. Bromley, "Vibration Analysis by Holographic Interferometry", J. Accous. Society of America, Vol. 44, 1968, p. 1225-1231.

89. Waddell, P. and W. Kenedy, "Vibration Studies of Engineering Components by Time Averaged Holograms", Symp. on Engineering Uses of Holography, Strathclyde, 1968, p. 347-354.

90. Grant, R. and W. Von Winkle, "Interferometric Holography as a Tool for the Study of Flexural in Active Sonar Tranducers", First International Conference on Laser Applications, Paris, 1967.

91. Peter, A., "Practical Holographic Mode Shapes on Turbine Blades", A.S.M.E. paper 69-VIBR-32.

92. Pastorius, W. and Z. Reif, "Application of Holographic Techniques to Turbine Disc Vibrations", A.S.M.E. paper 71-VIBR-105.

93. Hockley, B. and J. Butters, "Holography as a Routine Method of Vibration Analysis", J. Mechanical Engineering Science, Vol.12, 1970, p. 37-47.

94. Aprahamian, R., and D. Evensen, "Application of Holography to Dynamics:High Frequency Vibrations of Beams", A.S.M.E. Journal of Applied Mechanics, 1970, p. 287-291.

95. Archbold, E., and A. Ennos, "Observation of Surface Vibration Modes by Stroboscopic Hologram Interferometry", Nature, Vol. 217, 1968, p. 942-943.

96. Shajenko , P. and C. Johnson, "Stroboscopic Holographic Interferometry", Applied Physics Letters, Vol. 13, 1968, p. 44-46.

97. Aleksoff, C., "Time Average Holography Extended", Applied Physics Letters, Vol. 14, 1969, p. 23-24.

98. Watrasiewicz, B. and P. Spicer, "Vibration Analysis by Stroboscopic Holography", Nature, Vol. 217, 1968, p. 1142-1143.

99. Fryer, P., "Inexpensive System for Live Stroboscopic Holographic Interferometry", Optics Technology, 1970, p. 36-39.

100. Brandt, W., "Practical Holography for Vibration Studies", Optical Spectra, 1970, p. 26-31.

101. Zaidel, A. et. al., "Holographic Strobe Method for Studying Vibrations", Soviet Physics-Technical Physics, Vol. 13, 1969, p. 1470- 1473.

102. Erf, R. and J. Waters, "Holographic Characterization of Aerospace Components", A.S.M.E. paper 71-GT-74.

103. Waters, J. and H. Aas, "Holographic Analysis of Turbine Blades", A.S.M.E. paper 71-GT-84.

104. Fryer, P., "A Scanning Technique for Allowing Whole VibrationCycles to be Stored on One Hologram", Applied Optics, Vol. 9, 1970, p. 1216.

105. Waddell, A. et. al., "Vibration Analysis for Static and Rotating Objects by Stroboscopic Holography", Proc. Symp. on Holographic Applications, Besancon France, 1970.

106. Kennedy, W. et. al., "Stroboscopic Holography Using an Electro-Optic Modulator", Proc. Symp. on Electro-Optical Systems Design, Brighton, 1971.

107. Hagell, C. and S. Liem, "Vibration Analysis by Interferometric Fringe Modulation", Int. Symp. on the Applications of Holography, Besancon France, 1970.

108. Timoshenko, S. and Woinowskey-Krieger, Theory of Plates and Shells, 2nd Edition, McGraw-Hill, New York, 1959.

109. Cooley, W. and P. Lohnes, Multivariate Procedures for the Behavioral Sciences, J. Wiley and Sons, 1962.

110. Rogers, G., "The Design of Experiments for Recording and Reconstructing Three Dimensional Objects in Coherent Light", J. Scientific Instruments, Vol. 43, 1966, p. 677-684.

111. Lehmann, M., "Holography-Technique and Practice", Symp. on Engineering Uses of Holography, Strathclyde, 1968, p. 1-24.

112. Brooks, R., "Low Angle Holographic Interferometry Using Tri-X Pan Film", Applied Optics, Vol. 6, 1967, p. 1418-1419.

113. Nassenstein, H.,et. al., "An Investgation of the Properties of Photographic Materials for Holography", Symp. on Engineering Uses of Holography, Strathclyde, 1968, p. 25-43.

114. Schultze, D., "Red Sensitized High-Resolution Emulsions for Laser Photography", Laser Focus, 1968, p. 23-25.

115. Frecska, S., "Characteristics of the Agfa-Gevaert Type 10E70 Holographic Film", Applied Optics, Vol. 7, 1968, p. 2312-2314.

116. Young, M., and F. Kittredge, "Amplitude and Phase Holograms Exposed on Agfa-Gevaert 10E75 Film", Applied Optics, Vol. 8, 1969, p. 2353-2354.

117. Smith, H., "Photographic Releif Image", J. Optical Society of America, Vol. 58, 1968, p. 533-539.

118. Urbach, J. and R. Meier, "Properties and Limitations of Hologram Recording Materials", Applied Optics, Vol. 8, 1969, p.2269-2281.

119. Leonard, C. and A. Smirl, "Holographic Recording With Limited Laser Light", Applied Optics, Vol. 10, 1971, p. 625-663.

120. Pennington, K. and J.Harper, "Techniques for Producing Low Noise, Improved Efficiency Holograms", Applied Optics, Vol. 9, 1970, p. 1643-1650.

121. Schmackpfeffer, A. et. al.,"High Efficiency Phase-Hologram Gratings", I.B.M. J. Research and Development, 1970, p. 533-537.

122. --- , "Scientific Photography", Technical Information, Agfa Gevaert, Mortsel Belgium, Oct. 1967.

123. Upatnieks, J. and C. Leonard, "Diffraction Efficiency of Bleached, Photographically Recorded Interference Patterns", Applied Optics, Vol. 8, 1969, p. 85-89.

124. Kaspar, F. and R. Lamberts, "Effects of Some Photographic Characteristics on the Light Flux in a Holographic Image", J. Optical Society of America, Vol. 58, 1968, p. 970-976.

125. Biedermann, K., "Attempts to Increase the Holographic Exposure Index of Photographic Materials", Applied Optics, Vol. 10, 1971, p. 584-595.

126. Ruff, B., "The Production of Holograms by a Single Axial Mode Ruby Laser", M.A.Sc. Thesis, University of Rochester, 1966.

127. Gregor, E. and J. Davis, "Design Considerations for Nanosecond Holography," Electro- Optical Systems Design, July-Aug. 1969.

128. Barton, M. "Vibration of Rectangular and Skew Cantilever Plates", A.S.M.E. Journal of Applied Mechanics, Vol. 73, 1951, p.129-134.

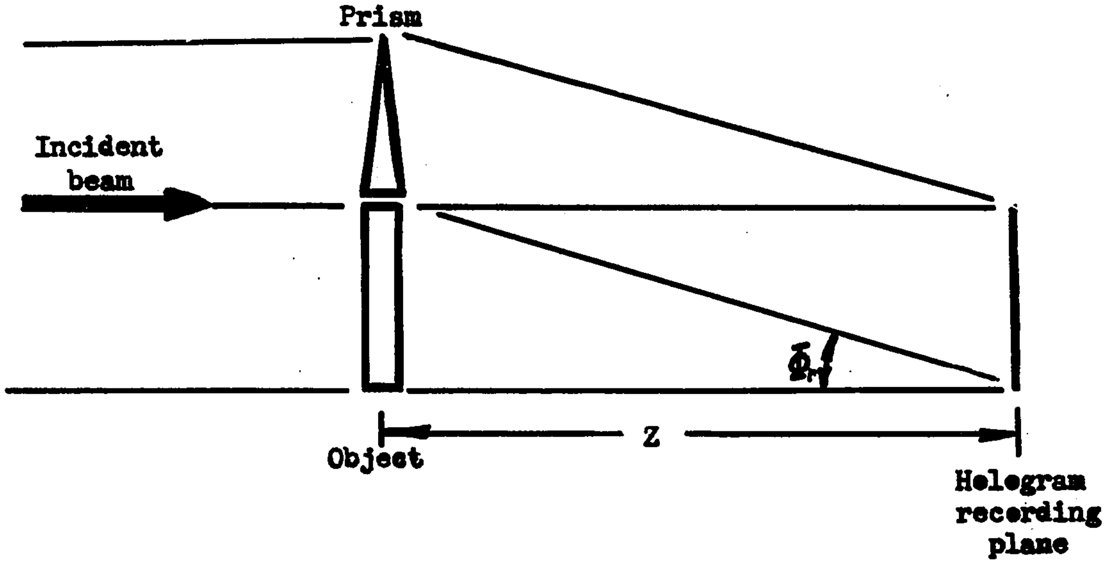

Fig. 1. Recording a Two Beam Hologram
(Transmission Mode)

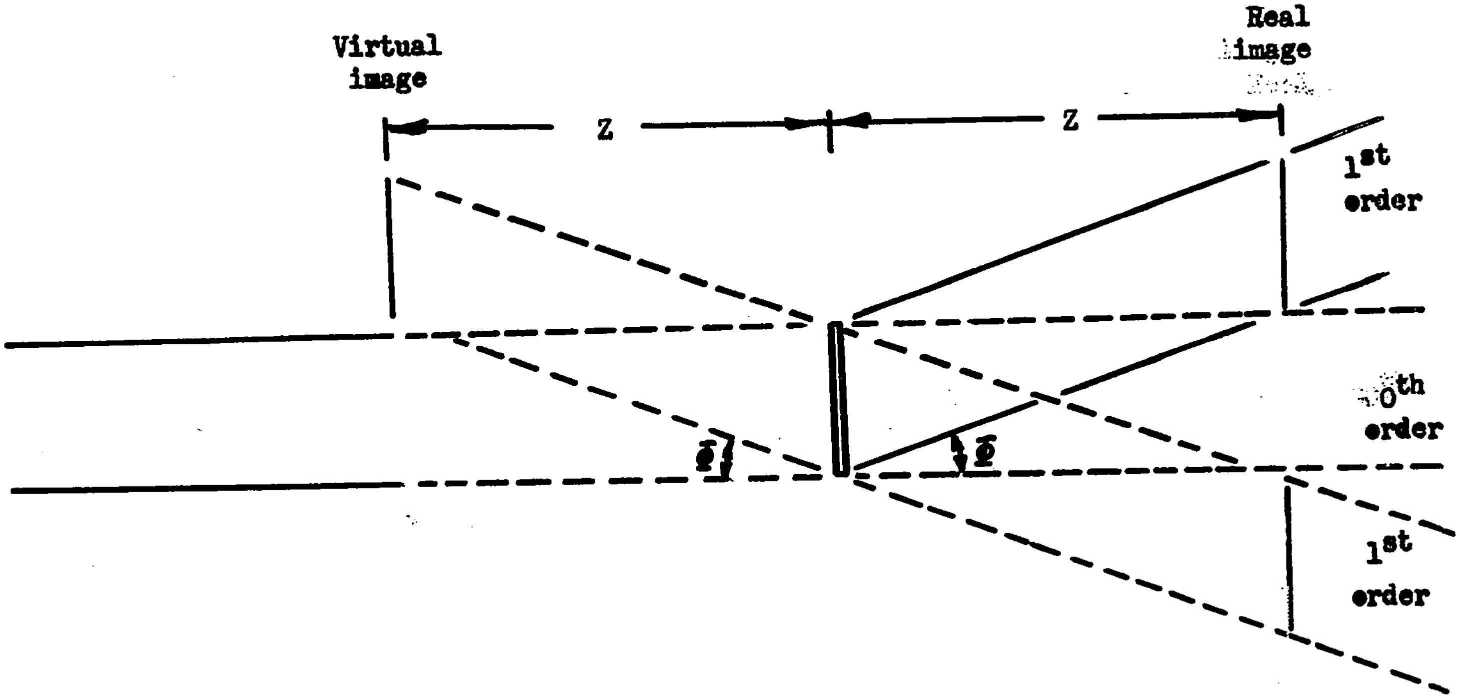

Fig. 2. Reconstructing a Two Beam Hologram
(Transmission Mode)

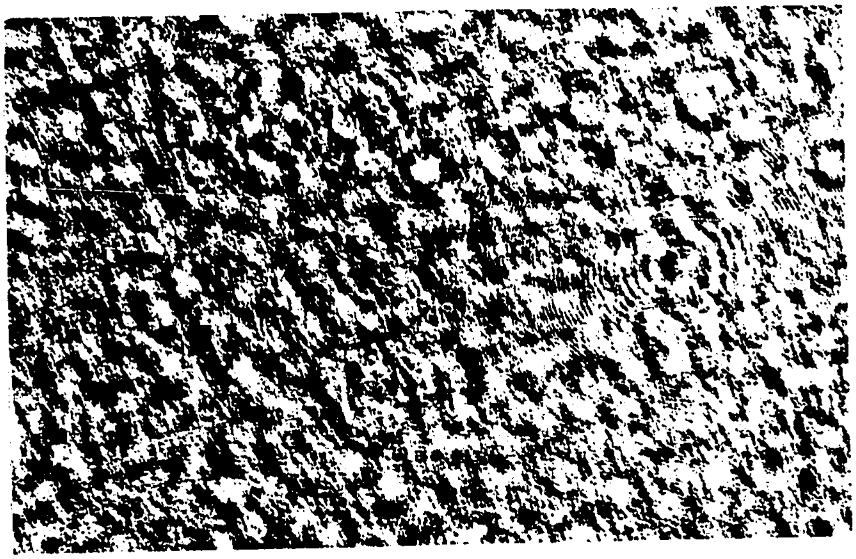

Fig. 3. Photo of Hologram (Approx. 4X)

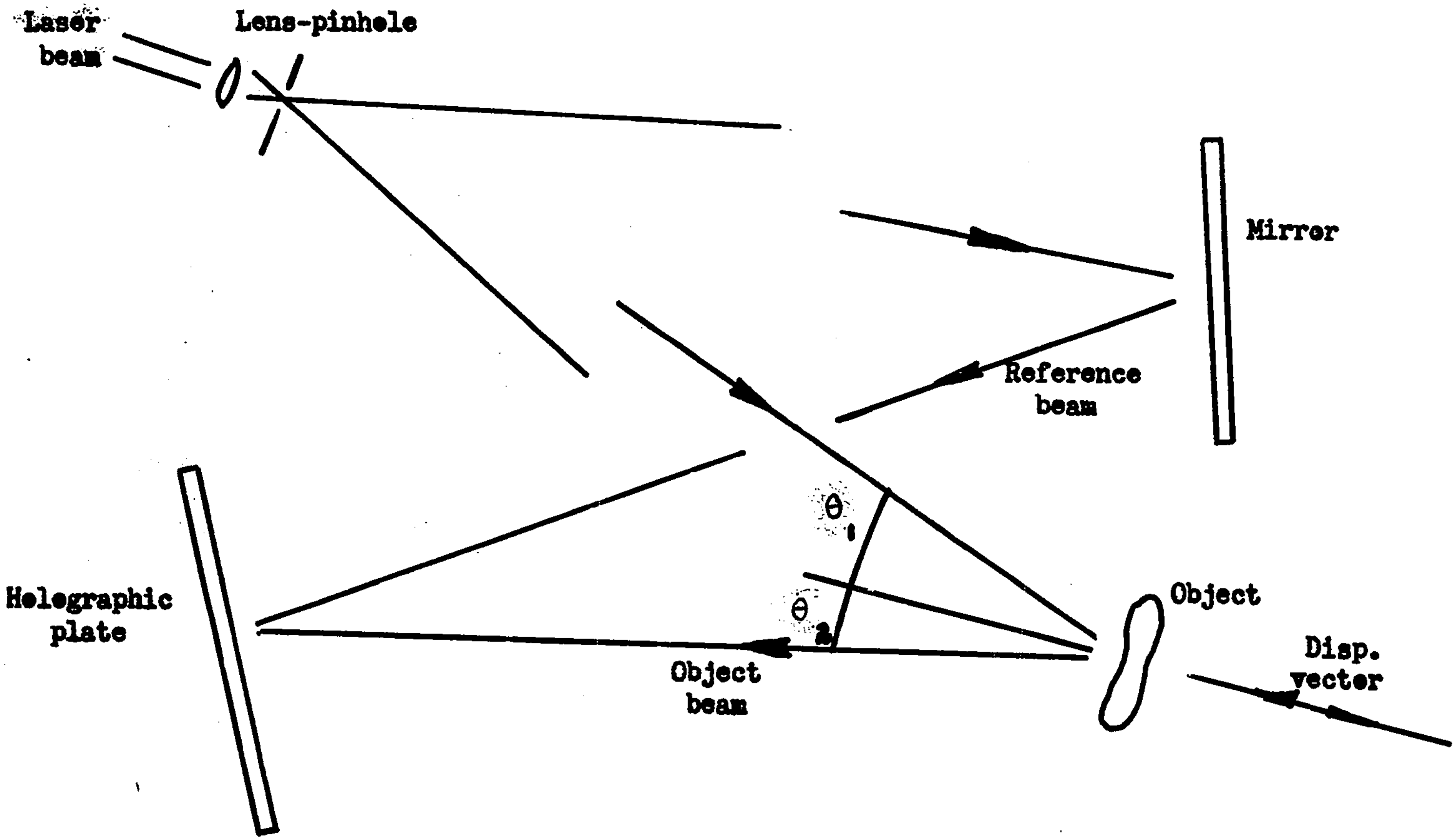

Fig. 4. Recording a Two Beam Hologram
(Three Dimensional Object)

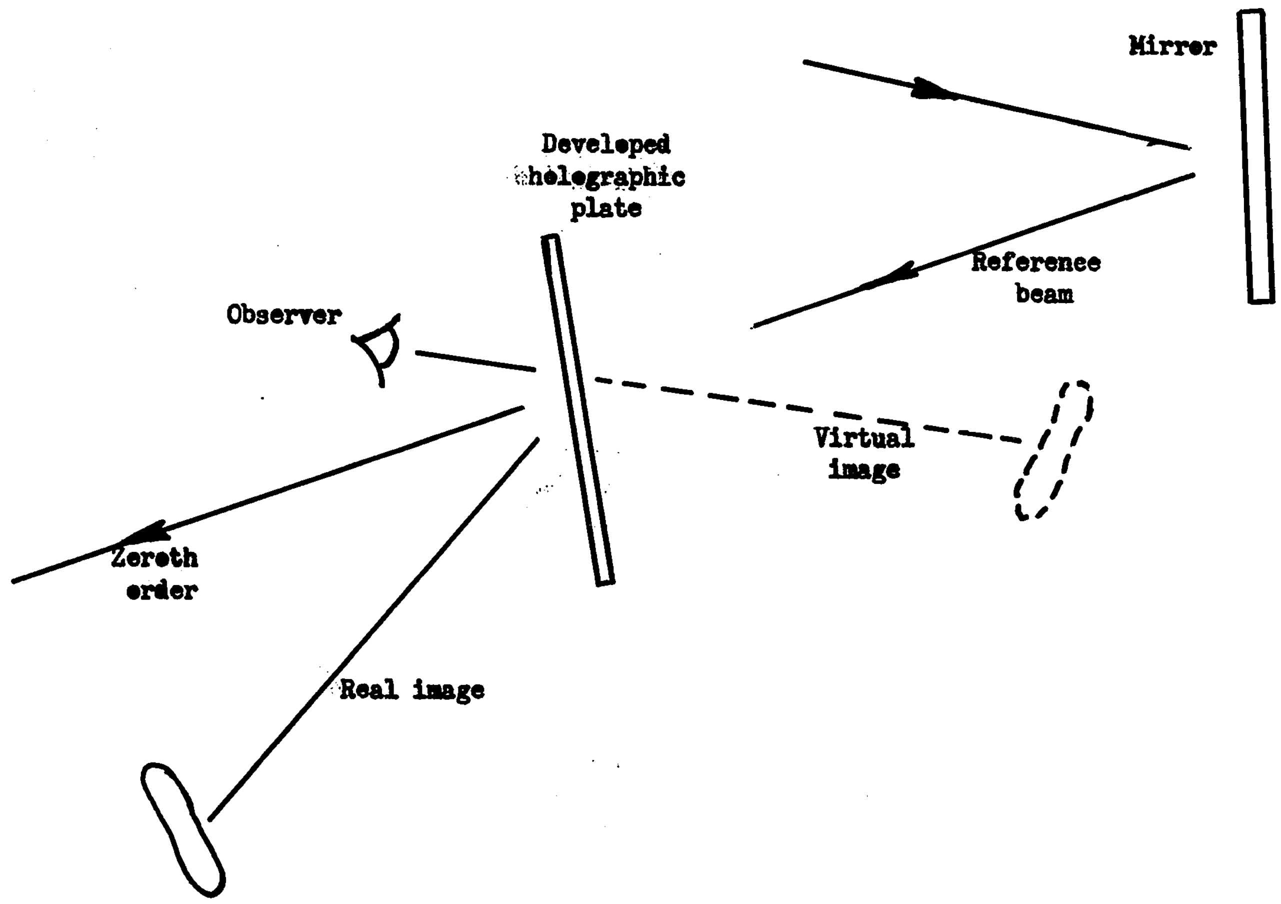

Fig. 5. Reconstructing a Two Beam Hologram
(Three Dimensional Object)

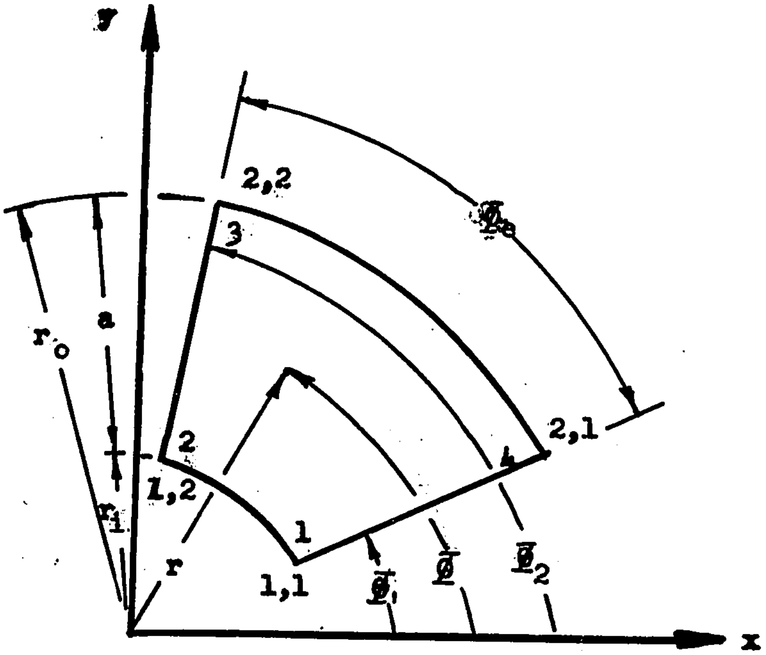

w transverse displacement within an element

w_{ij} transverse displacement at node i,j

Fig. 6. Secter Element Geometry

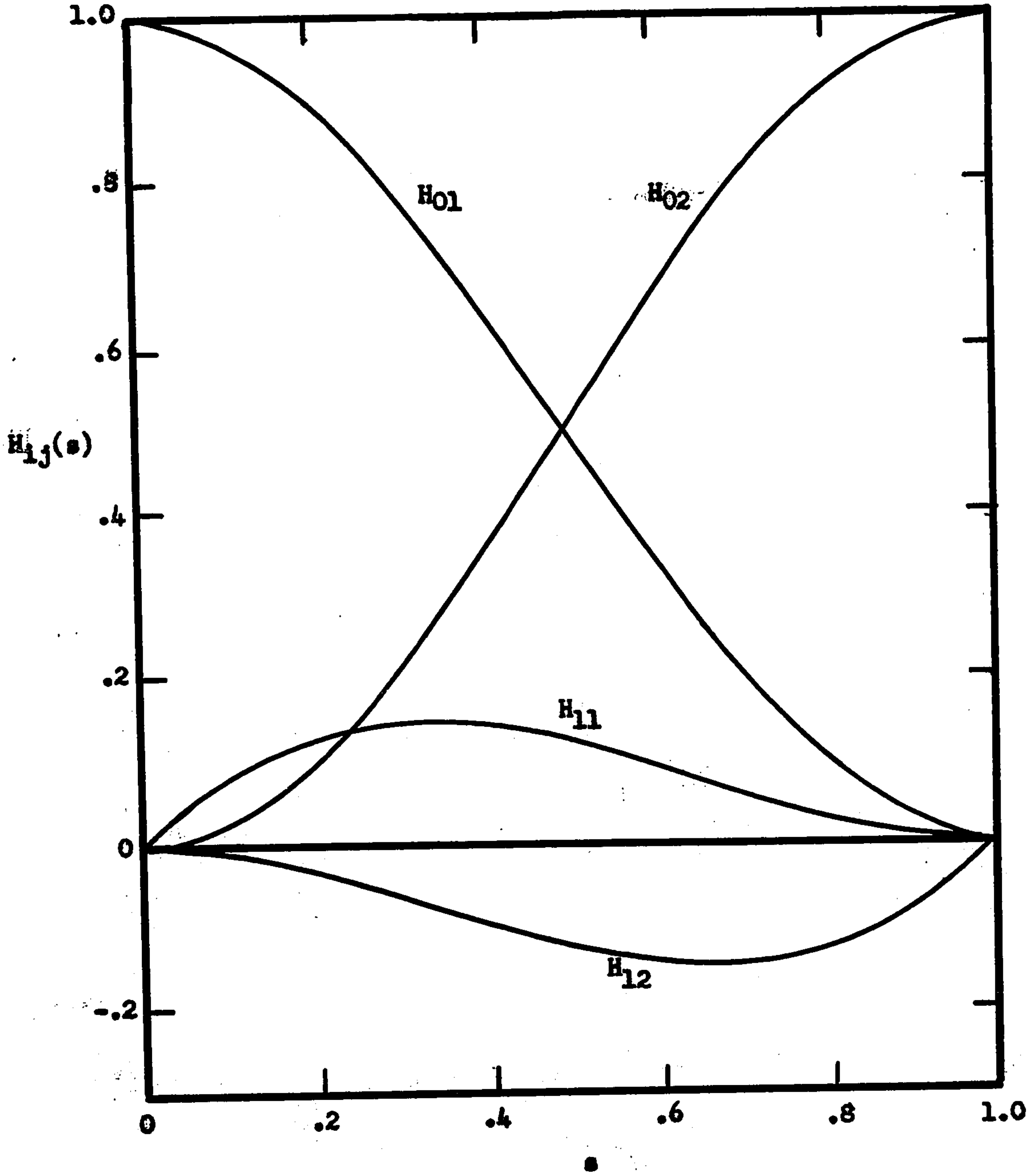

Fig. 7. Osculatory Interpolation Polynomials

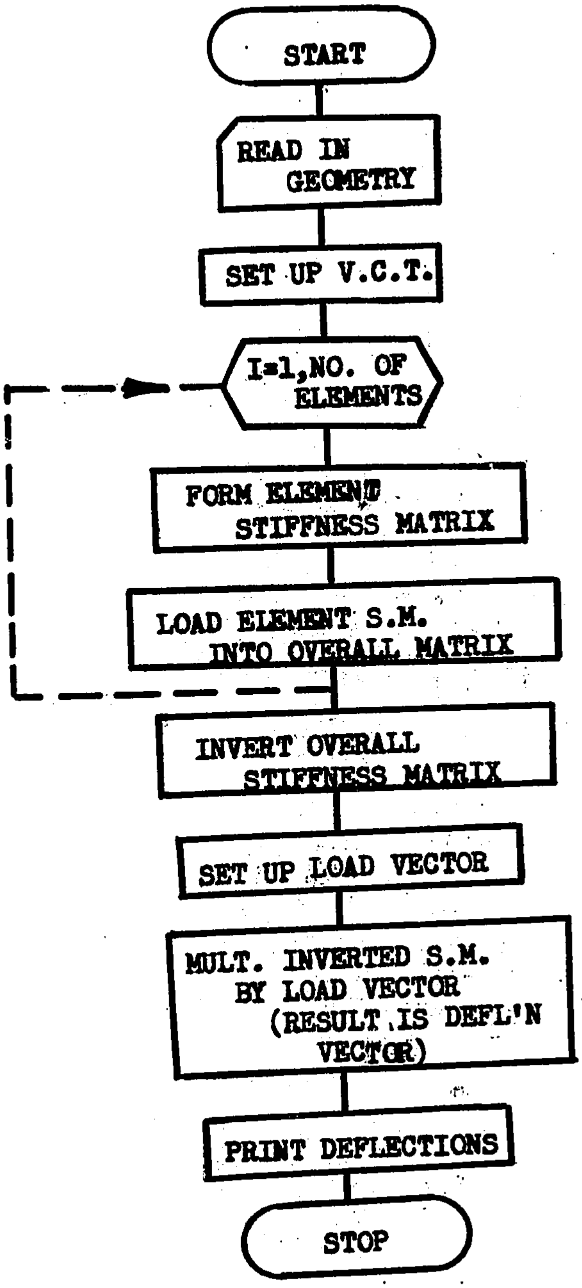

Fig. 8. Flowchart of Static Analysis Program

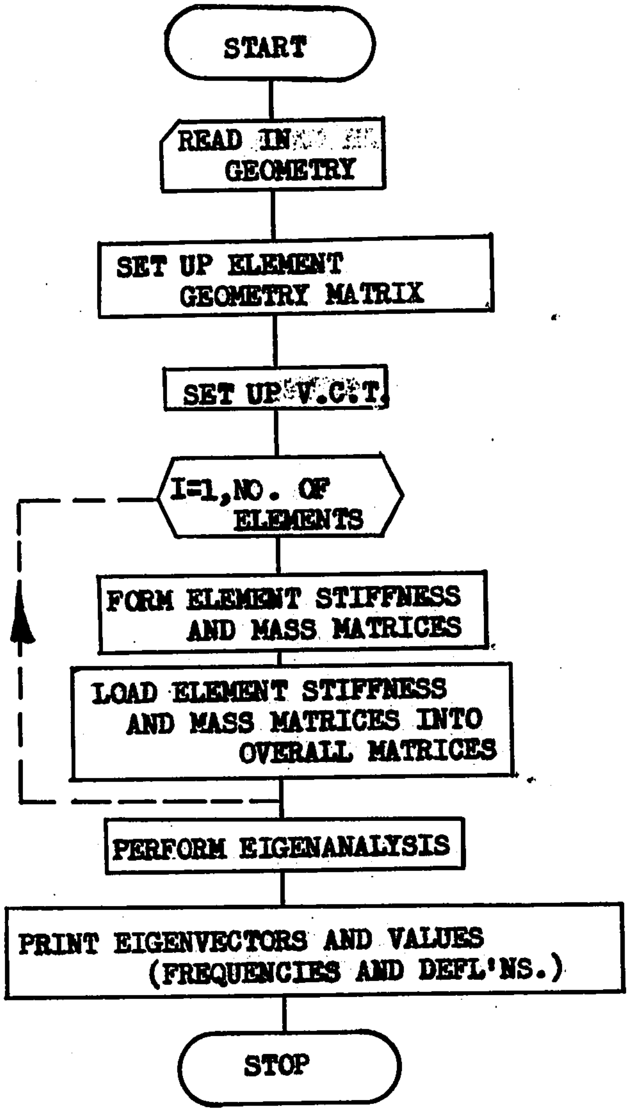

Fig. 9. Flowchart of Dynamic Analysis Program

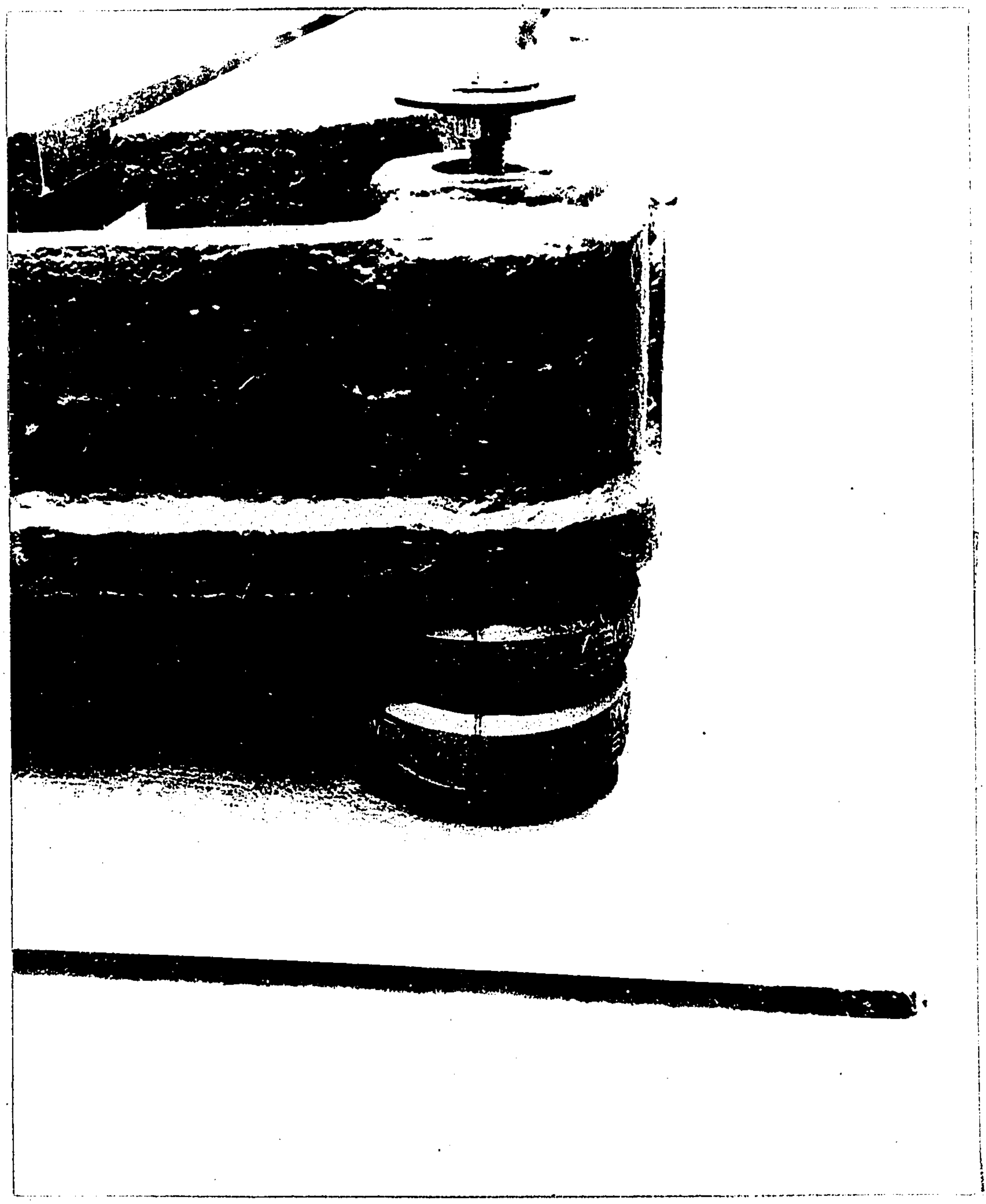

Fig. 10. Rubber Spring Isolation System

Fig. 10. Rubber Spring Isolation System

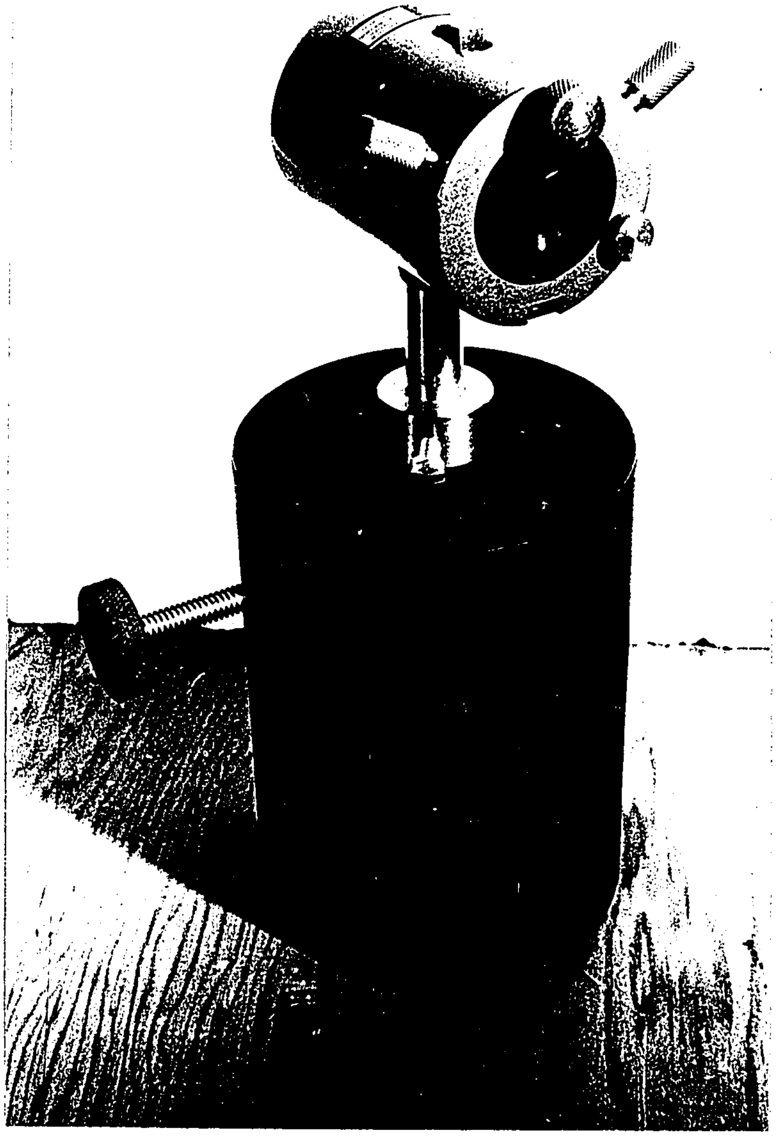

Fig. 11. Optical Component Mount

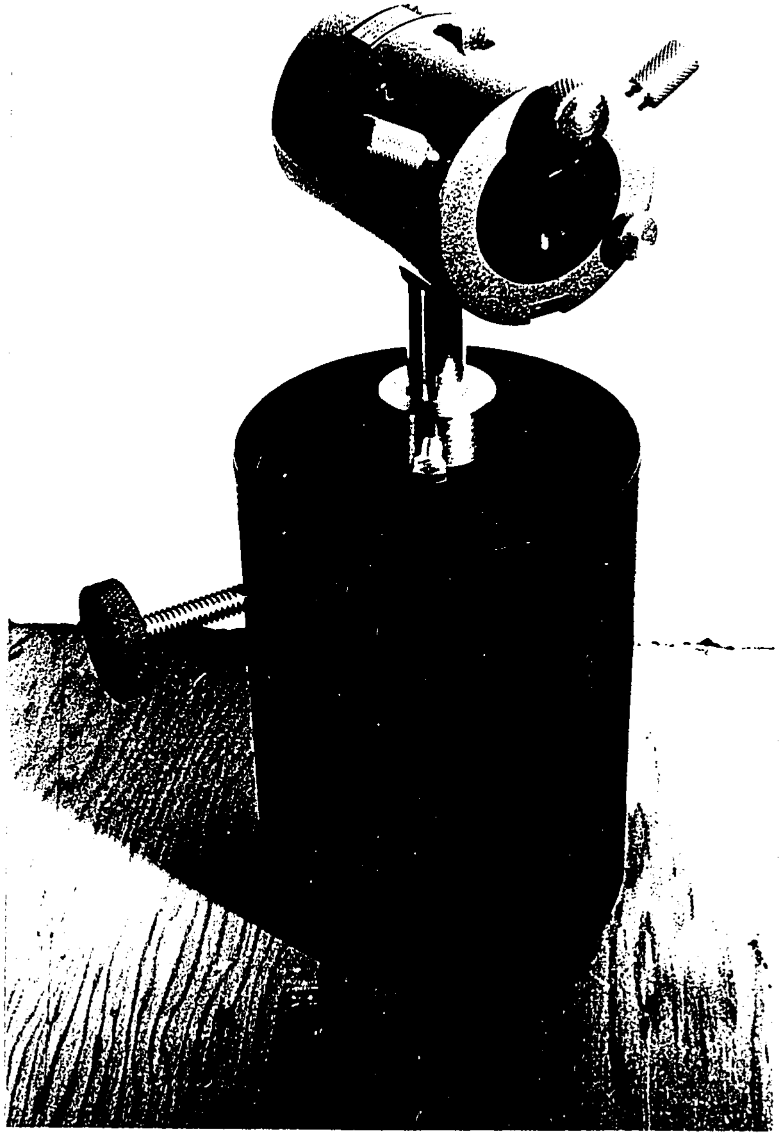

Fig. 11. Optical Component Mount

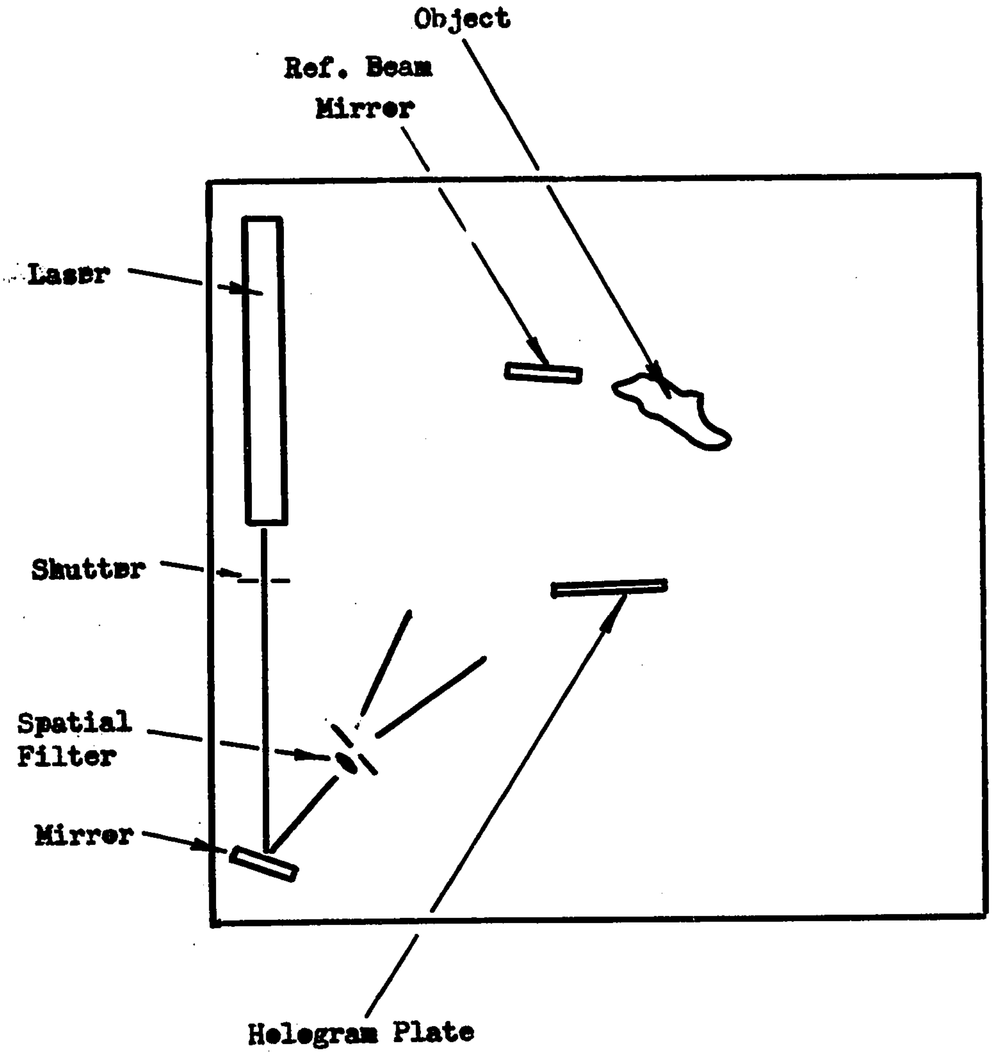

Fig. 12. Simple Component Layout

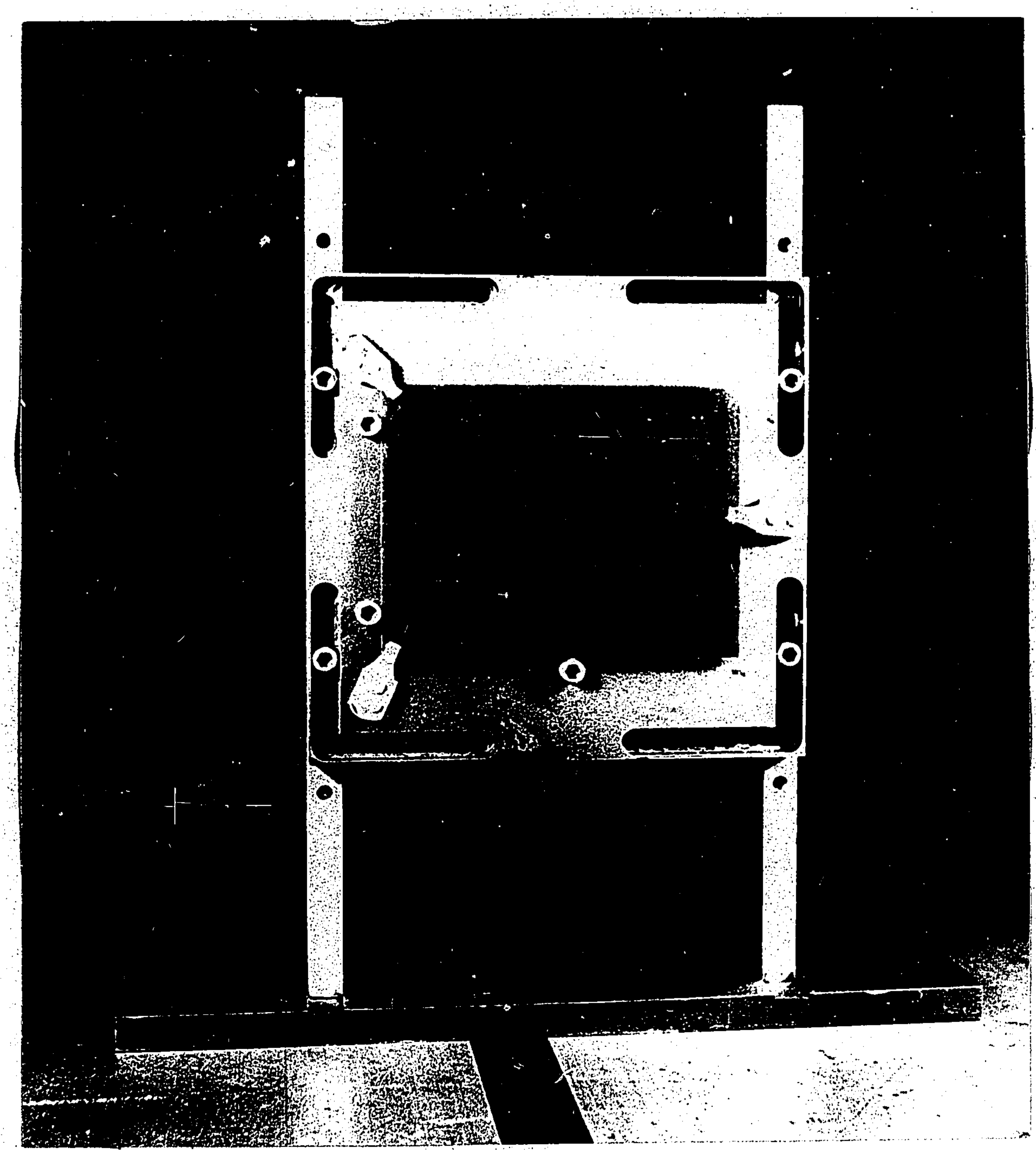

Fig. 13. Holographic Live Fringe Plateholder

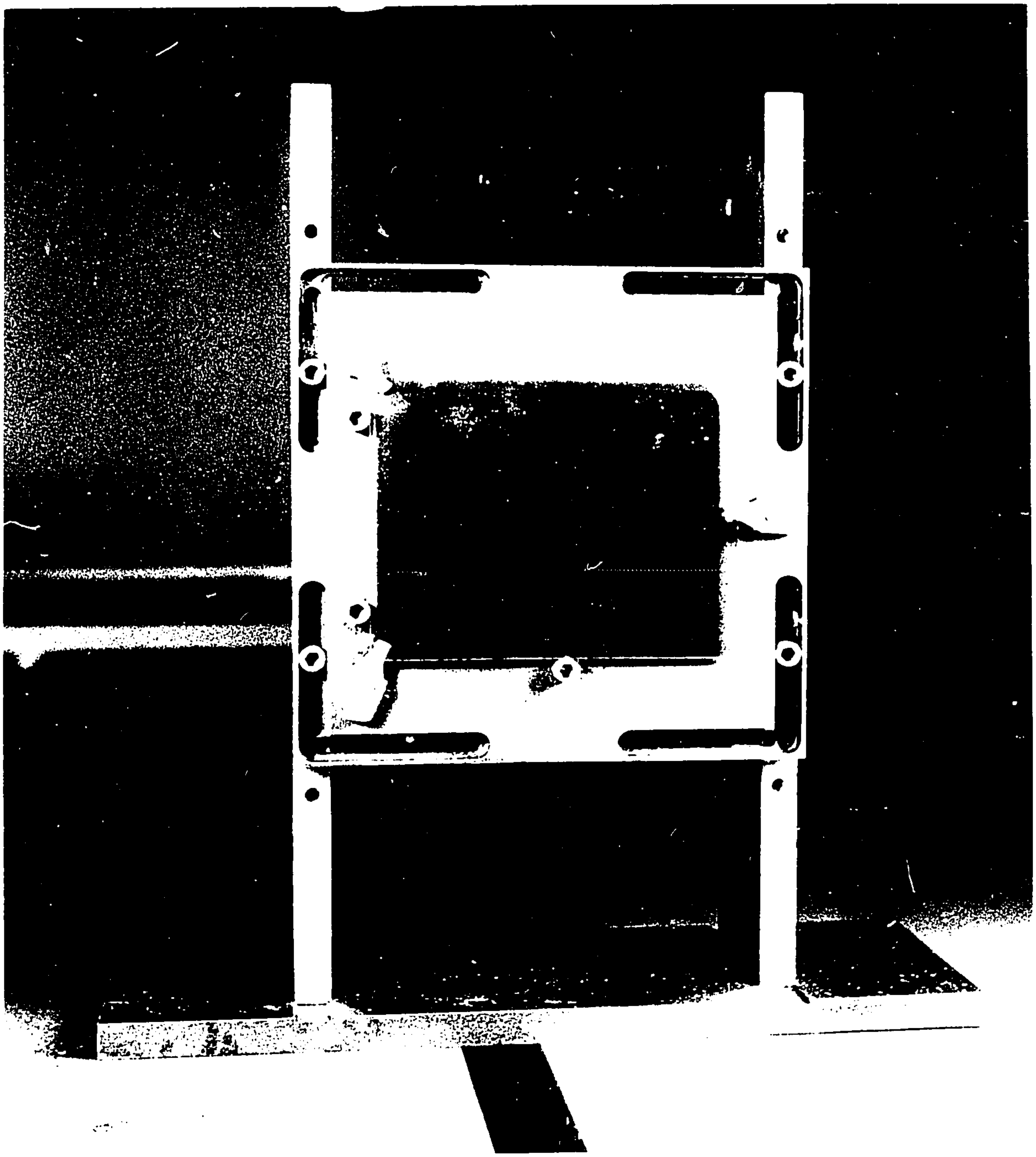

Fig. 15. Holographic Live Fringe Plateholder

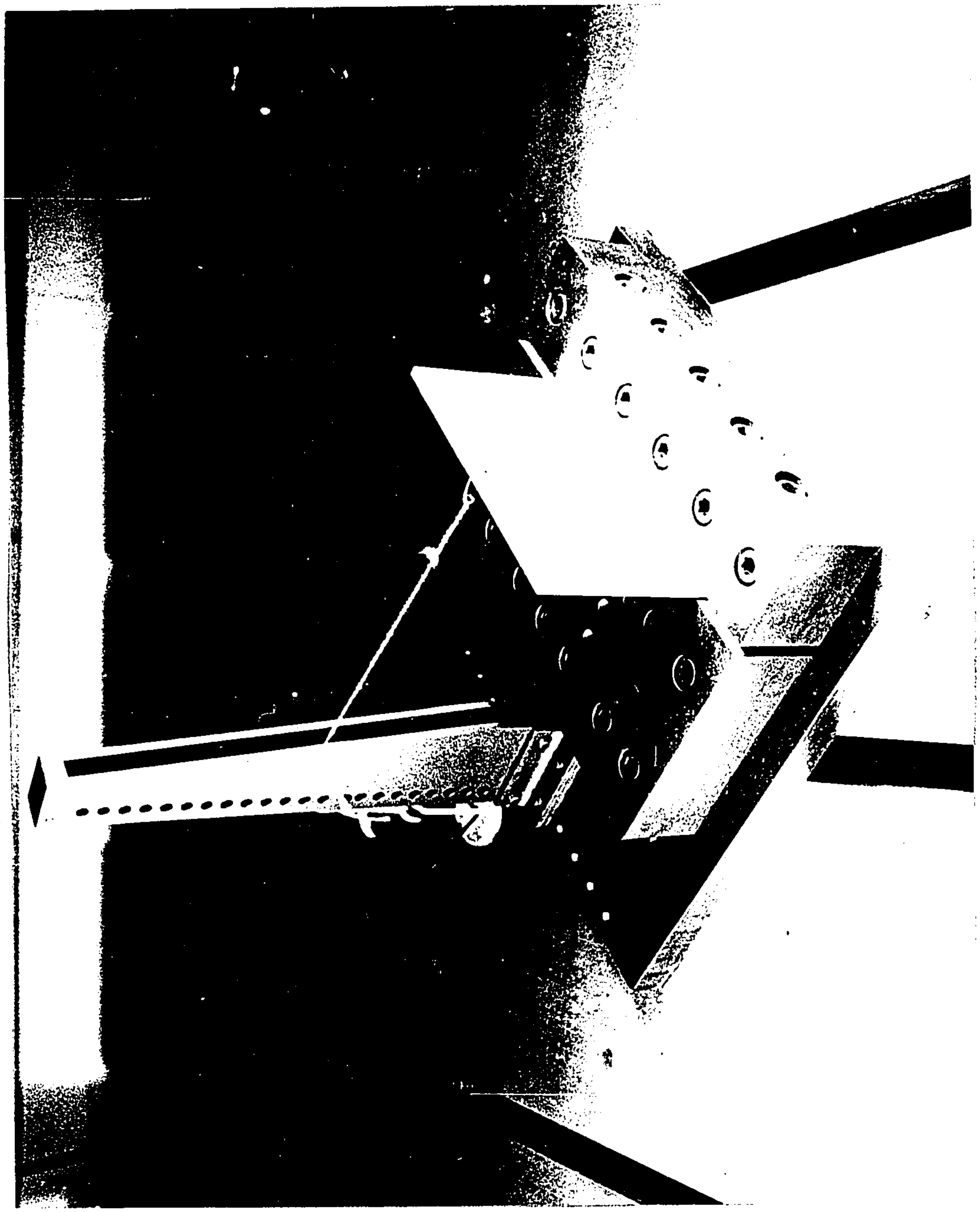

Fig. 14 Cantilever Plate Fixture

14

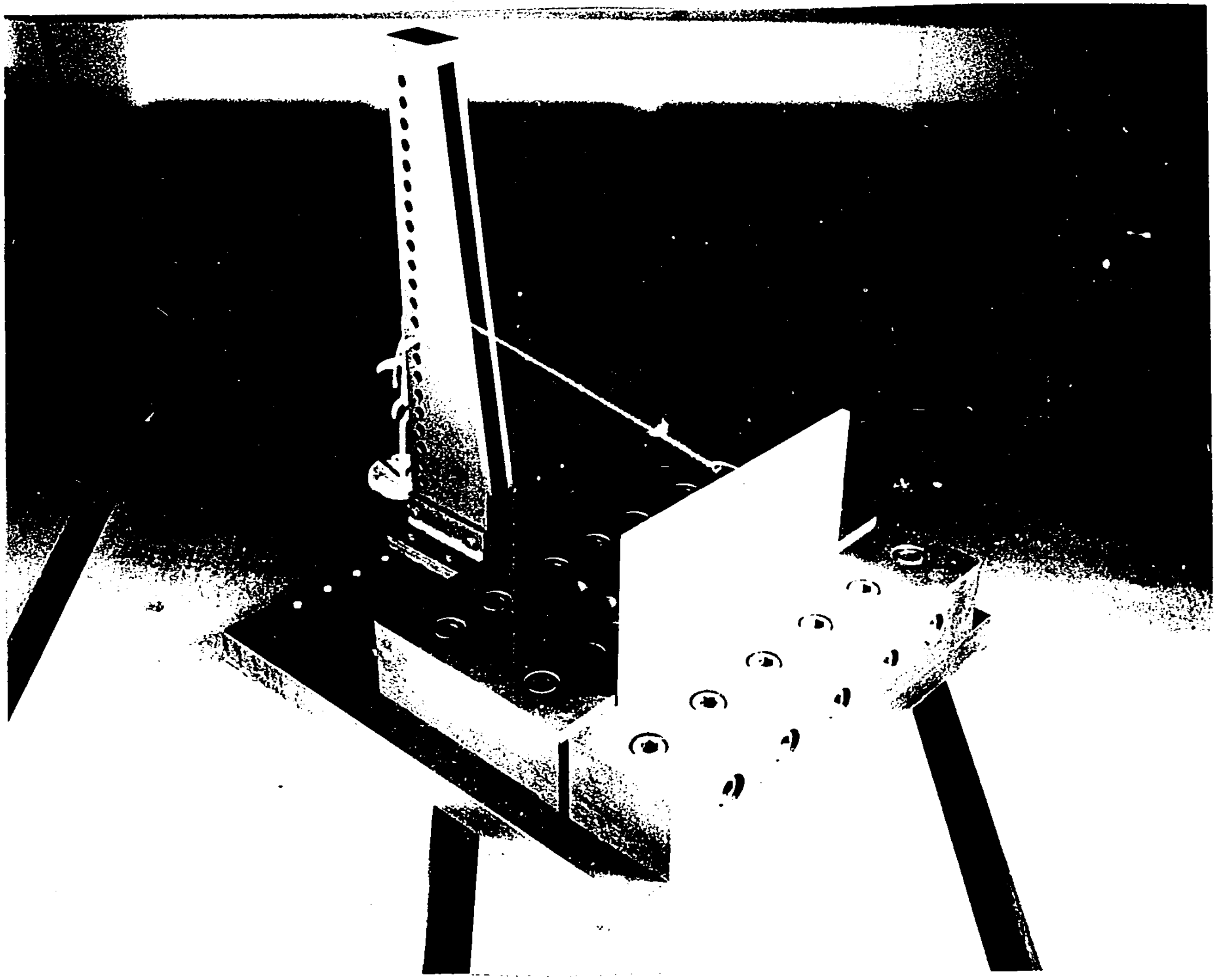

Fig. 14 Cantilever Plate Fixture

Fig. 15 Disc Fixture

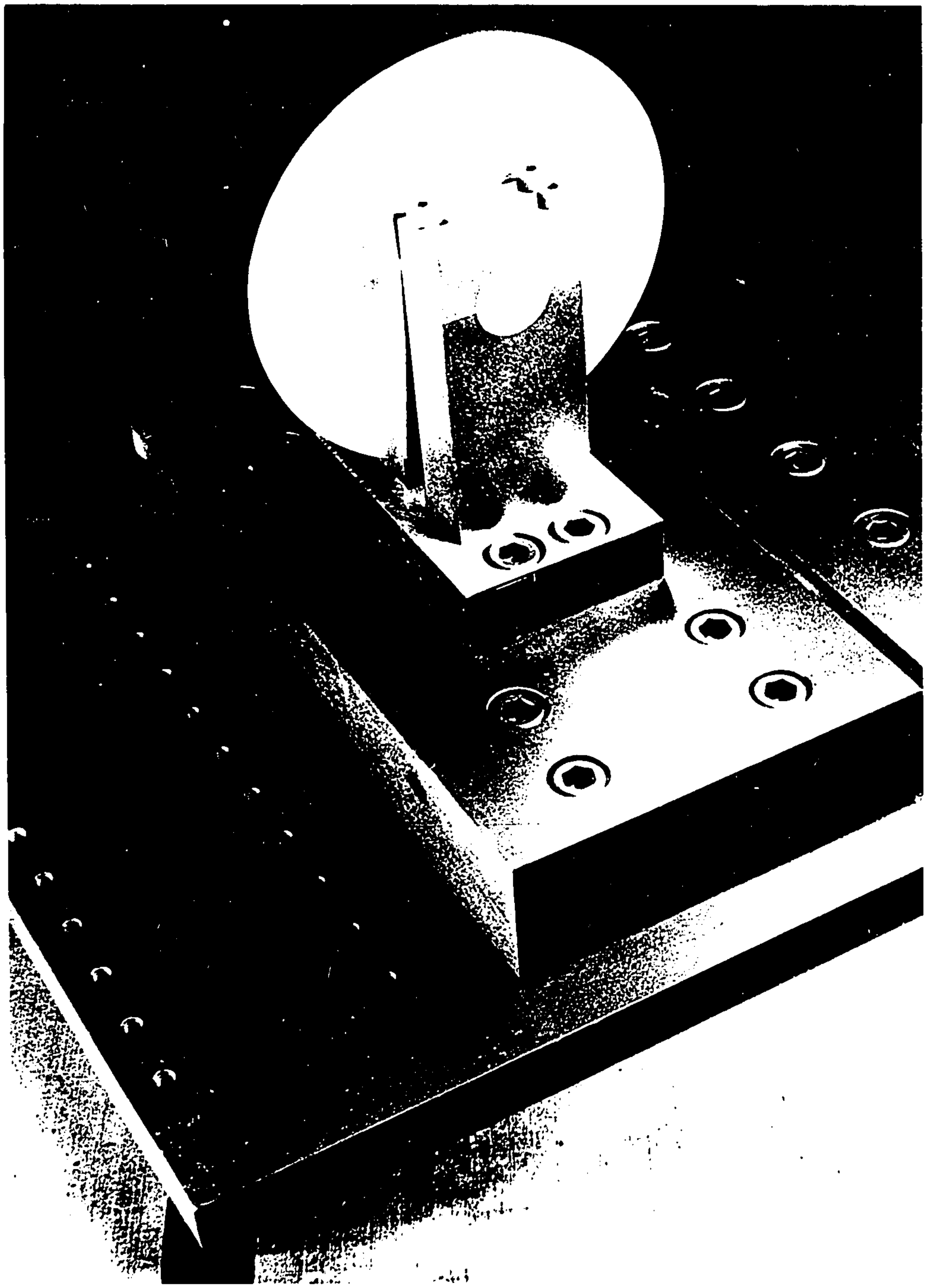

Fig. 15 Disc Fixture

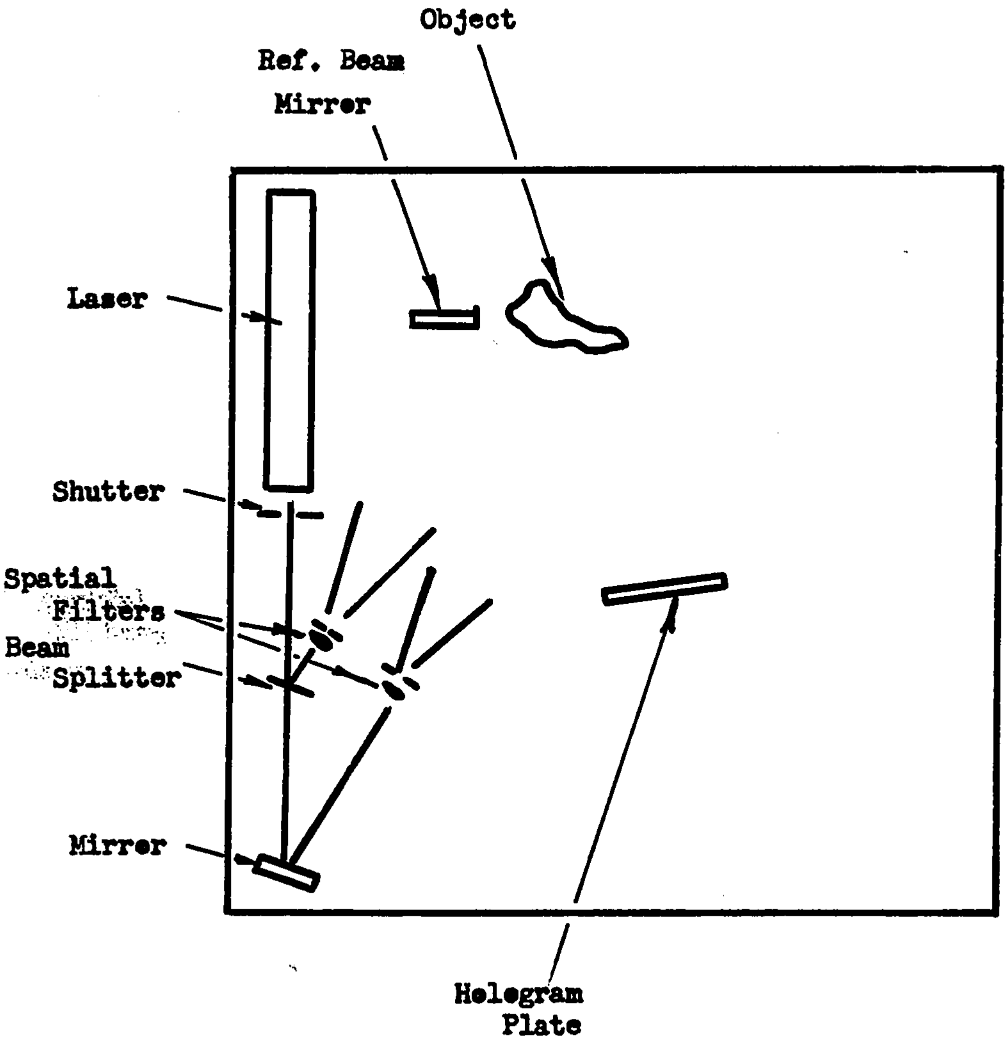

Fig. 16. Discrete beam Component Layout

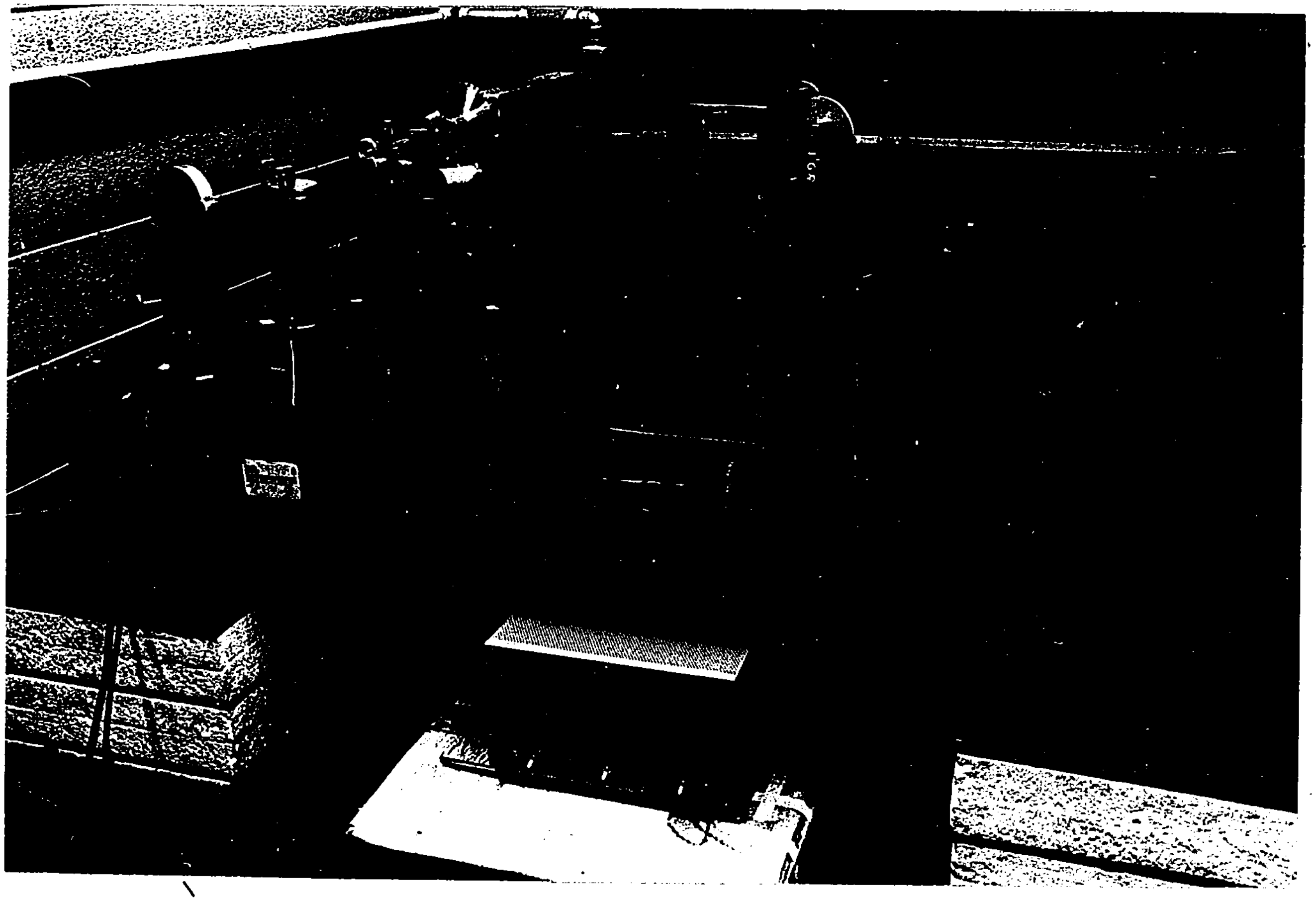

Fig. 17. Overall Holographic System

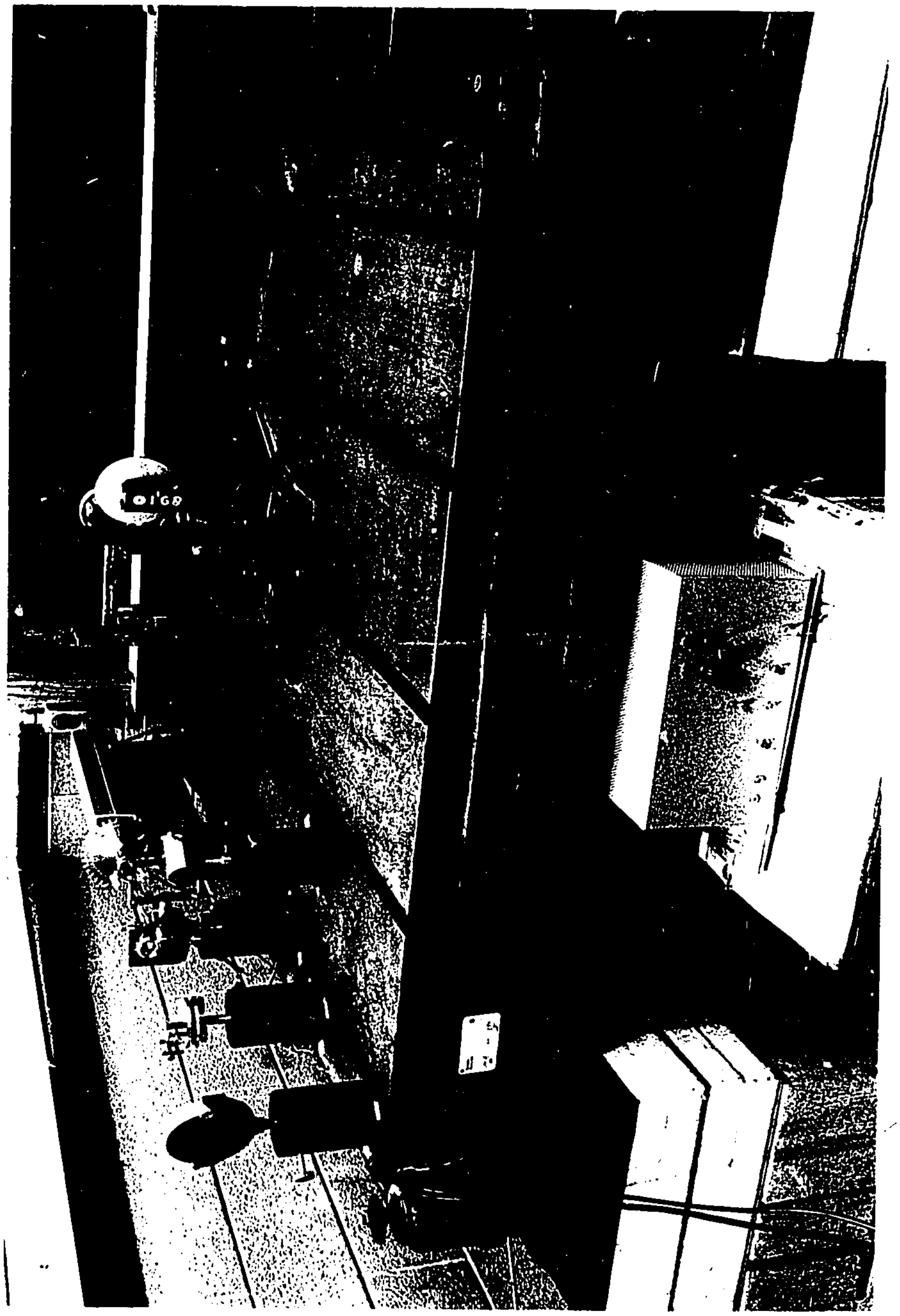

Fig. 17. Overall Holographic System

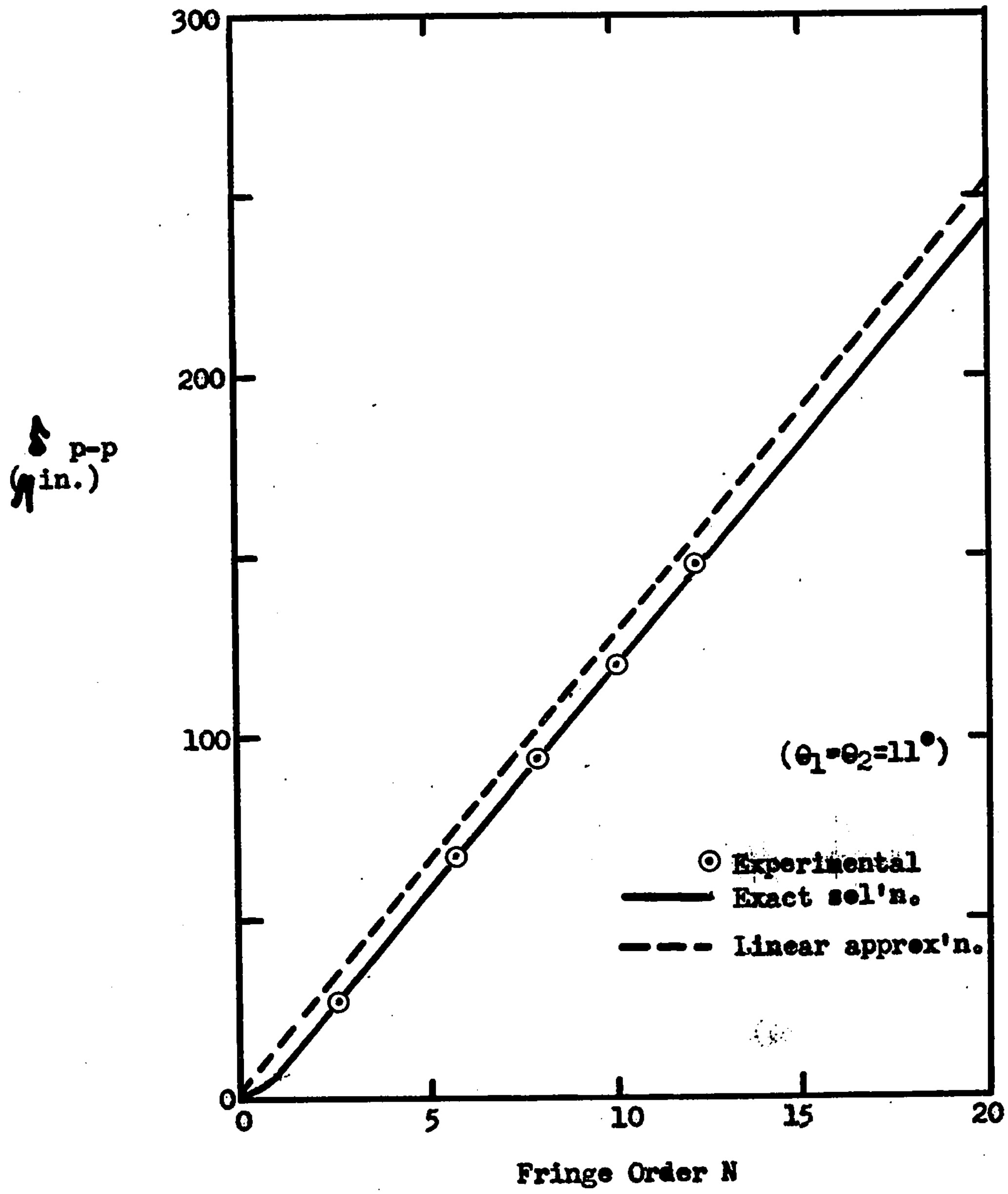

Fig. 18. Time Average Fringe Positions

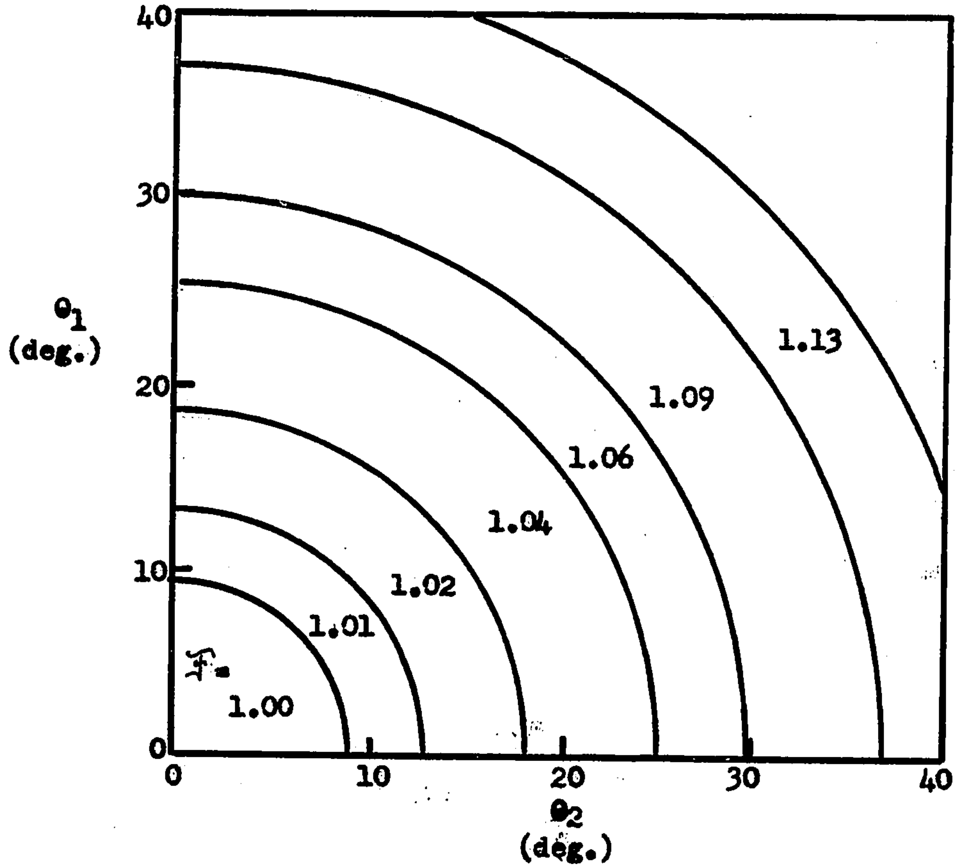

$$\frac{M}{N}=\frac{\lambda}{\cos\,\theta_1+\cos\,\theta_2}=\frac{\mathfrak{F}\,\lambda}{2}$$

Fig. 19. Sensitivity Factor

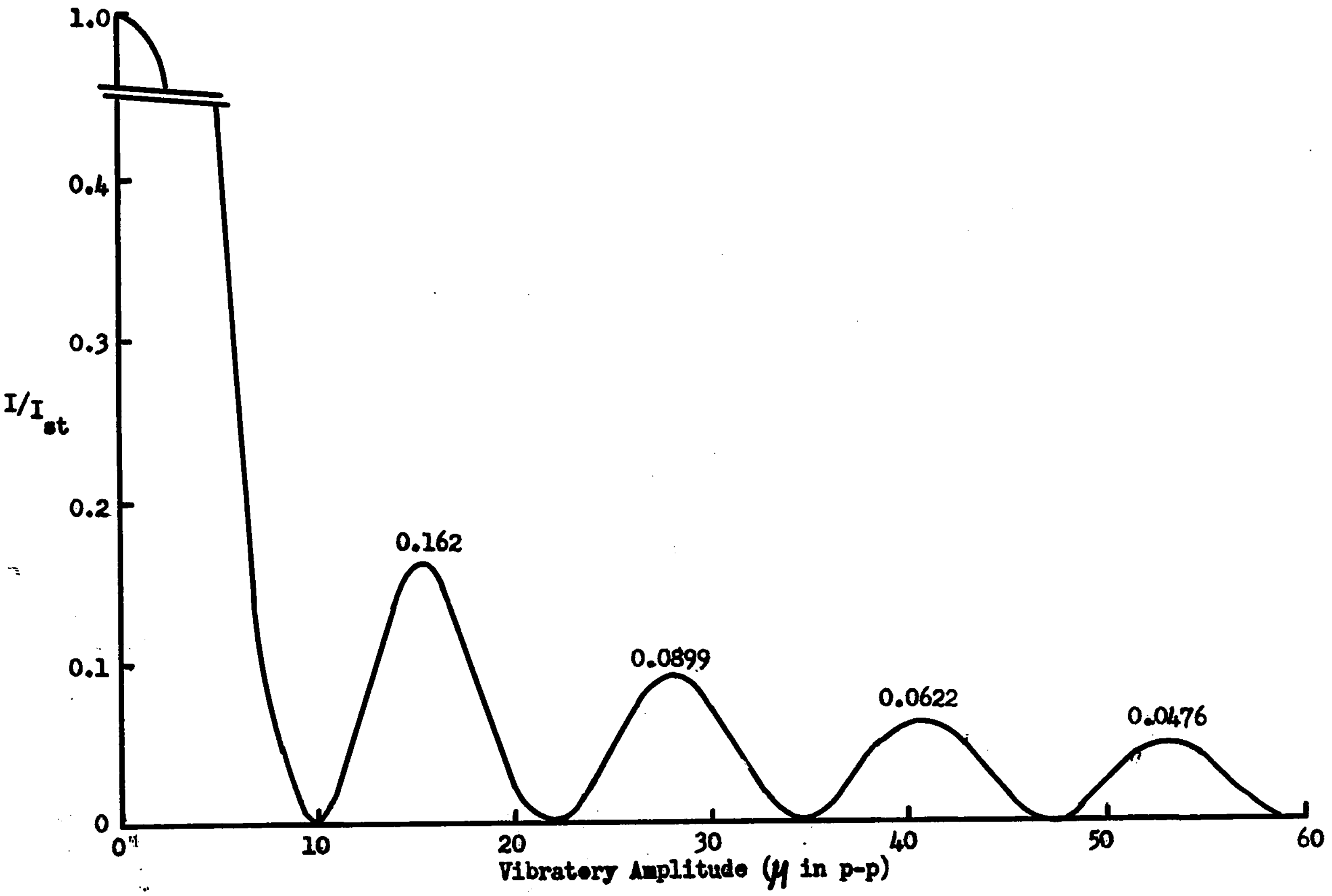

Fig. 20. Time Average Fringe Centrast

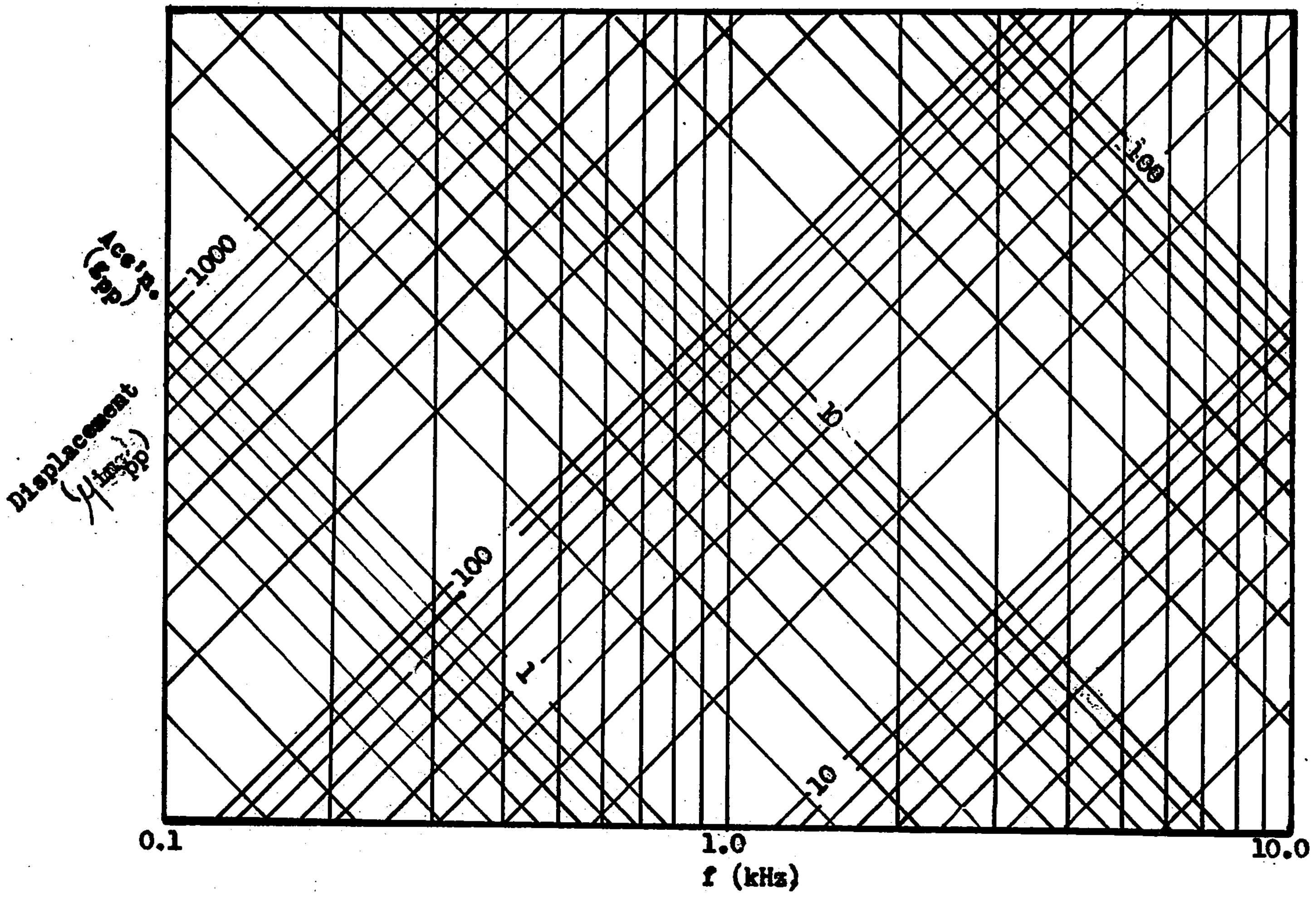

Fig. 21. Simple Harmonic Motion Conversions

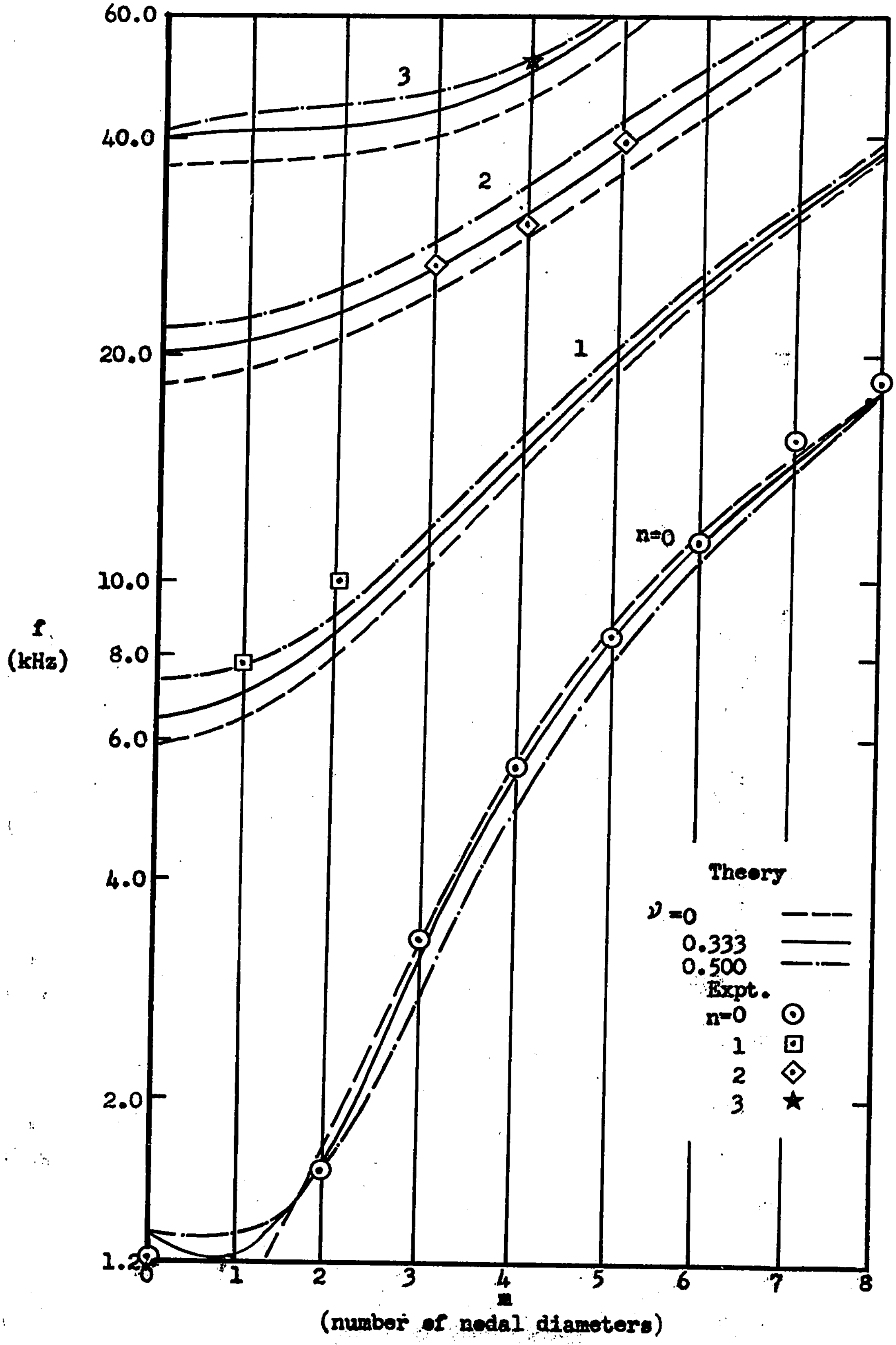

Fig. 22. Uniform Thickness Disc Natural Frequencies

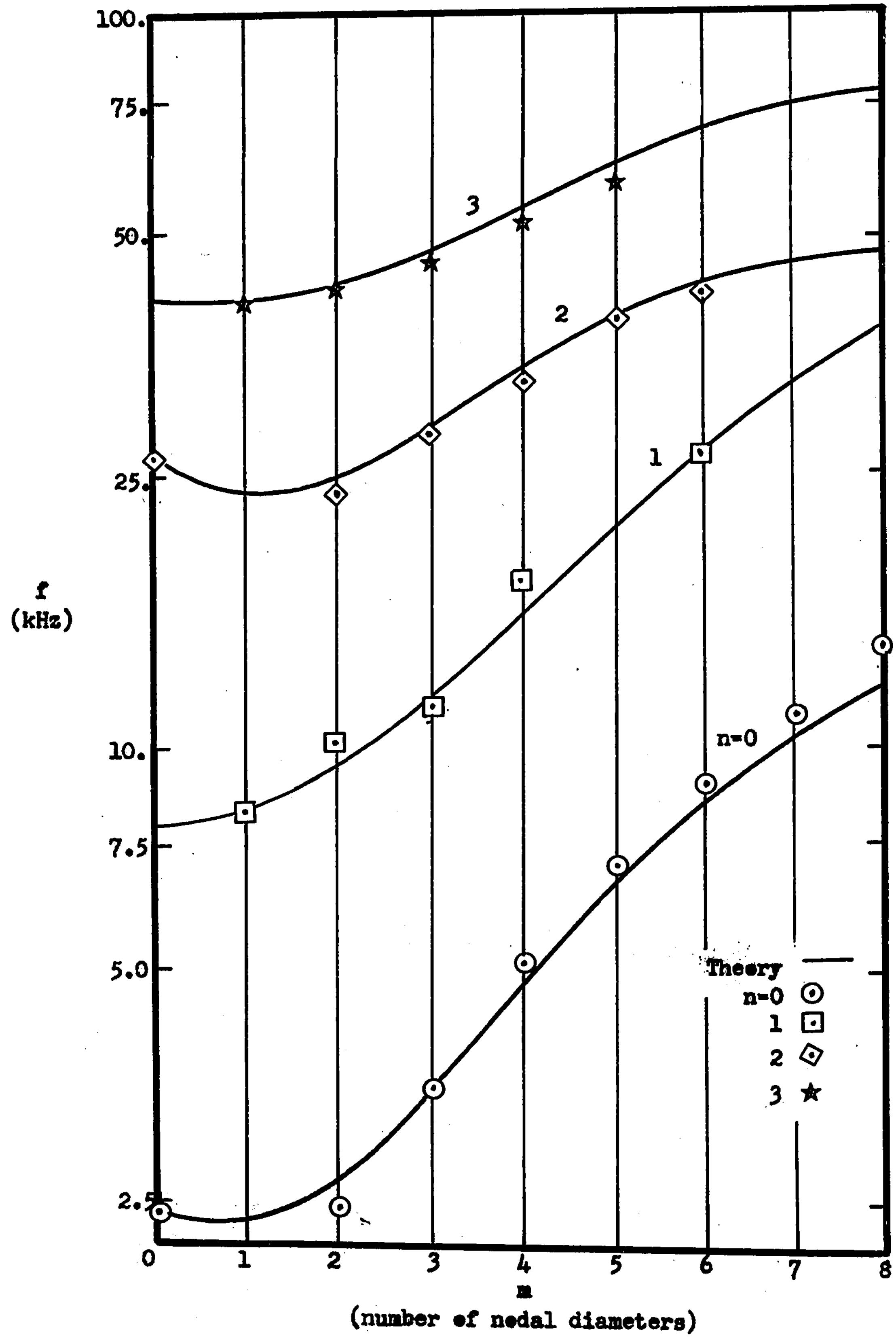

Fig. 23. Linear Taper Disc Natural Frequencies

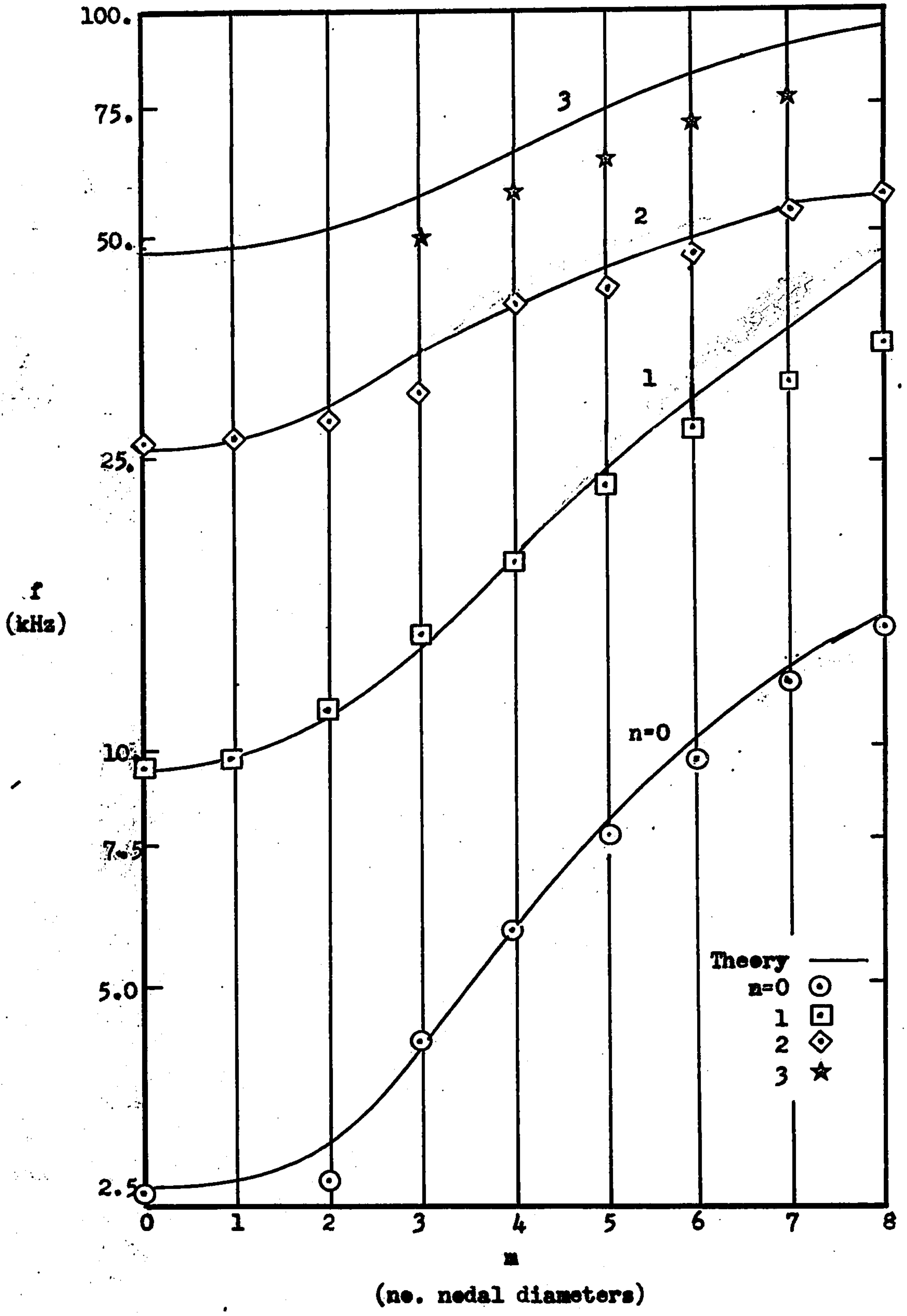

Fig. 24. Constant Stress Disc Natural Frequencies

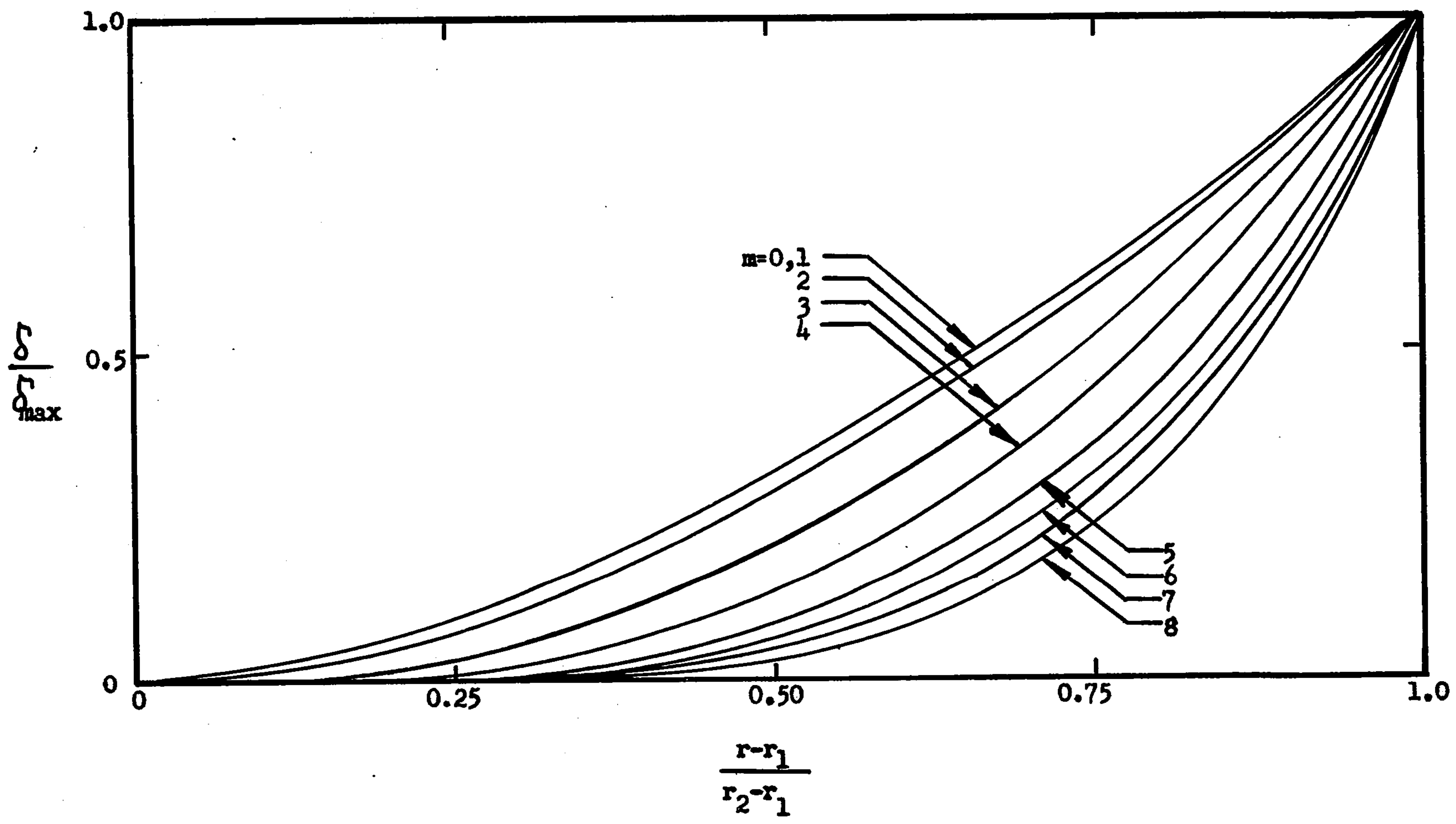

Fig. 25. Constant Stress Disc Radial Profile of Deflection (n=0)

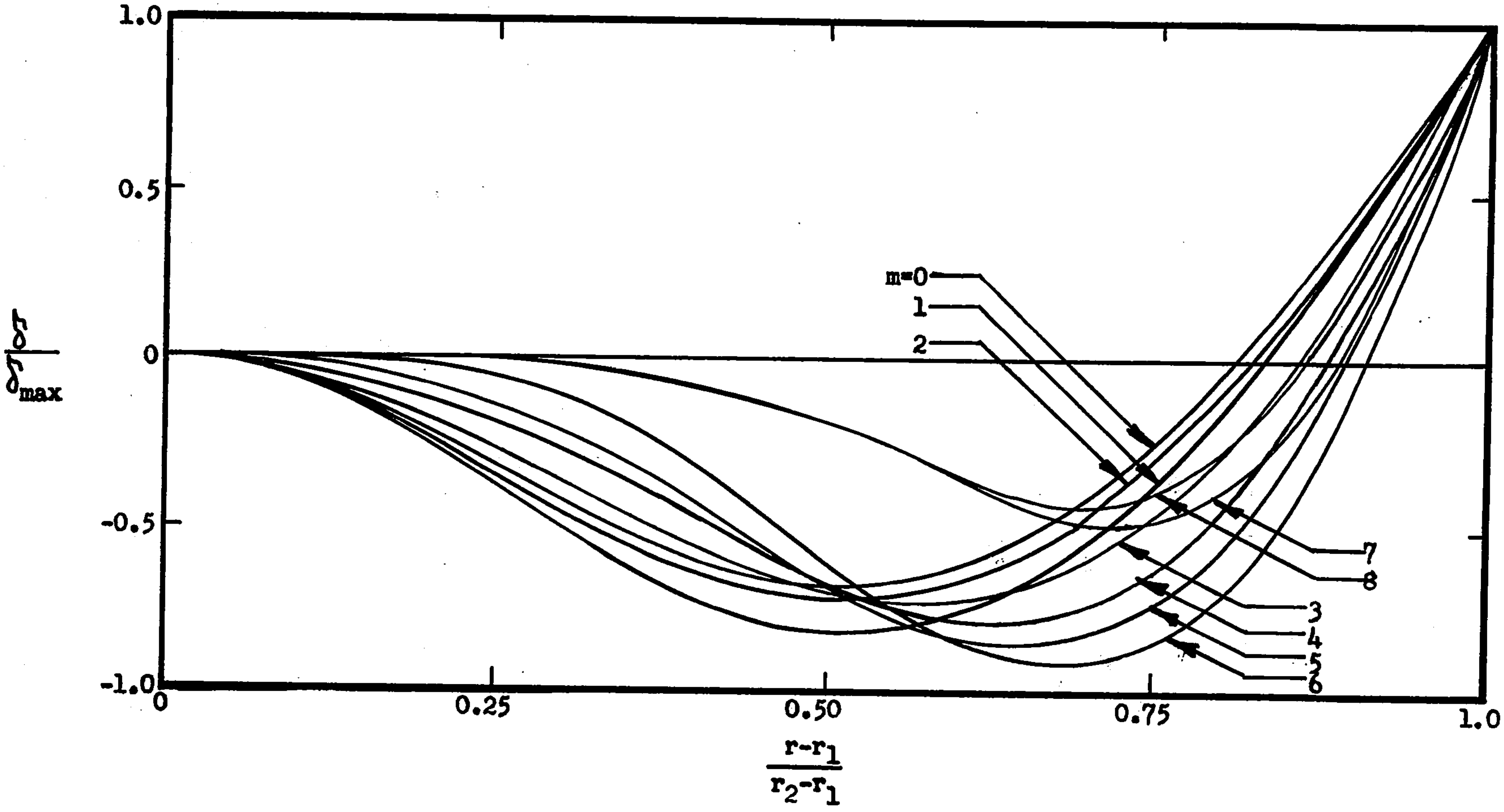

Fig. 26. Constant Stress Disc Radial Profile of Deflection (n=1)

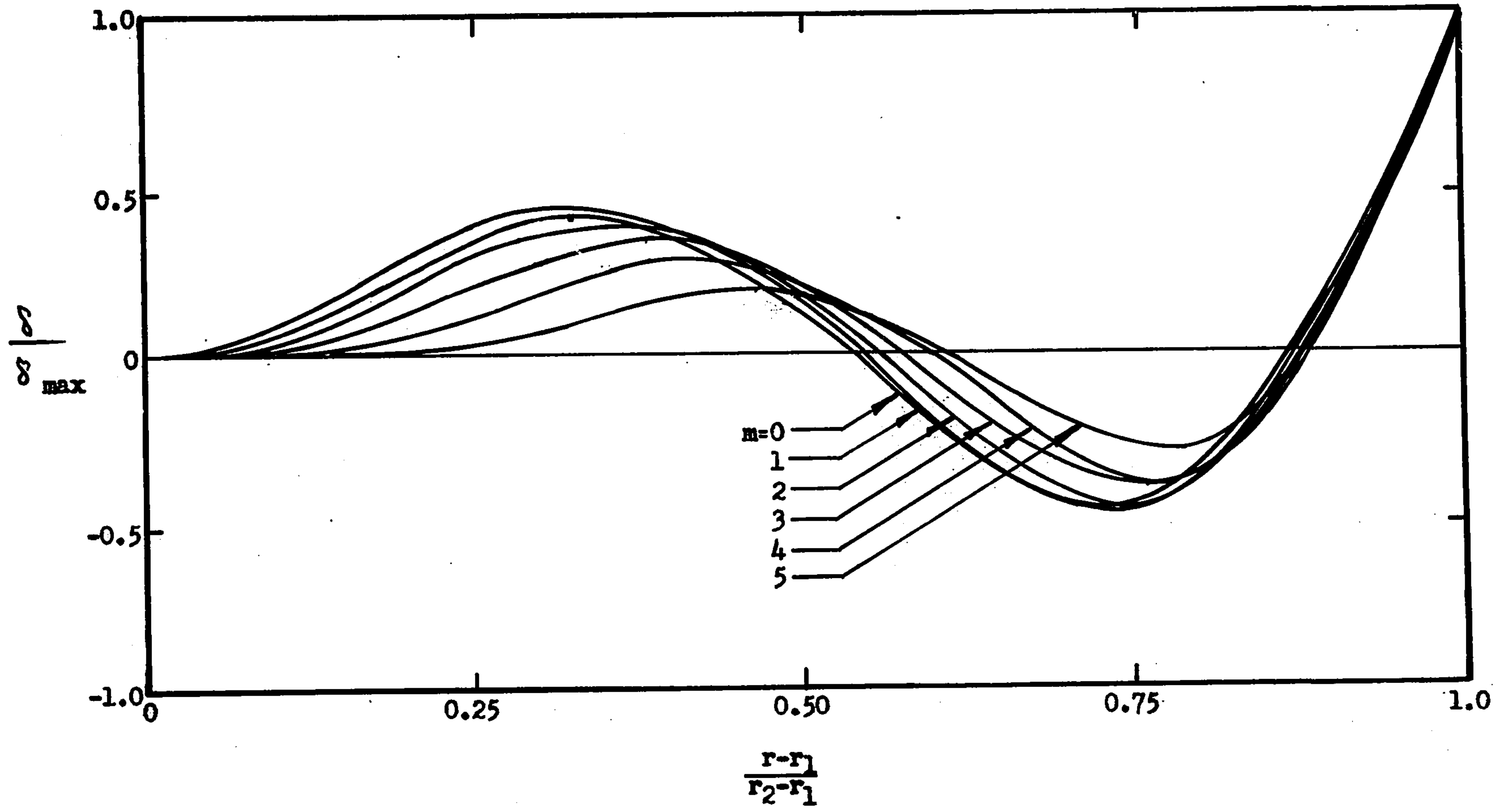

Fig. 27. Constant Stress Disc Radial Profile of Deflection (n=2)

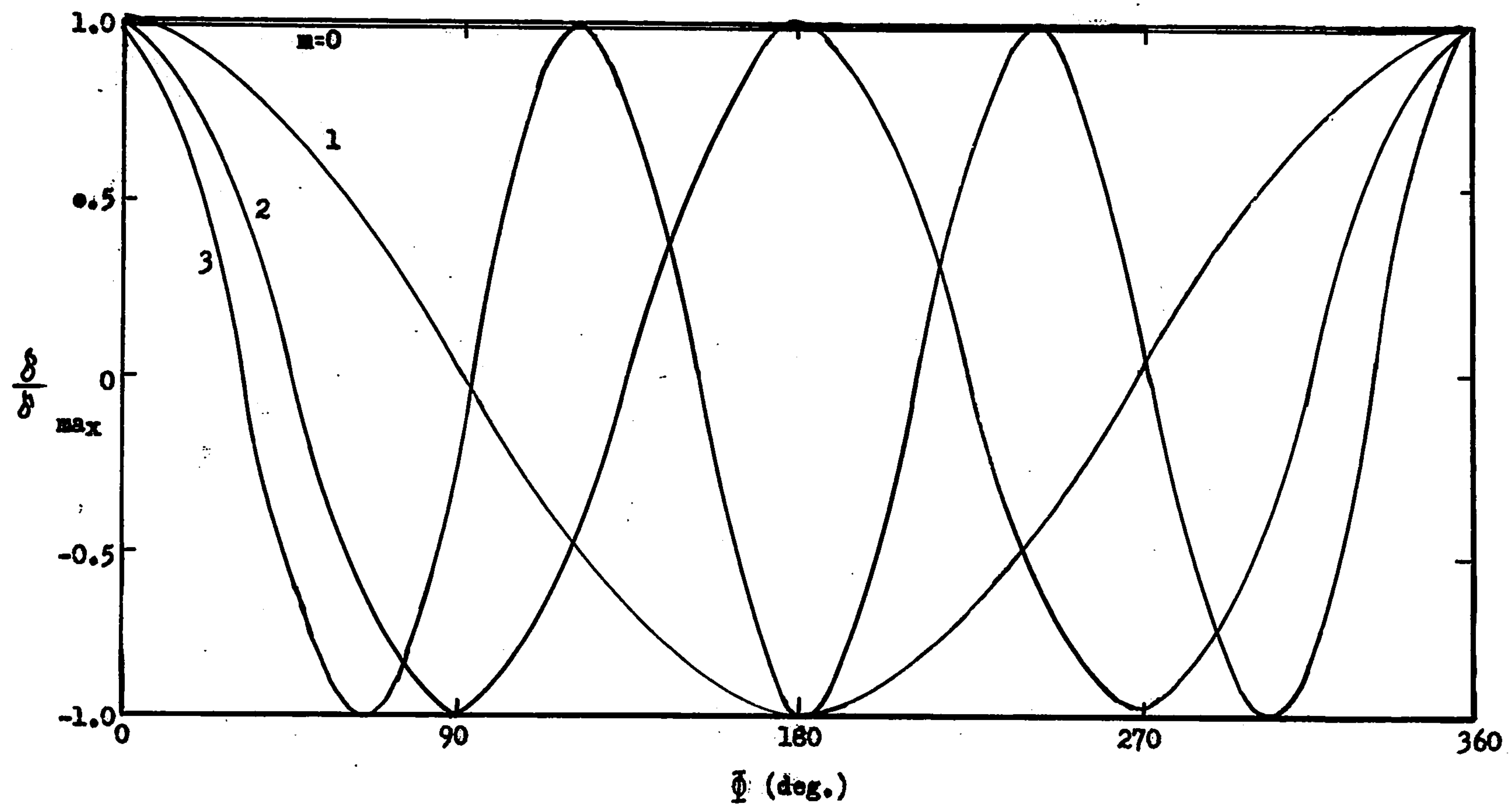

Fig. 28. Constant Stress Disc Tangential Profile of Deflection (n=0)

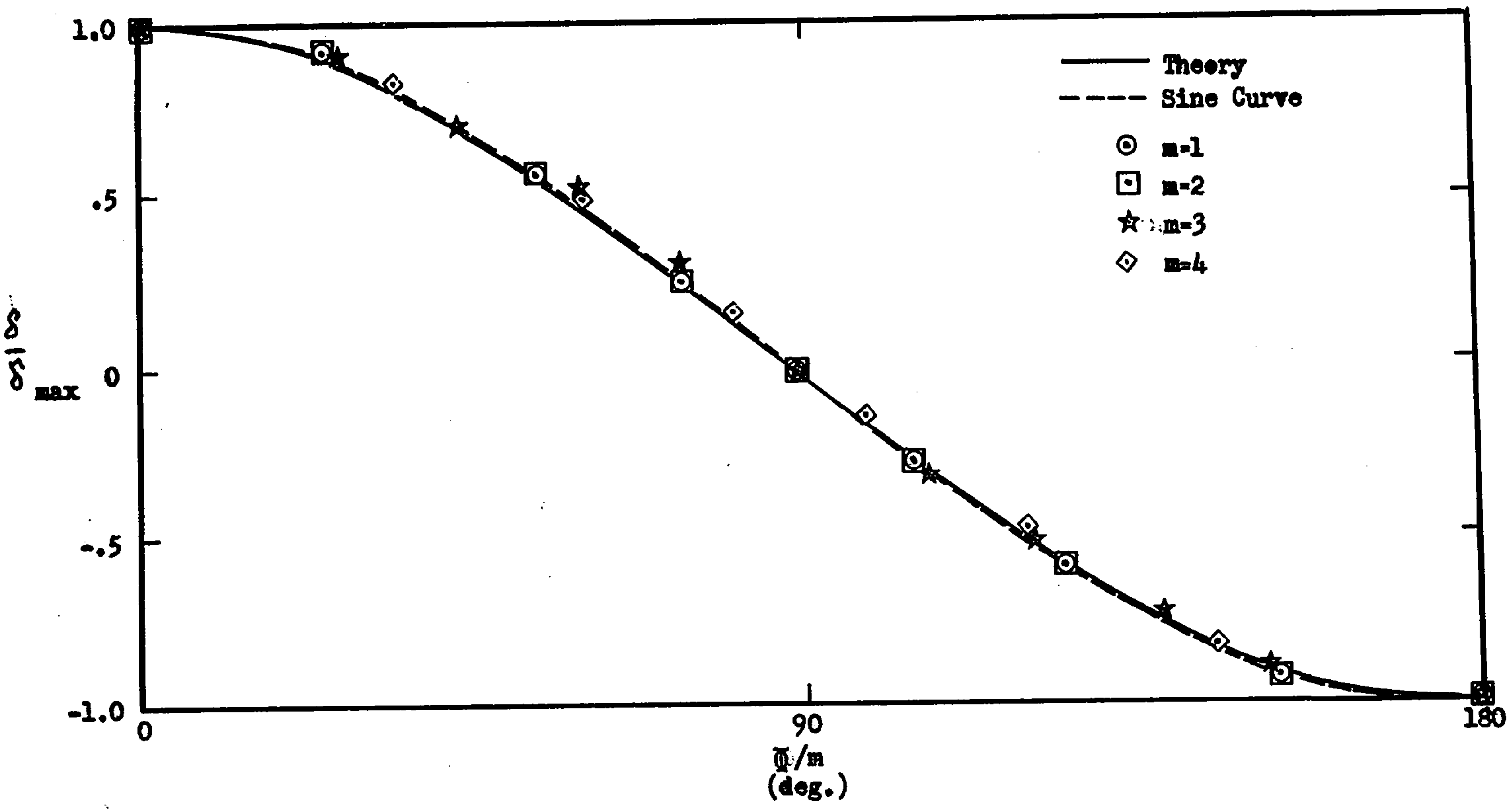

Fig. 29. Constant Stress Disc Normalized Deflection Profile (n=0)

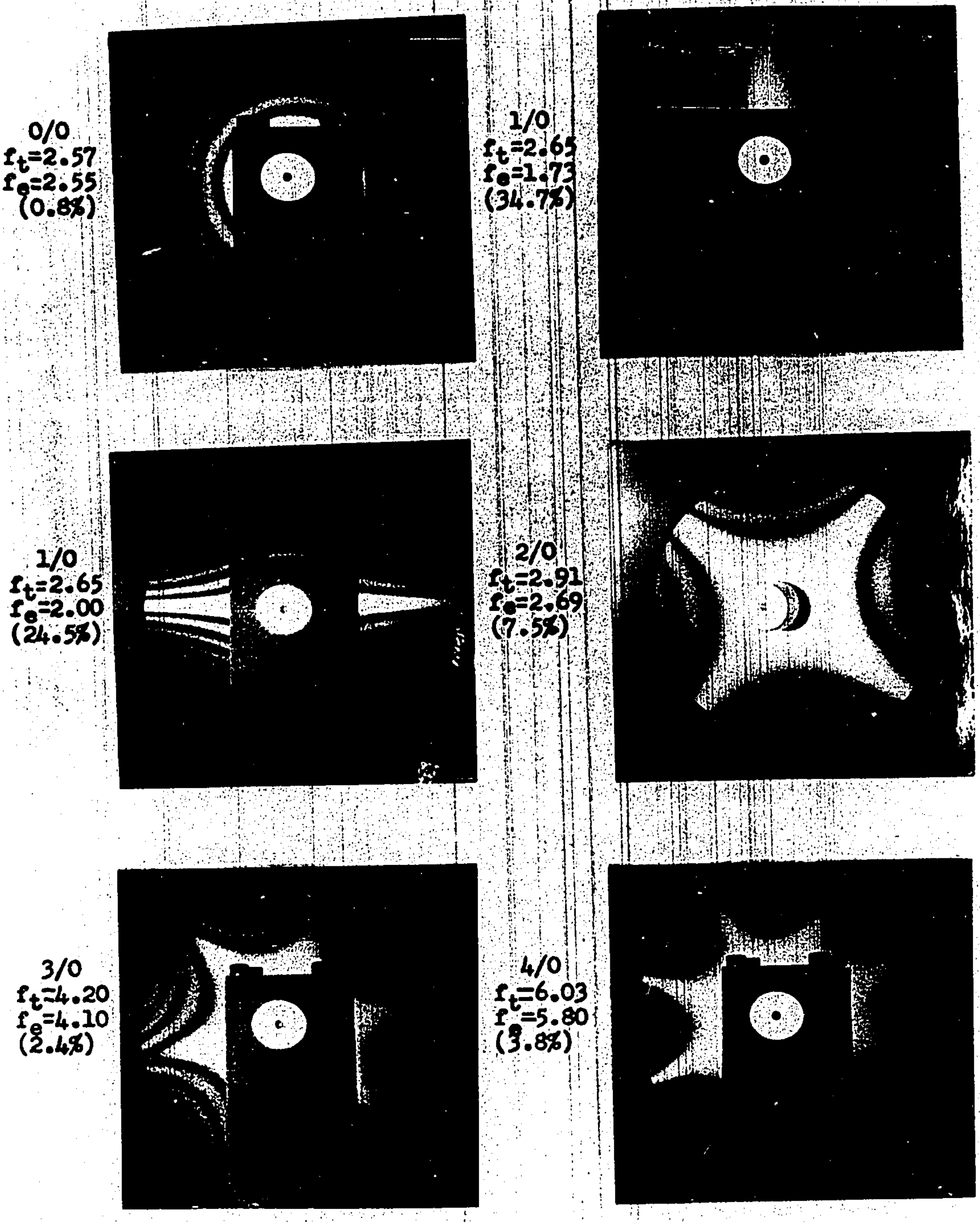

(all frequencies in kHz)

Fig. 30. Constant Stress Disc Interferograms (n=0)

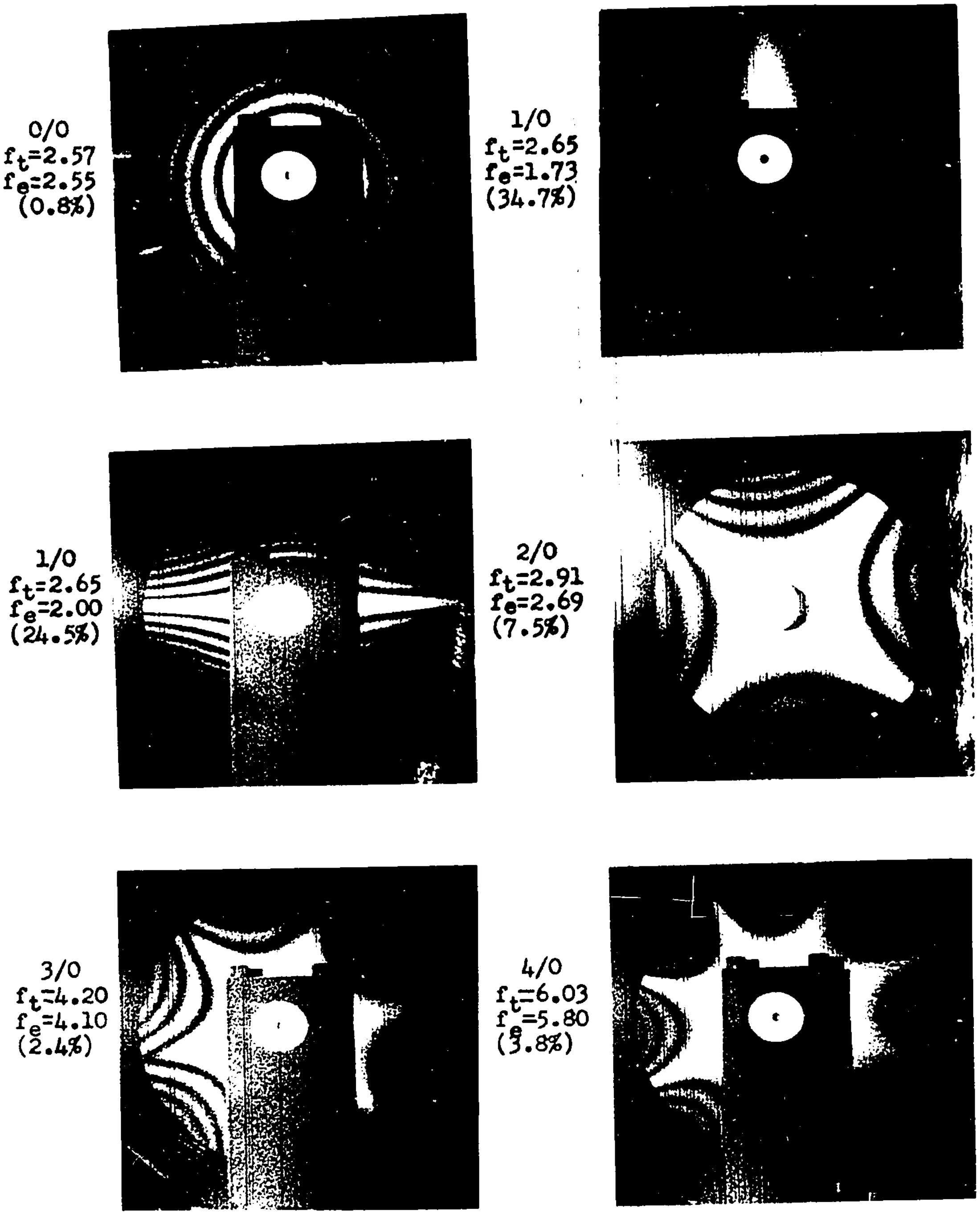

0/0
f_t=2.57
f_e=2.55
(0.8%)

1/0
f_t=2.65
f_e=1.73
(34.7%)

1/0
f_t=2.65
f_e=2.00
(24.5%)

2/0
f_t=2.91
f_e=2.69
(7.5%)

3/0
f_t=4.20
f_e=4.10
(2.4%)

4/0
f_t=6.03
f_e=5.80
(3.8%)

(all frequencies in kHz)

Fig. 30. Constant Stress Disc Interferograms (n=0)

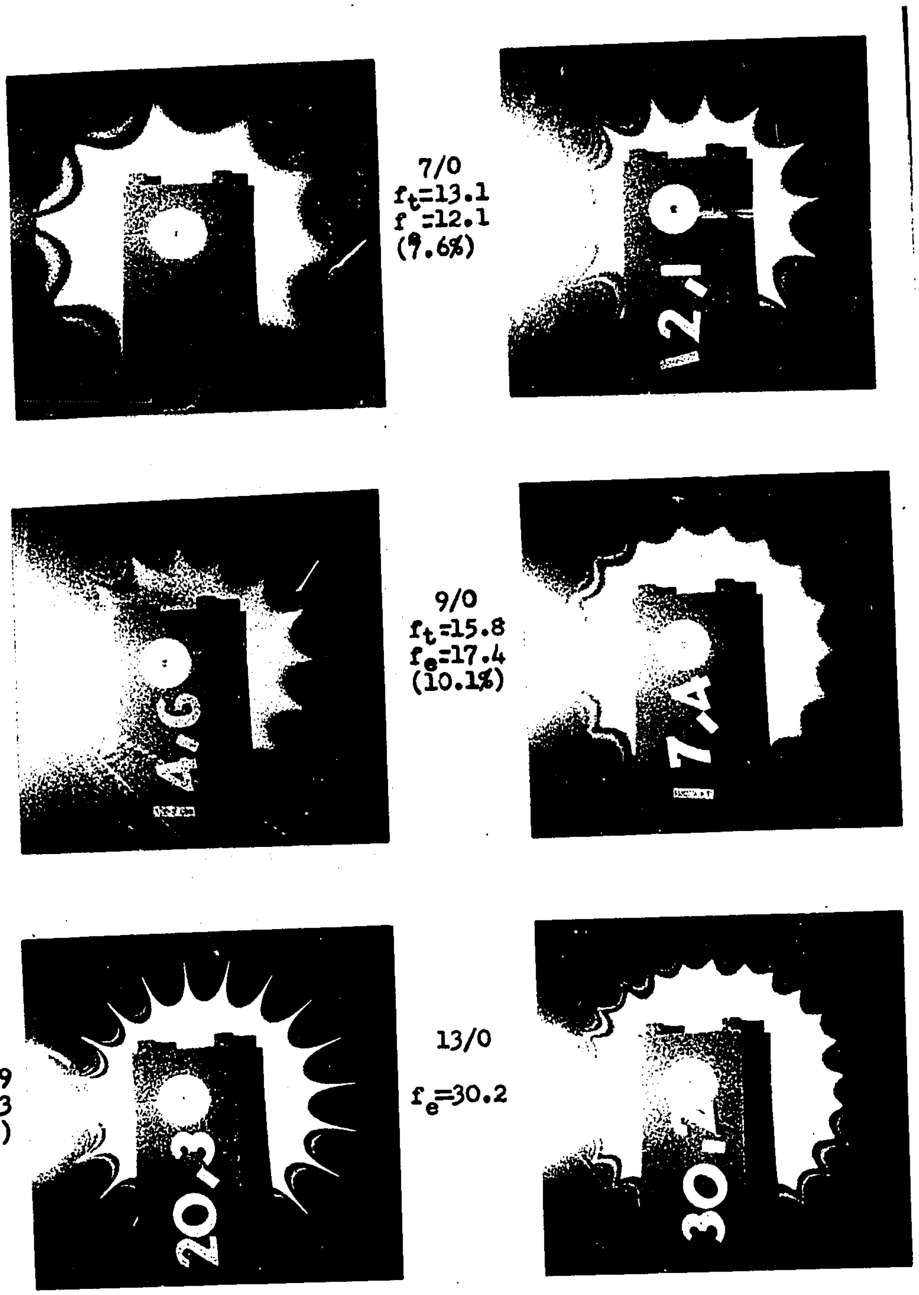

5/0
f_t=8.15
f_e=7.68
(5.8%)

7/0
f_t=13.1
f_e=12.1
(7.6%)

8/0
f_t=15.5
f_e=14.6
(5.8%)

9/0
f_t=15.8
f_e=17.4
(10.1%)

10/0
f_t=22.9
f_e=20.3
(11.3%)

13/0

f_e=30.2

(all frequencies in kHz)

Fig. 31. Constant Stress Disc Interferograms (n=0)

5/0
f_t=8.15
f_e=7.68
(5.8%)

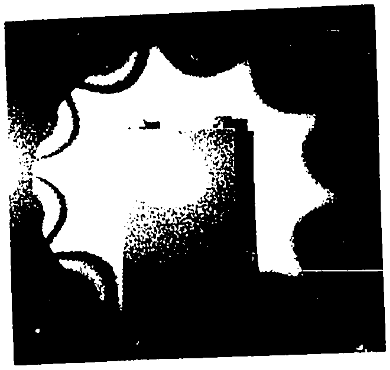

7/0
f_t=13.1
f_e=12.1
(7.6%)

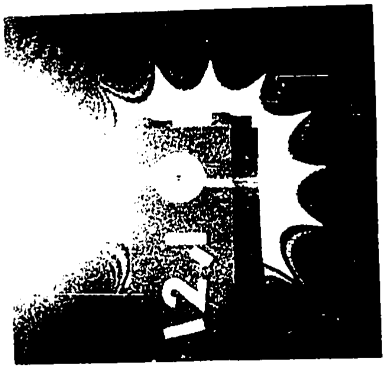

8/0
f_t=15.5
f_e=14.6
(5.8%)

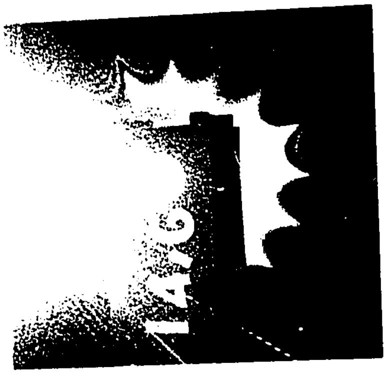

9/0
f_t=15.8
f_e=17.4
(10.1%)

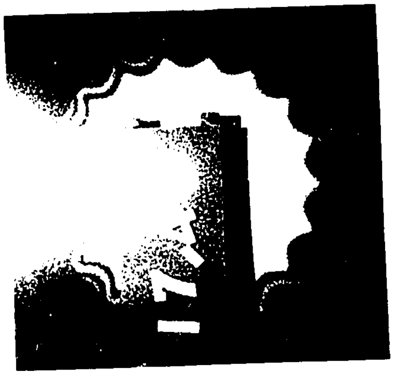

10/0
f_t=22.9
f_e=20.3
(11.3%)

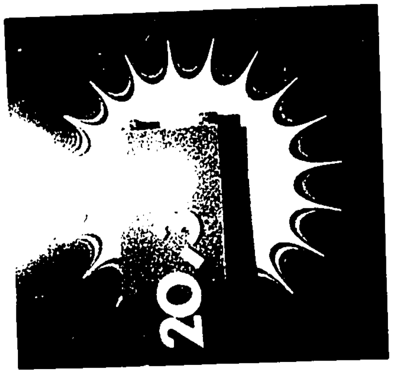

13/0

f_e=30.2

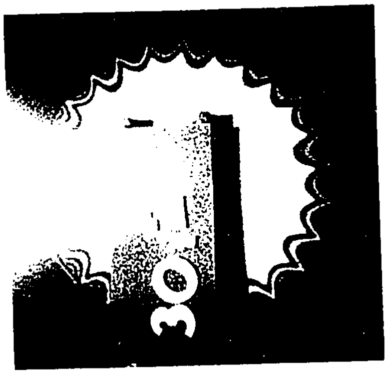

(all frequencies in kHz)

Fig. 31. Constant Stress Disc Interferograms (n=0)

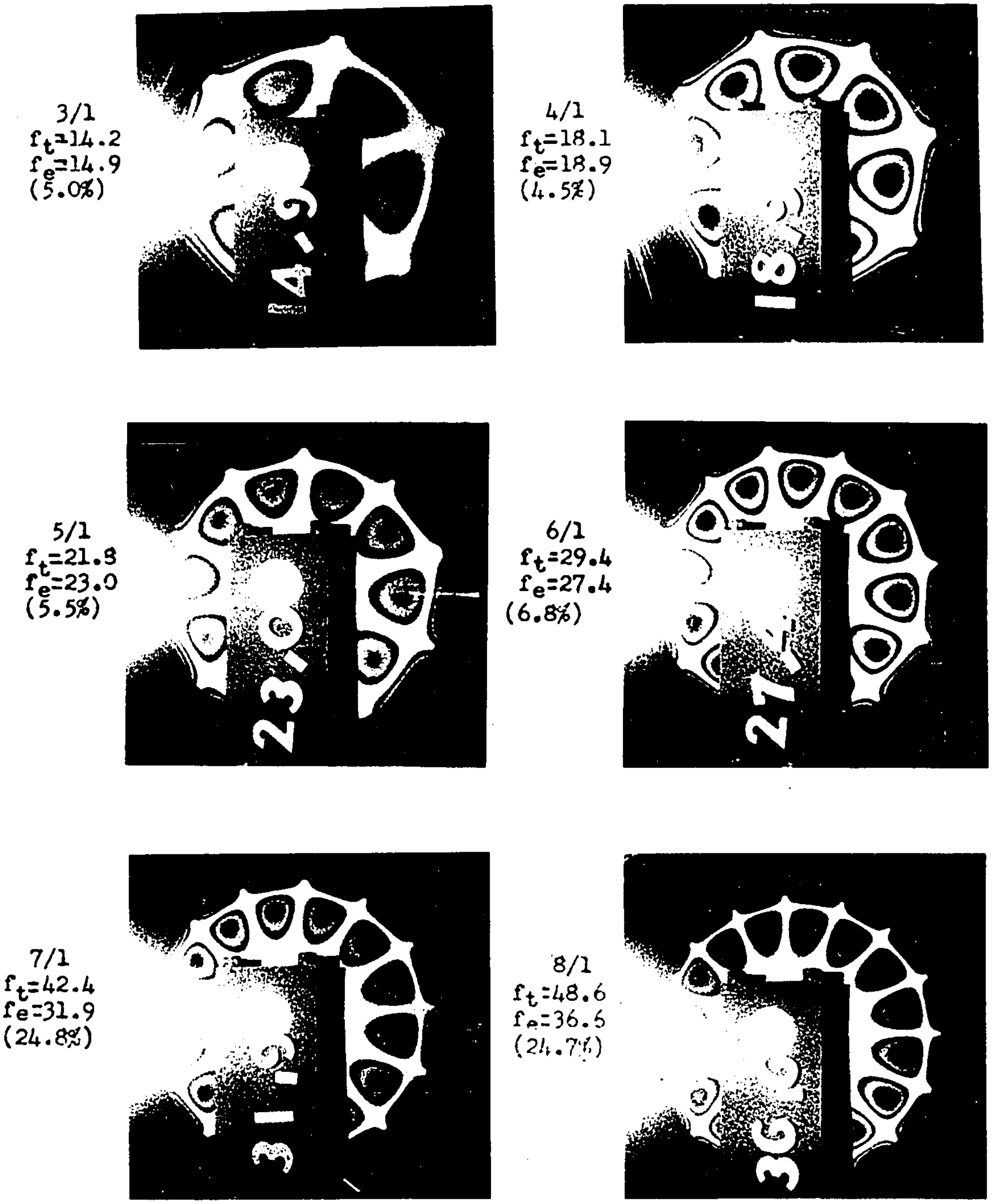

3/1
f_t=14.2
f_e=14.9
(5.0%)

4/1
f_t=18.1
f_e=18.9
(4.5%)

5/1
f_t=21.8
f_e=23.0
(5.5%)

6/1
f_t=29.4
f_e=27.4
(6.8%)

7/1
f_t=42.4
f_e=31.9
(24.8%)

8/1
f_t=48.6
f_e=36.6
(24.7%)

(all frequencies in kHz)

Fig. 32. Constant Stress Disc Interferograms (n=1)

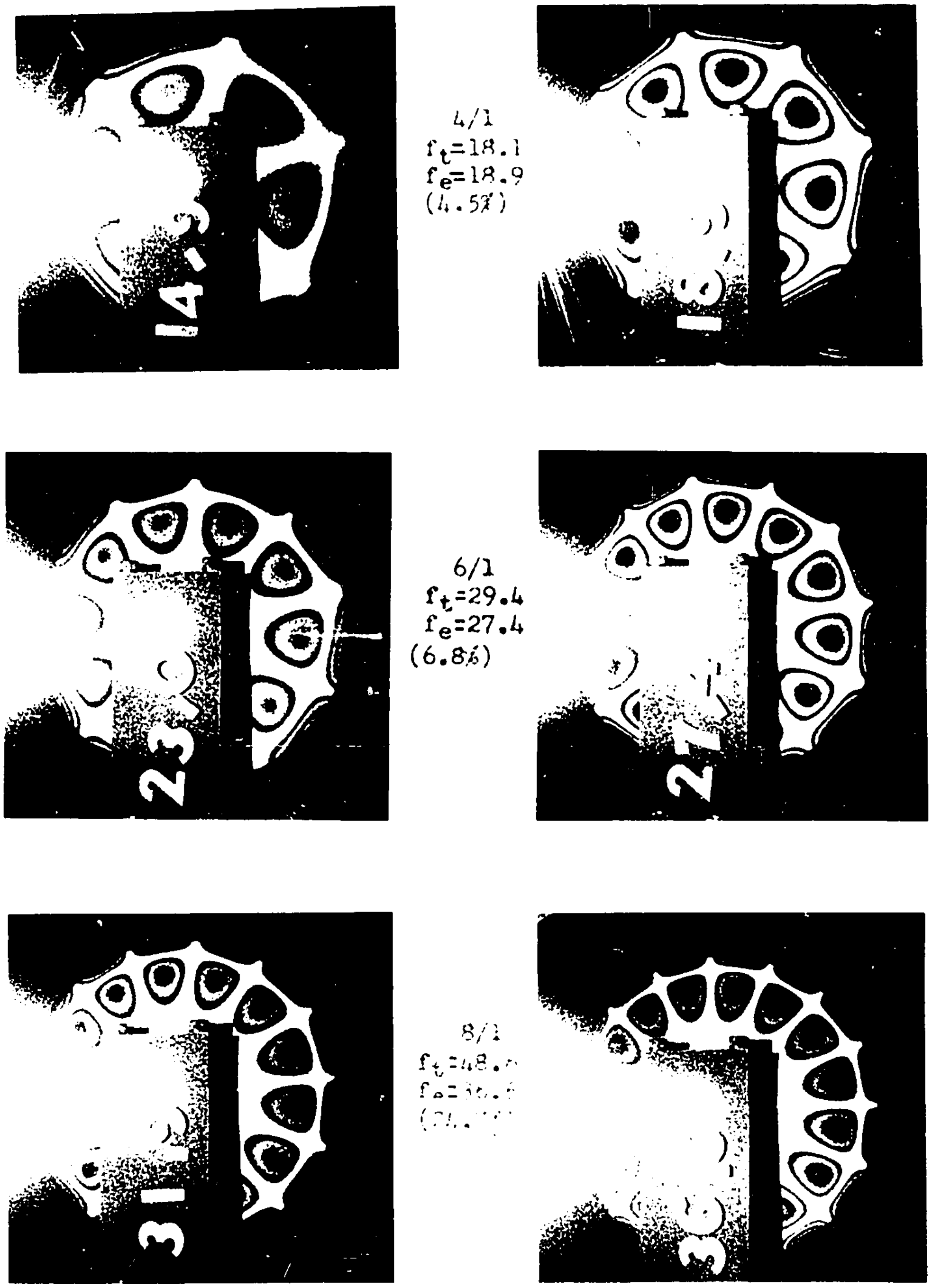

3/1
f_t=14.2
f_e=14.9
(5.0%)

4/1
f_t=18.1
f_e=18.9
(4.5%)

5/1
f_t=21.8
f_e=23.0
(5.5%)

6/1
f_t=29.4
f_e=27.4
(6.8%)

7/1
f_t=42.4
f_e=31.9
(24.8%)

8/1
f_t=48.[illegible]
f_e=36.[illegible]
(24.[illegible])

(all frequencies in kHz)

Fig. 32. Constant Stress Disc Interferograms (n=1)

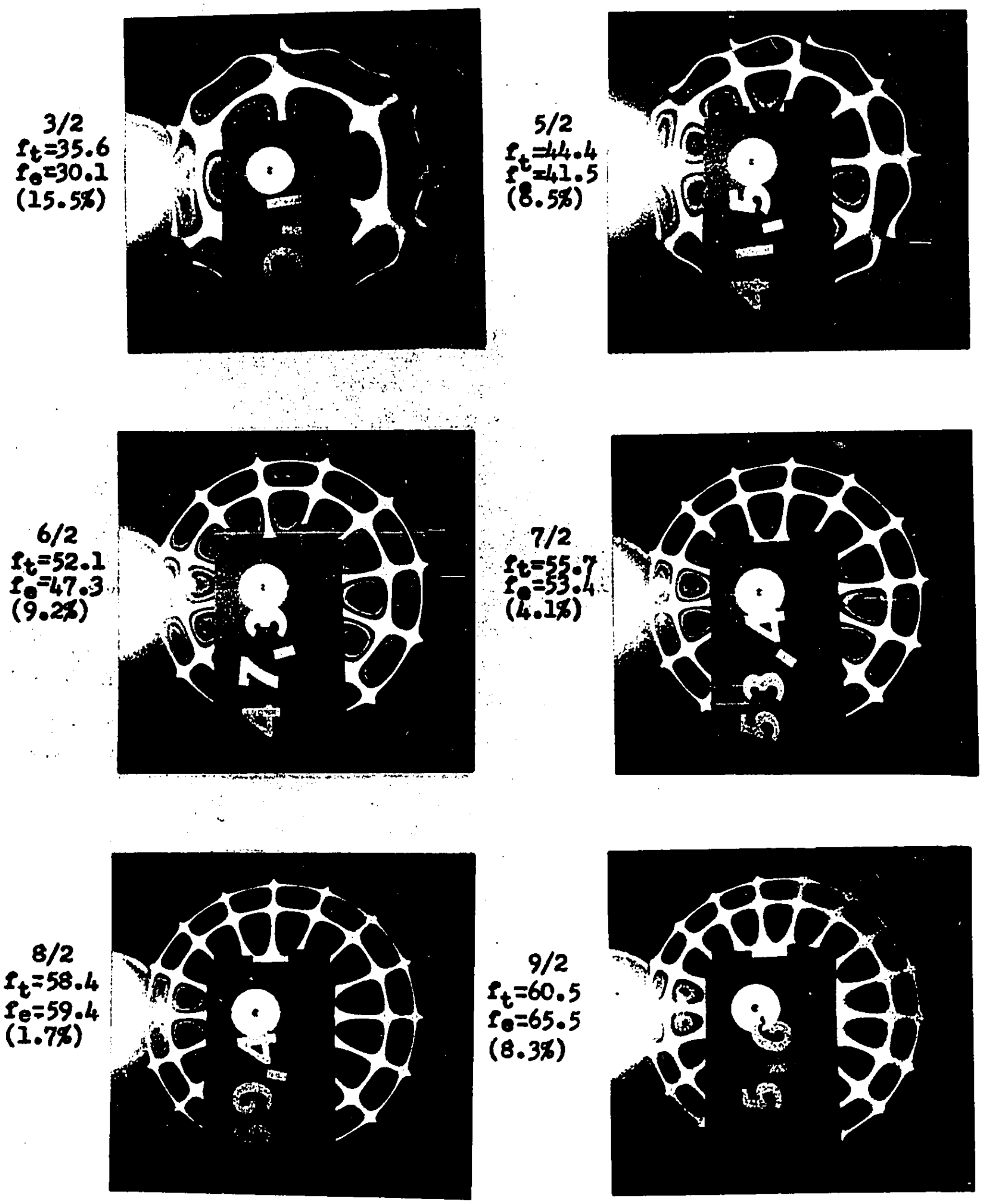

3/2
f_t=35.6
f_e=30.1
(15.5%)

5/2
f_t=44.4
f_e=41.5
(6.5%)

6/2
f_t=52.1
f_e=47.3
(9.2%)

7/2
f_t=55.7
f_e=53.4
(4.1%)

8/2
f_t=58.4
f_e=59.4
(1.7%)

9/2
f_t=60.5
f_e=65.5
(8.3%)

(all frequencies in kHz)

Fig. 33. Constant Stress Disc Interferograms (n=2)

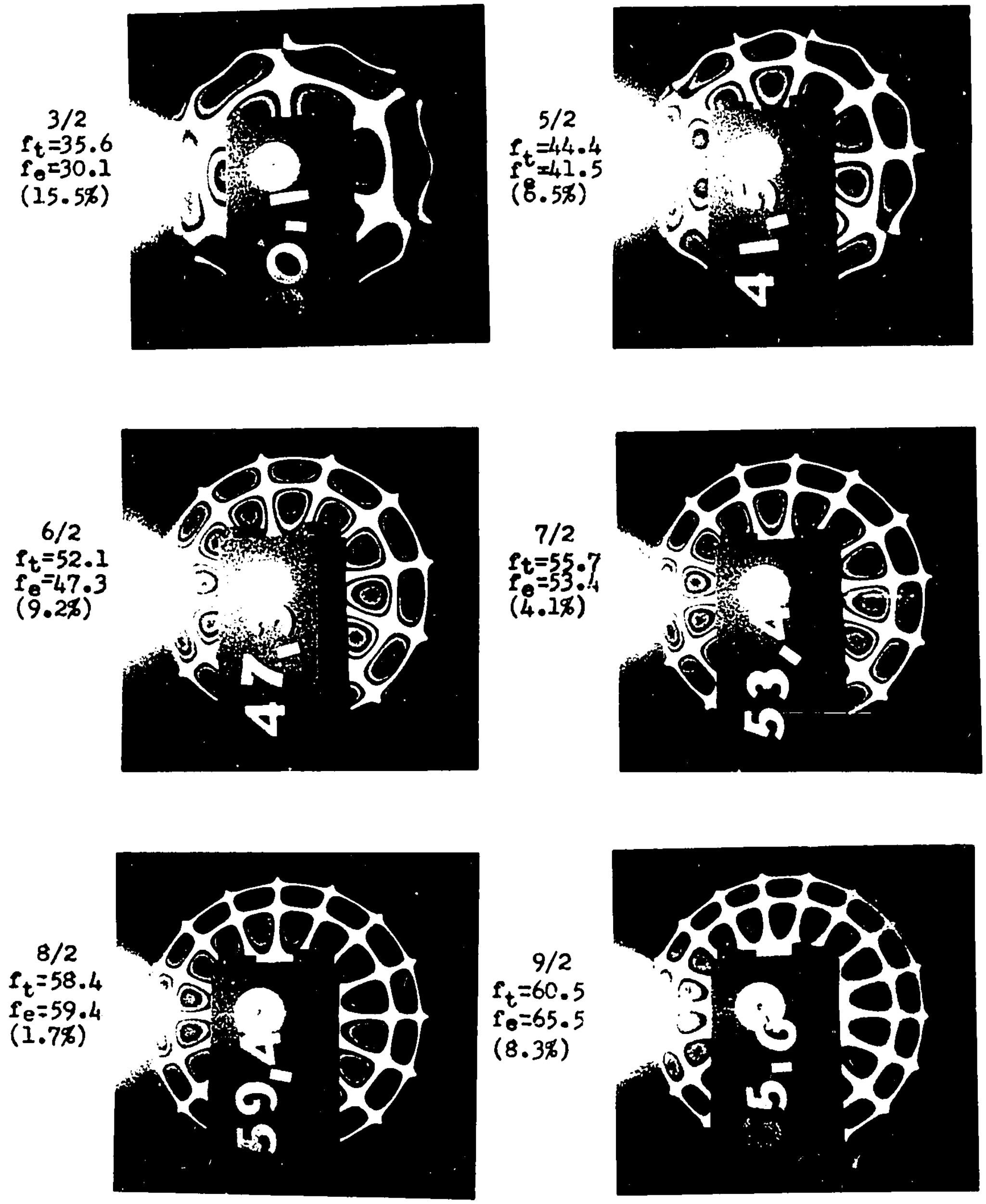

3/2
f_t=35.6
f_e=30.1
(15.5%)

5/2
f_t=44.4
f_e=41.5
(6.5%)

6/2
f_t=52.1
f_e=47.3
(9.2%)

7/2
f_t=55.7
f_e=53.4
(4.1%)

8/2
f_t=58.4
f_e=59.4
(1.7%)

9/2
f_t=60.5
f_e=65.5
(8.3%)

(all frequencies in kHz)

Fig. 33. Constant Stress Disc Interferograms (n=7)

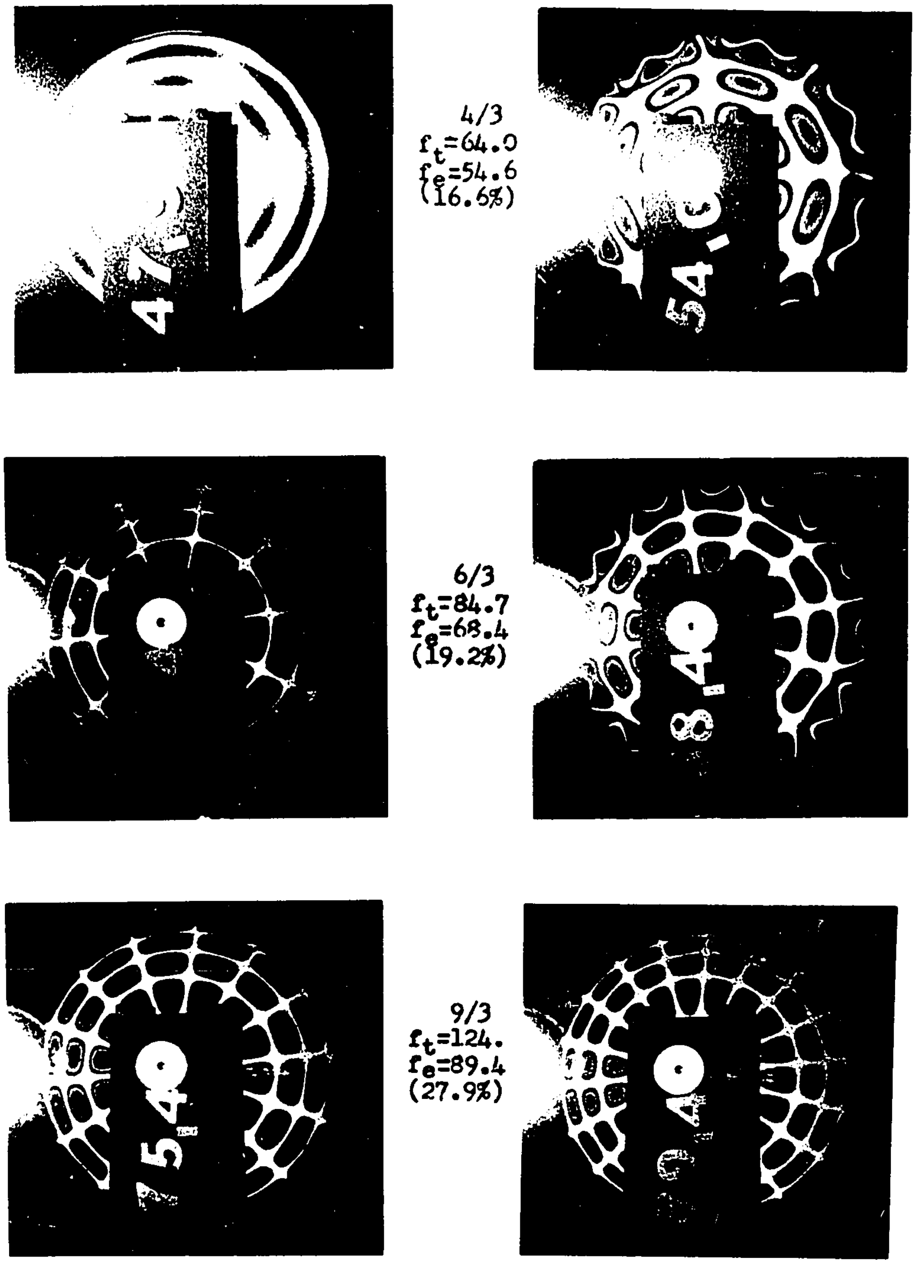

3/3
f_t=56.0
f_e=47.9
(14.4%)

4/3
f_t=64.0
f_e=54.6
(16.6%)

5/3
f_t=74.6
f_e=61.4
(15.0%)

6/3
f_t=84.7
f_e=68.4
(19.2%)

7/3
f_t=91.8
f_e=75.4
(17.9%)

9/3
f_t=124.
f_e=89.4
(27.9%)

(all frequencies in kHz)

Fig. 34. Constant Stress Disc Interferograms (n=3)

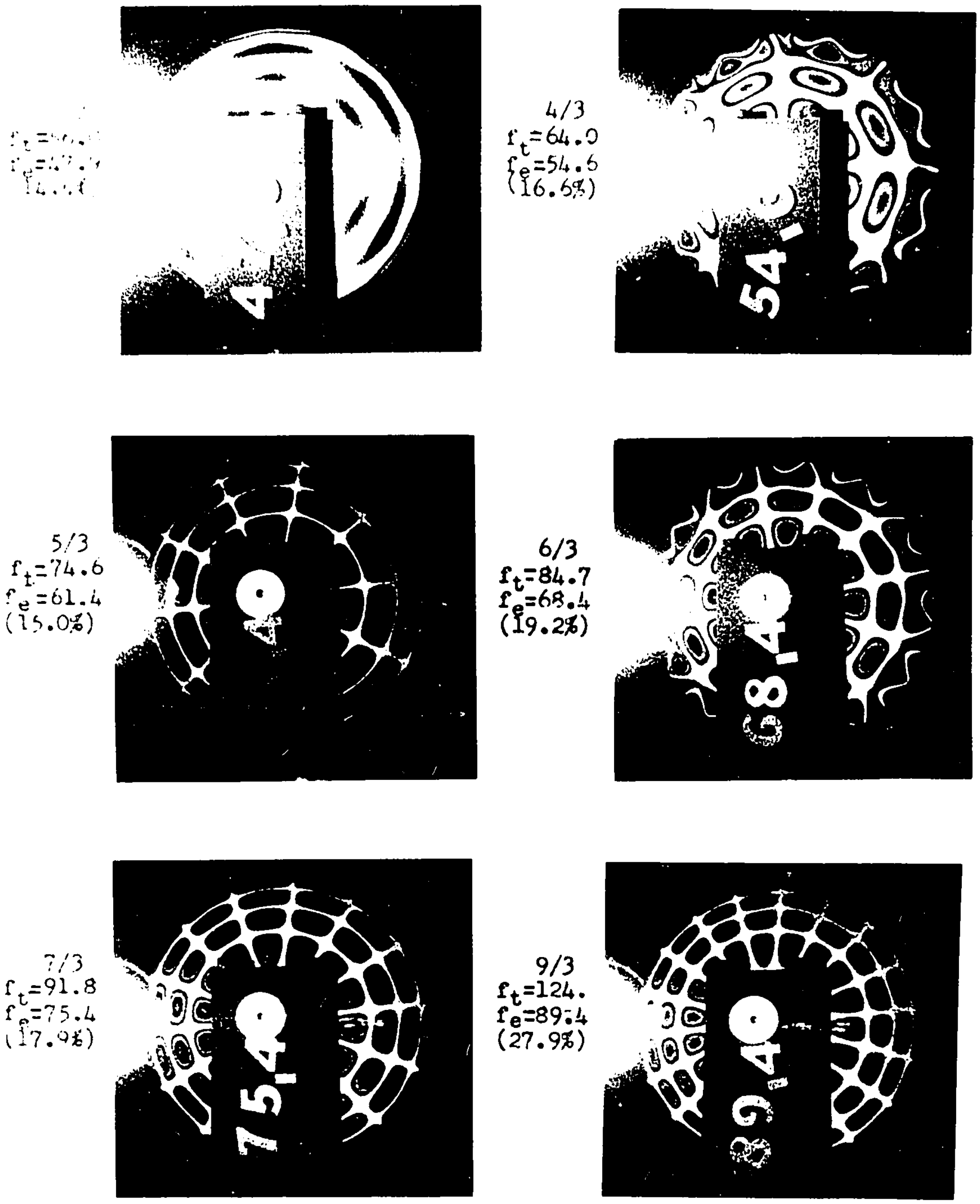

[illegible]
f_t=[illegible]
f_e=[illegible]
(14.[illegible])

4/3
f_t=64.0
f_e=54.6
(16.6%)

5/3
f_t=74.6
f_e=61.4
(15.0%)

6/3
f_t=84.7
f_e=68.4
(19.2%)

7/3
f_t=91.8
f_e=75.4
(17.9%)

9/3
f_t=124.
f_e=89.4
(27.9%)

(all frequencies in kHz)

Fig. 34. Constant Stress Disc Interferograms (n=3)

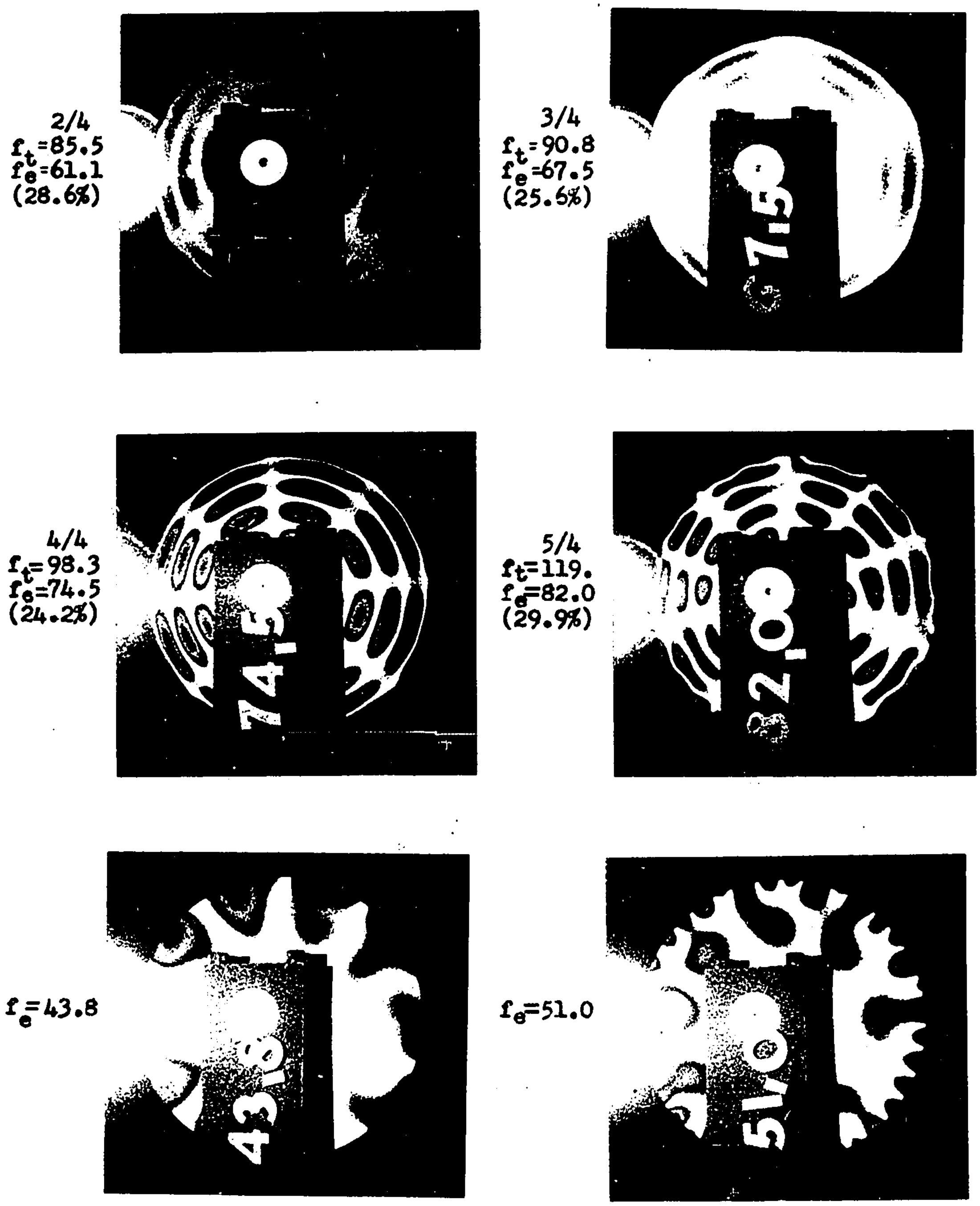

2/4
$f_t=85.5$
$f_e=61.1$
(28.6%)

3/4
$f_t=90.8$
$f_e=67.5$
(25.6%)

4/4
$f_t=98.3$
$f_e=74.5$
(24.2%)

5/4
$f_t=119.$
$f_e=82.0$
(29.9%)

$f_e=43.8$

$f_e=51.0$

(all frequencies in kHz)

Fig. 35. Constant Stress Disc Interferograms (n=4)

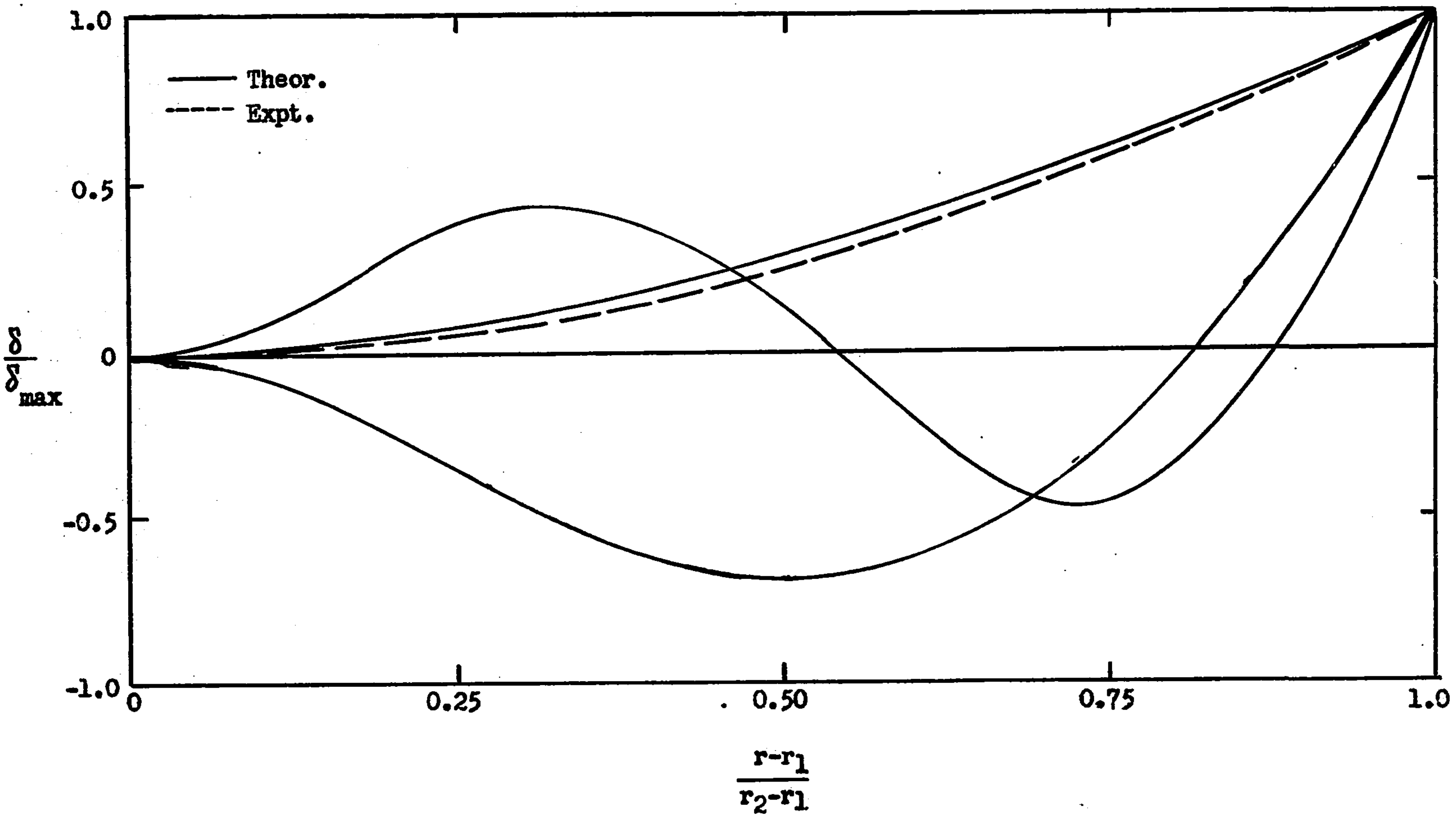

Fig. 36. Constant Stress Disc Radial Profile of Deflection (m=0)

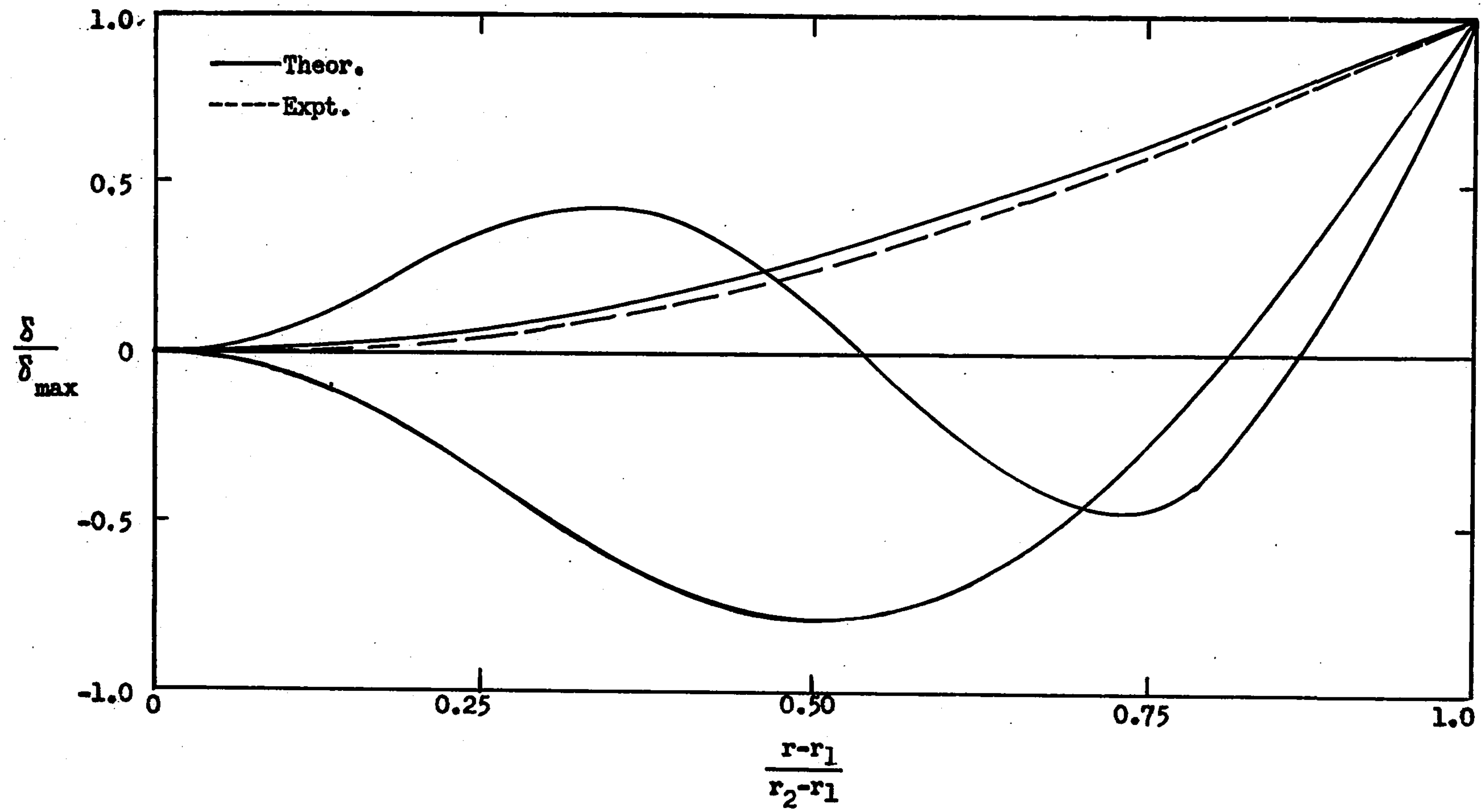

Fig. 37. Constant Stress Disc Radial Profile of Deflection (m=1)

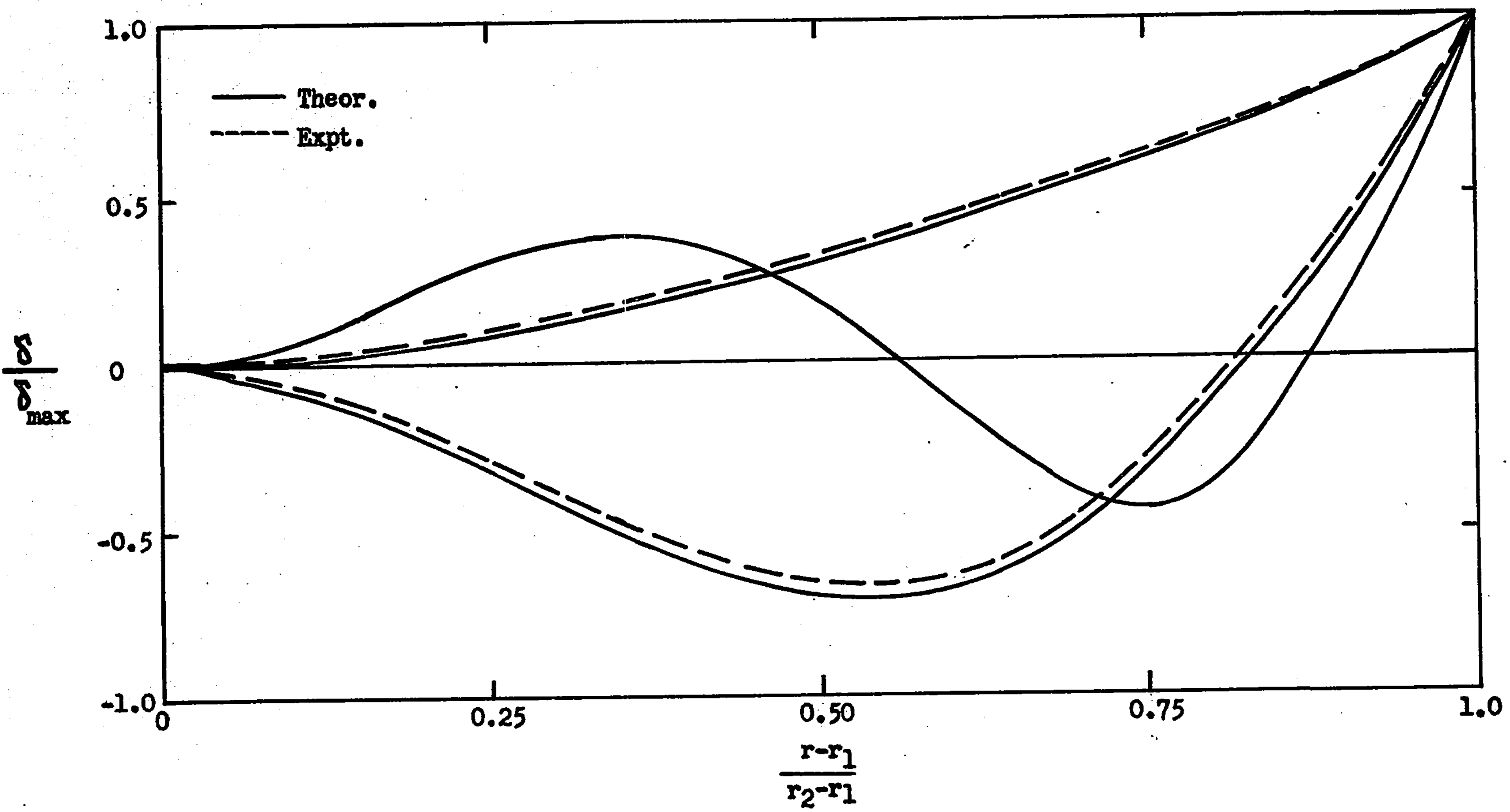

Fig. 38. Constant Stress Disc Radial Profile of Deflection (M=2)

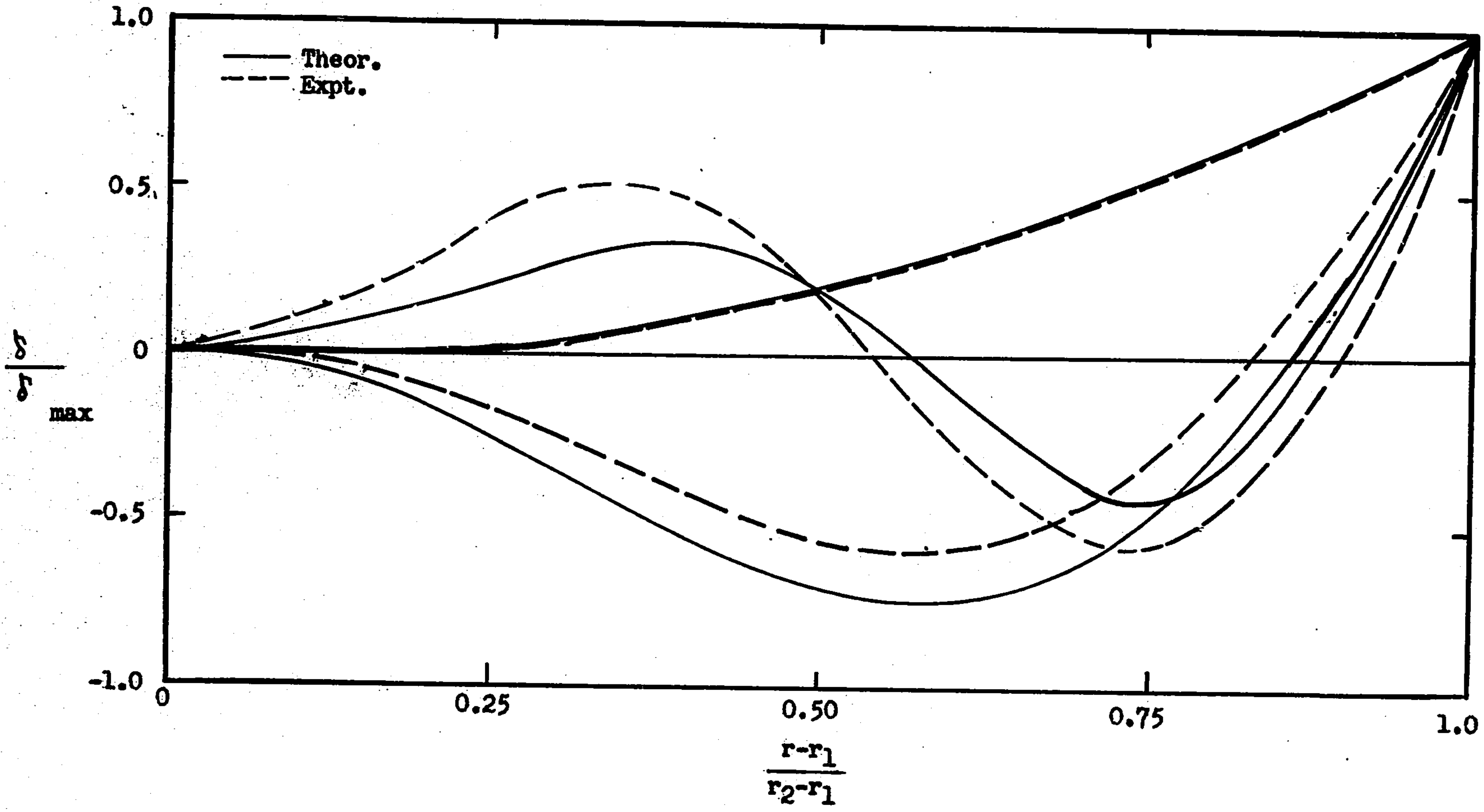

Fig. 39. Constant Stress Disc Radial Profile of Deflection (m=3)

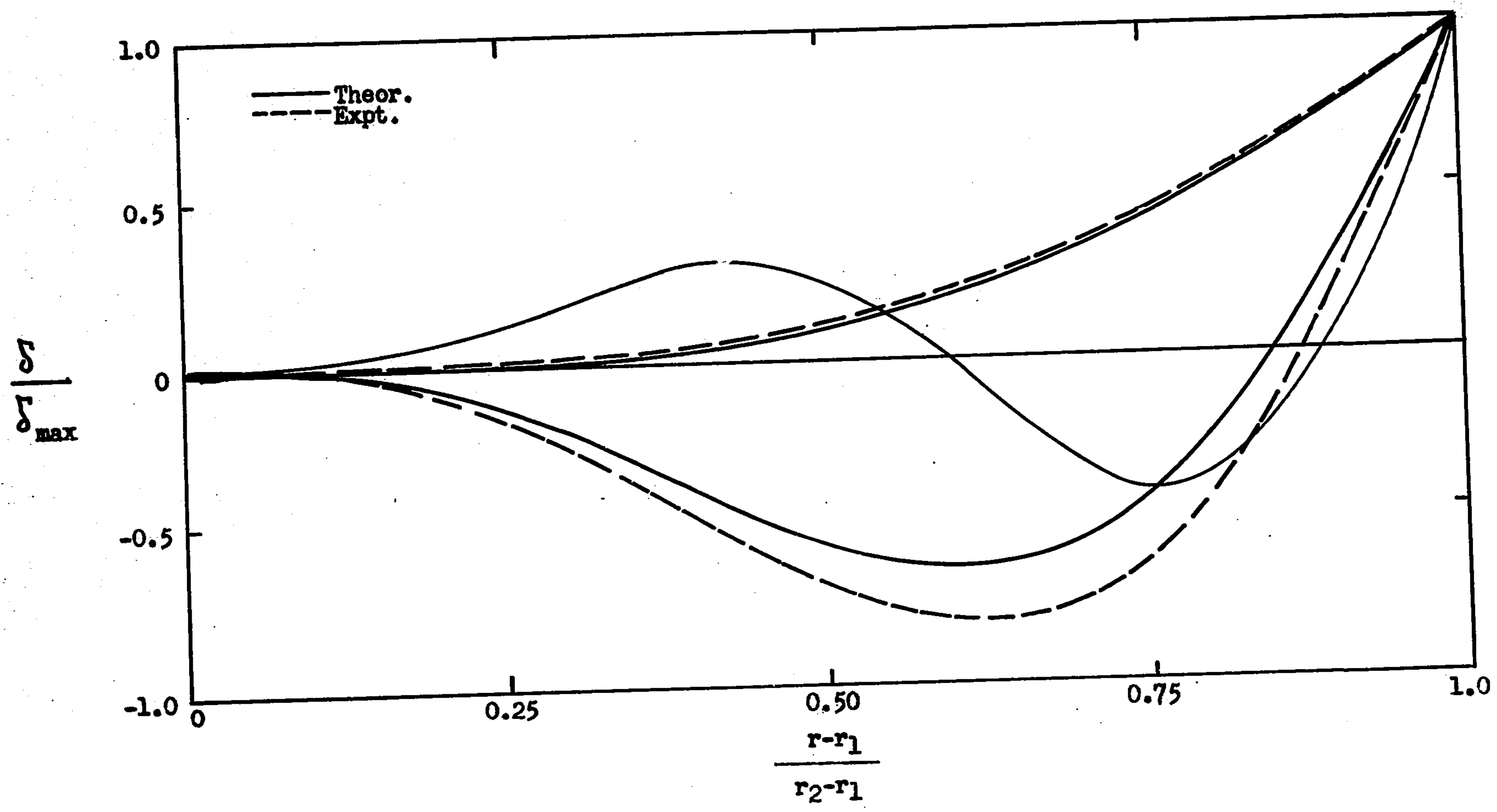

Fig. 40. Constant Stress Disc Radial Profile of Deflection (m=4)

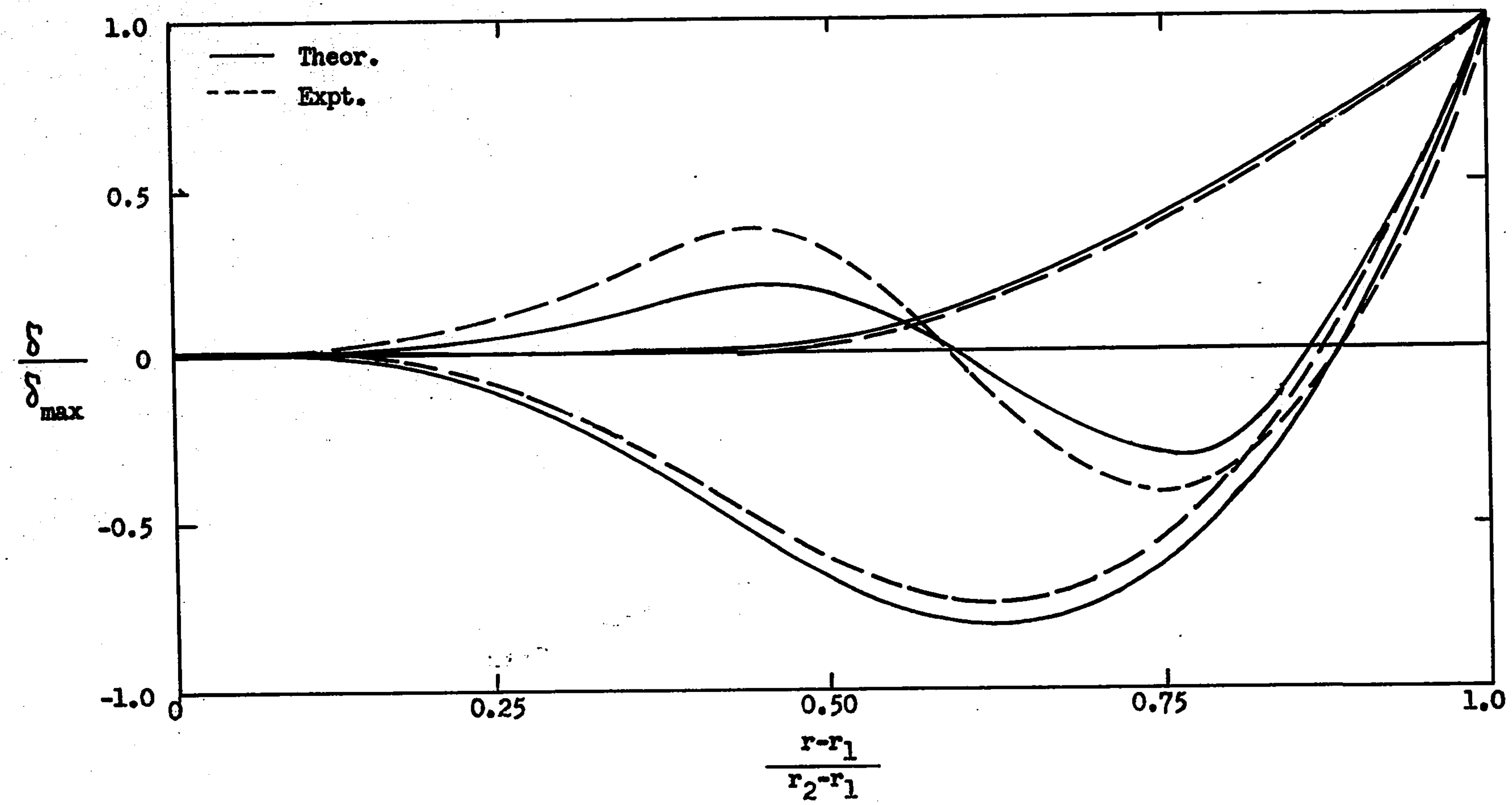

Fig. 41. Constant Stress Disc Radial Profile of Deflection (m=5)

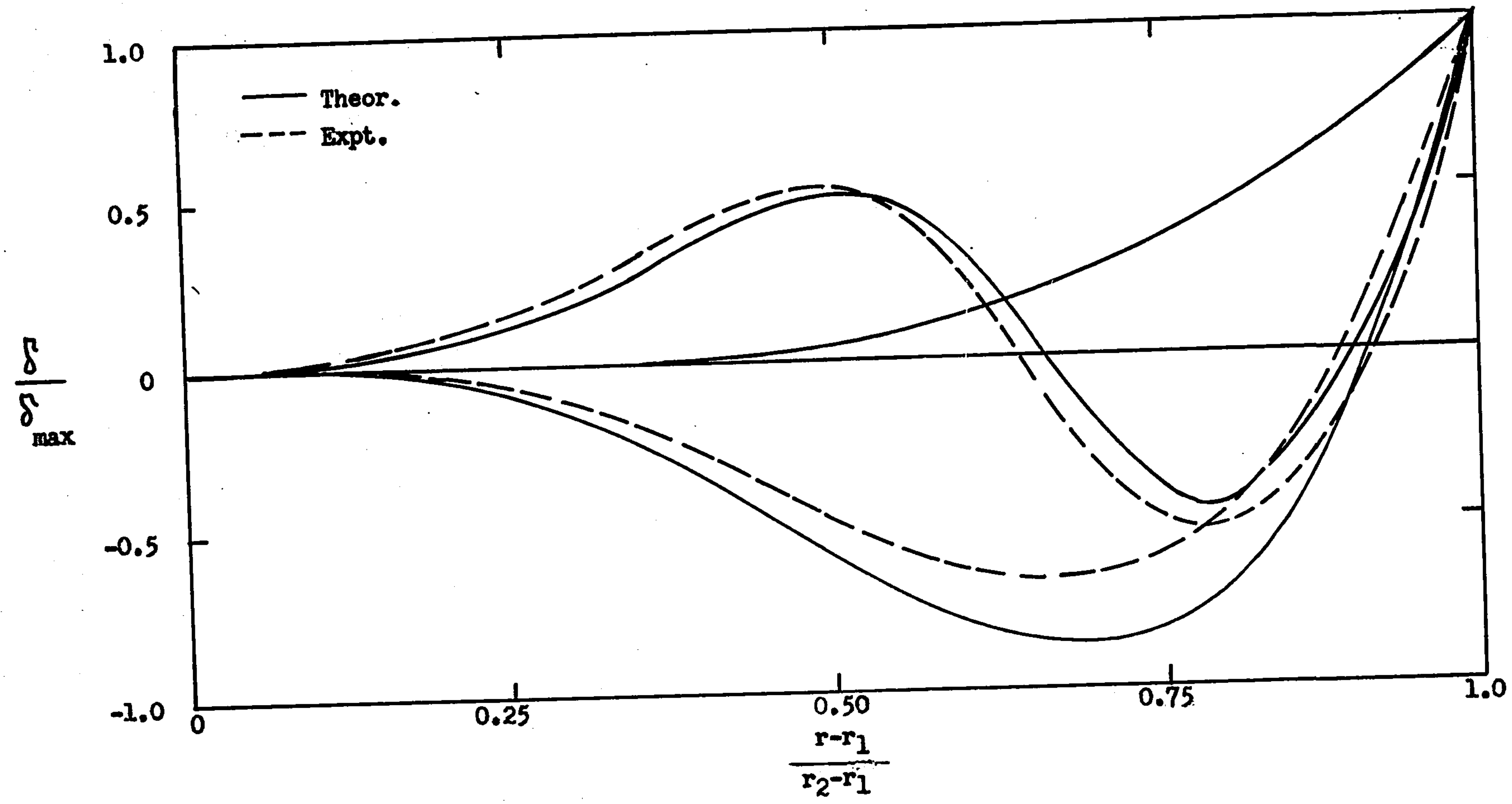

Fig. 42. Constant Stress Disc Radial Profile of Deflection (m=6)

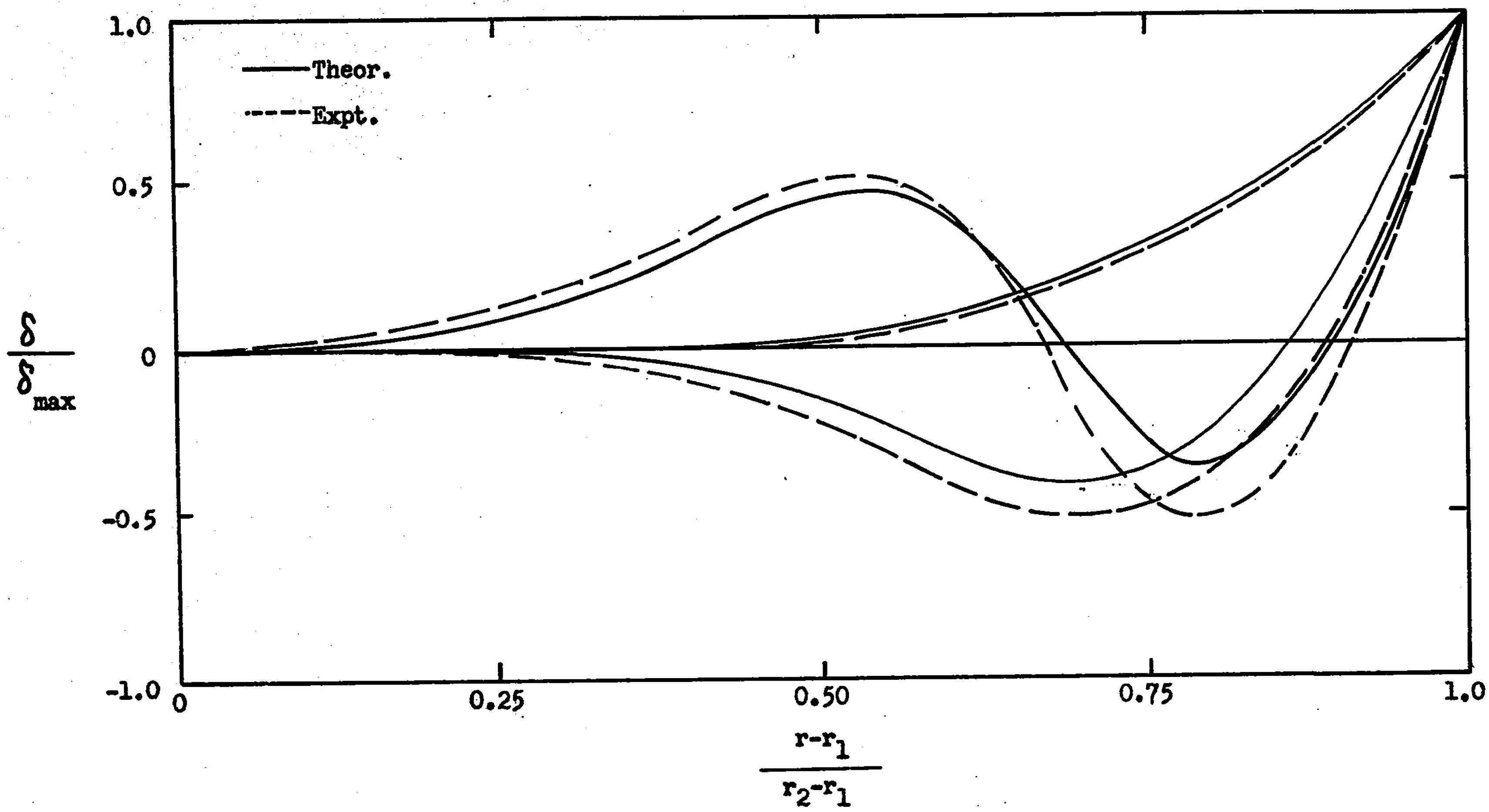

Fig. 43. Constant Stress Disc Radial Profile of Deflection (m=7)

8

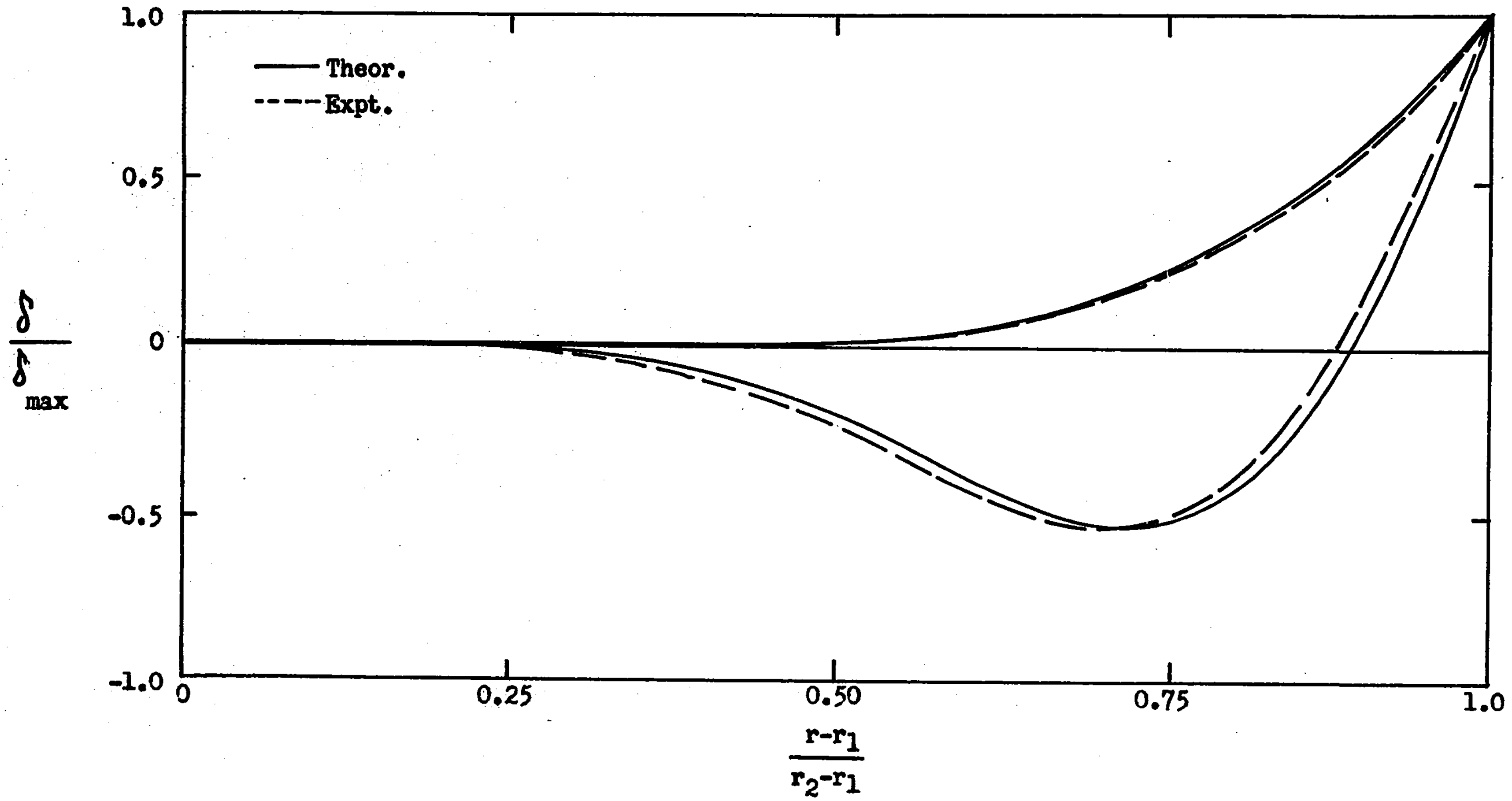

Fig. 44. Constant Stress Disc Radial Profile of Deflection (m=8)

Type	649-F	SO-243	8E75	10E70	10E75	14C70	He-Ne-1
Mfr.	Kodak	Kodak	Agfa-Gevaert	Agfa-Gevaert	Agfa-Gevaert	Agfa-Gevaert	Ilford
Base*	G&P	P	G	G&P	G&P	P	G
Sens'y. (ergs/cm2) @ 6328 A	900	5	200	50	80	3	5
Resolution† (1/mm.)	2000	400	3000	2800	2800	1500	2000
Emulsion Thick.(μ)	17&6	-	7	7&5	7&5	5	9

* G glass
P plastic

† Derived from hologram reconstruction

Table 1. Properties of Various Holographic Emulsions

CASE NO. \ DEG. FREEDOM	2	4	6	8	10	12	14	REF. 108
1	86.5	87.6	87.6	87.7	87.6	-	-	87.7
2	5.10	5.10	5.10	5.10	5.10	-	-	5.10
3	211	220	221	223	223	223	-	-
4	205	298	326	338	344	345	345	345
5	25.6	37.2	40.8	42.2	43.0	43.0	-	43.1
6	162	144	136	131	129	128	127	-
7	107	87.3	81.3	78.8	77.6	76.4	76.5	-

Maximum Deflection (μ in.)

Table 2. Results of Static Analysis

No. of Elements	Frequency (kHz)		
	0/0	0/1	0/2
2	1.54	9.89	43.4
3	1.39	8.49	25.0
4	1.34	8.26	24.3
5	1.32	7.96	22.1
6	1.30	7.08	20.1
7	1.28	6.82	20.4
8	1.26	6.46	20.4
9	1.27	6.76	-
Ref. 7	1.28	7.45	21.5

Table 3. Convergence of Frequencies

APPENDIX A

PROPERTIES AND GEOMETRIES OF MODELS

A total of seven cases of simulated discs were used in the study; four of uniform thickness, three of linear taper and one of a more general cross sectional profile. The geometries are shown in Table A1.

All seven were analyzed theoretically in the static study of Section 3.3.2. Cases 1 through 5 were selected since they correspond to the analytical tables given by Timoshenko (108). Cases 3,6,and 7 correspond to actual models tested dynamically in the study. For the static analysis, a Poisson's ratio of 0.300 was used to agree with Timoshenko's values. Young's modulus was taken as 10×10^6 psi. and the load around the circumference was 10 pounds in total. In all cases, inner and outer radius boundary conditions were taken as fixed and free respectively.

Theoretical vibration analysis was done for cases 3,6 and 7, since these were available for experimental examination. Case 7 is of special interest since it is the constant centrifugal stress profile as found in Biezeno and Grammel (1). The thickness variation is given as

$$t = t_1 e^{-\frac{\omega_r^2 \rho}{2 \sigma} r^2} \qquad (A1)$$

The disc has constant and equal radial and tangential centrifugal stress. A plot of the thickness profile of the disc may be found in Fig. A 1. To obtain a stress of 10 ksi., this disc would rotate at approximately 36,000 rpm.

The discs were manufactured from solid six inch round 6061-T6 aluminum stock, leaving a one inch diameter shaft on each disc face.

The constant stress disc was manufactured on a lath using an incremental table of thickness at various radii, then lightly polished to remove machining marks. Although manufacturing the discs from a solid block involves a great deal of work, this was done to insure a fixed boundary condition at the inner radius. A 1/32 inch radius was left at the shaft to reduce the possibility of fatigue cracks at the root of the discs.

For theoretical vibration analysis, the handbook value of 0.333 for Poisson's ratio was used. Young's modulus was taken as 10×10^6 psi and the density as 0.098 lb/cu. in.

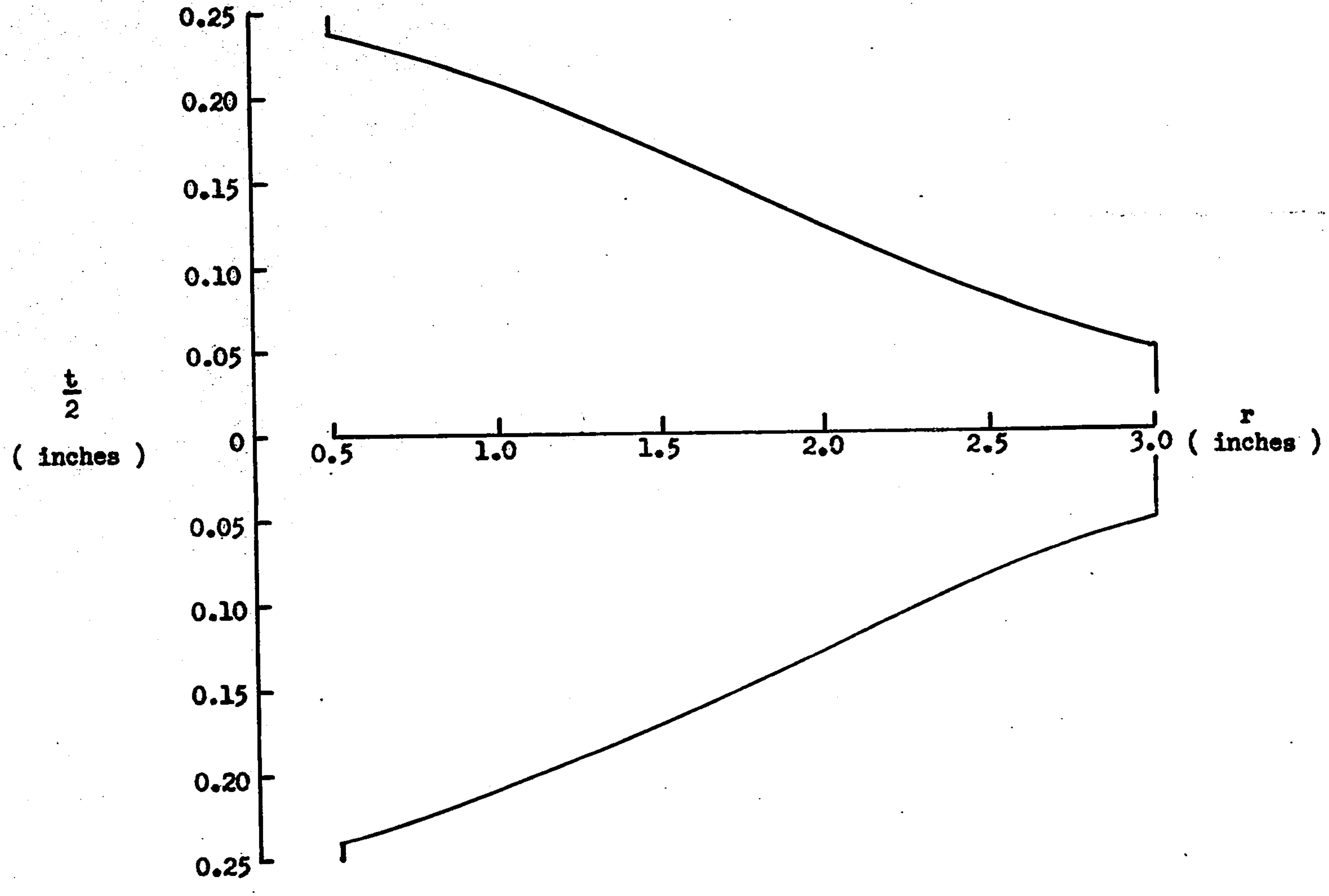

Fig. A1. Constant Stress Disc Profile

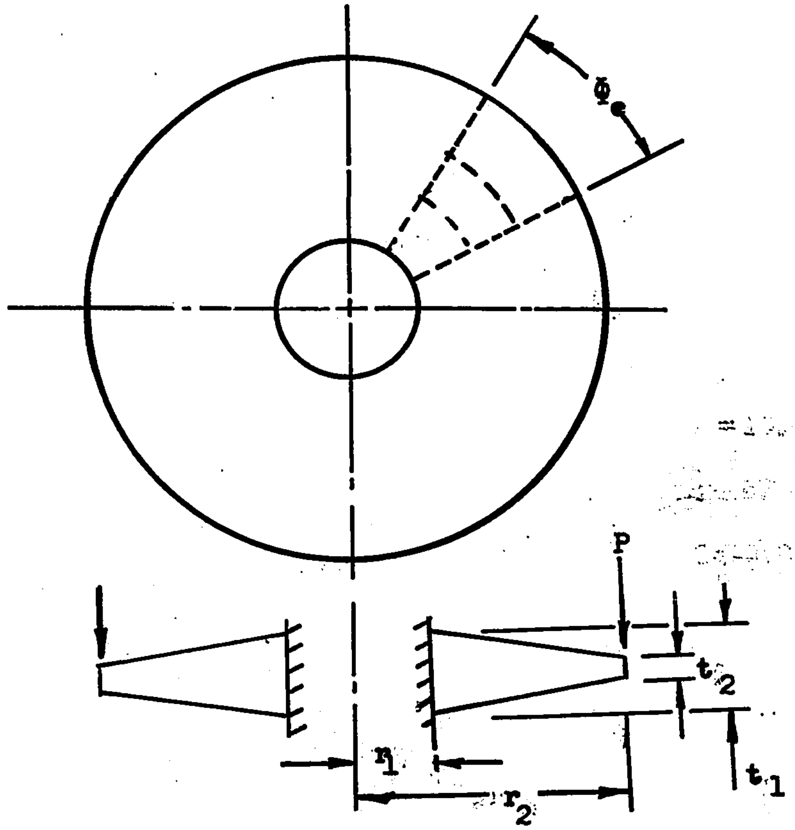

CASE NO.	r_1	r_2	t_1	t_2	THICKNESS PROFILE
1	0.50	1.00	0.100	0.100	Const. t
2	0.50	0.80	0.100	0.100	Const. t
3	0.50	2.98	0.248	0.248	Const. t
4	0.50	1.00	0.050	0.100	Lin. taper
5	0.50	1.00	0.100	0.200	Lin. taper
6	0.50	2.98	0.503	0.107	Lin. taper
7	0.50	2.98	0.479	0.111	Const. σ

Table A1. Geometries of Models

APPENDIX B

ACCURACY OF HOLOGRAPHIC TECHNIQUE

B.1. AMPLITUDE DETERMINATION

An initial approximation to the accuracy of amplitude determination may be obtained by analyzing the equivalent static linear approximation given by equation (5). The differentiation gives :

$$D(M) = \frac{\lambda}{\cos\theta_1 \cos\theta_2} + \frac{d(\lambda)}{\lambda} + \frac{d(N)}{N} + \frac{\sin\theta_1 d(\theta_1) + \sin\theta_2 d(\theta_2)}{\cos\theta_1 + \cos\theta_2} \qquad \text{(B-1)}$$

Dividing by equation (5) :

$$\frac{D(M)}{M} = \frac{d(\lambda)}{\lambda} + \frac{d(N)}{N} + \frac{\sin\theta_1 d(\theta_1) + \sin\theta_2 d(\theta_2)}{\cos\theta_1 + \cos\theta_2} \qquad \text{(B-2)}$$

For the component layout of Fig. 16, geometrical analysis shows $\theta_1 = 11 \pm 5.5^\circ$ and $\theta_2 = 13 \pm 6.1^\circ$. This includes the possible changes of angles from one side of the model to the other and from one side of the hologram to the other. Substituting these values in the equation (B-2) and neglecting the term for wavelength change (this is typically 0.008%):

$$\frac{D(M)}{M} = \frac{d(N)}{N} + 0.0448 \qquad \text{(B-3)}$$

Equation B-3 shows a maximum possible error due to uncertainties in angle determination of 4.48 %. If one wishes to decrease this error by selecting a fixed viewing position and including the variation of angle in equation (5), this error may be reduced to 0.37%.

The major source of error in equation B-3 is in fringe order determination. For five fringes, with an error of ±0.25 fringe, fringe order error is5 % making a total maximum possible error of 9.48 %. If high resolution is required, the fringes may be scanned with a photodensitometer which has typical resolution of ±0.05 fringe. If the local values of angle are used for the point of interest, maximum possible error may be reduced to 1.37 % for the fifth fringe.

For vibration analysis, a further error is introduced if equation (5) is used. Although the form of equation (4) is not suitable for error analysis, the form of the equation is similar to equation (5). It is reasonable to assume that if equation (4) is applied for time-average fringes, maximum possible errors should be less than 15 %. This is generally suitable for vibration analysis since the investigator is usually more concerned with frequency determination than with deflection profiles. If precise amplitude determination is required, densitometer analysis will reduce errors signifigantly. If this is combined with stroboscopic or ruby laser sources, the error becomes 1.37 %, the same as the static case.

For the current study, deflection profiles were obtained by plotting the individual fringe positions after conversion to displacement. If more points were desired for a curve, the half order or bright fringes were also used. This procedure is generally simpler than attempting to determine partial fringe orders at given positions.

B.2 RESONANT FREQUENCY DETERMINATION

Accuracy of resonant frequency analysis is a function of the width of the resonance curve. A typical response curve is shown in Fig. B.1. Resonance frequencies were determined by observation of live fringe holograms. Excitation frequency was varied manually until the maximum number of fringes was observed. Excitation frequency was then determined from a digital counter with resolution of ± 1 count. For a given mode, the resonant frequency was found to be repeatable to better than 1 % in all cases.

B.3 EXPERIMENTAL VERIFICATION OF HOLOGRAPHIC ACCURACY

The conversion of interferometric fringe order to deflection was verified both statically and dynamically. For the static analysis, a 6" X 1.5" X 0.100" beam of 6061-T6 aluminum was selected. Double exposure holographic interferograms of the beam were taken for four loads. A typical interferogram obtained is shown in Fig. B 2 . Results for the deflected profile are plotted in Fig. B 3 . Agreement between loads and elementary theory is excellent.

Dynamic verification was carried out for a 6" X 4" X 0.256" low carbon steel.cantilever plate.

A Kistler model 815 A7 accelerometer with nominal sensitivity of 10.66 mv/g was mounted near the plate tip. The accelerometer calibration was checked on a Bruel and Kjaer Type 4290 Calibration Exciter. Sensitivity agreed within 2% to the standard in the calibrator. The plate was accoustically excited in its fundamental mode at various amplitudes and time average interferograms taken. Typical interferograms are shown in Fig. B 4 . Fringe order at the accelerometer centreline was determined and the accelerometer reading converted to amplitude from the simple harmonic motion equations. Results are plotted in Fig. 18. Excellent agreement is shown with theory.

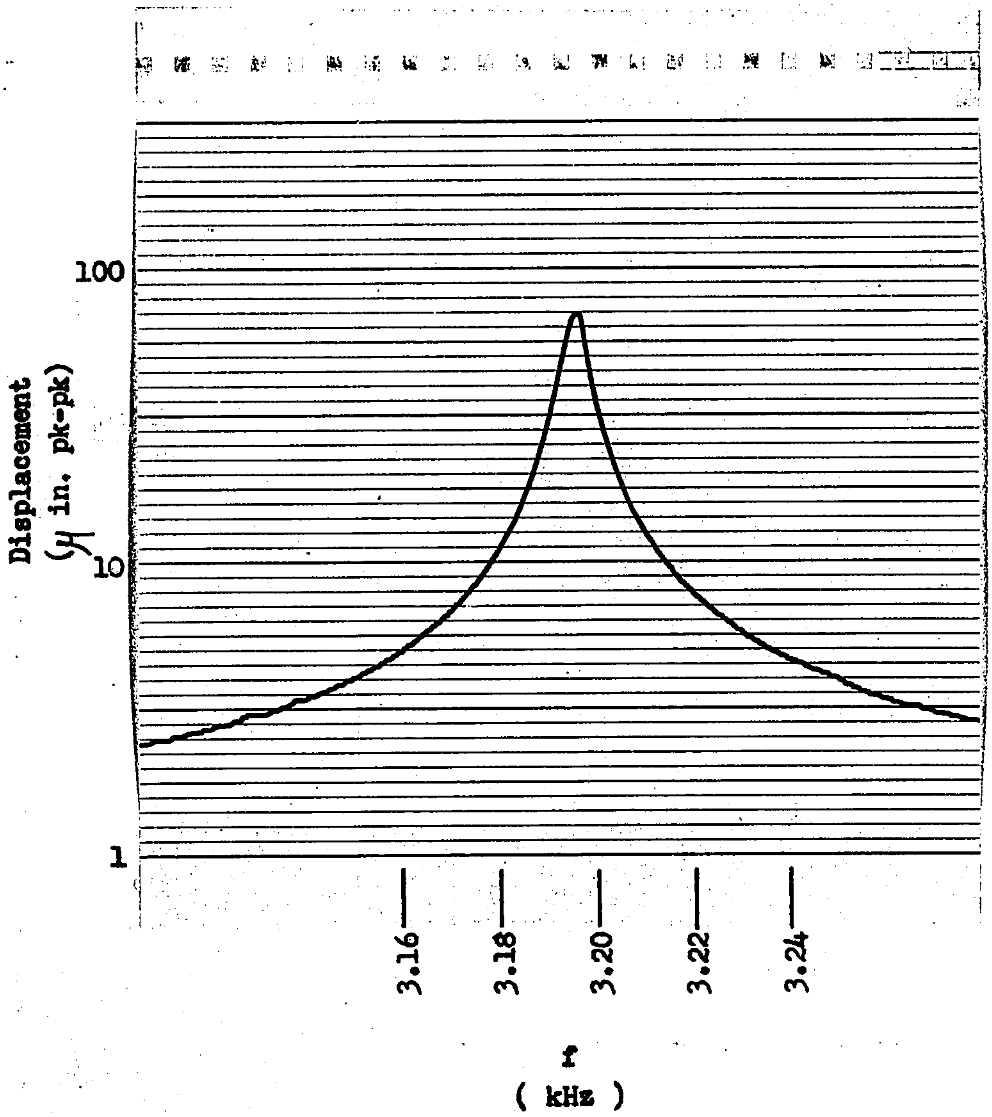

Fig. B1. Typical Resonance Response

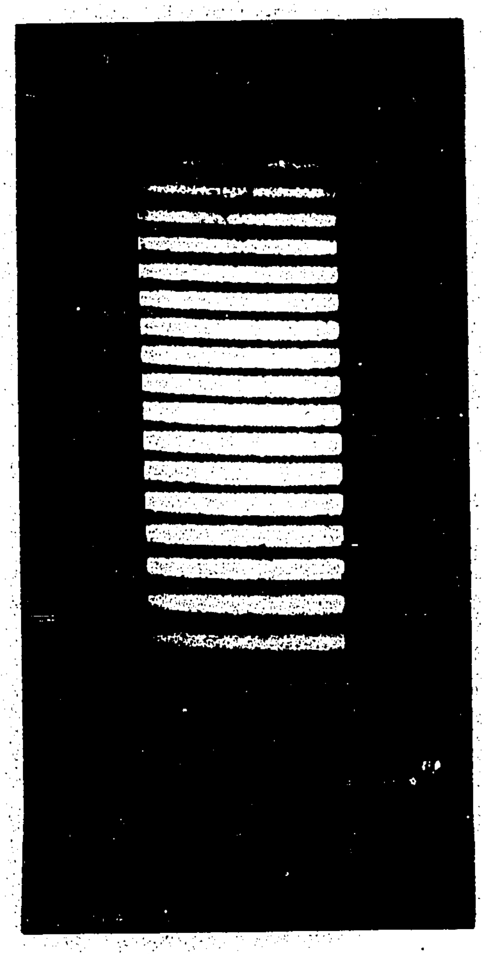

Fig. B2. Typical Static Verification Interferogram

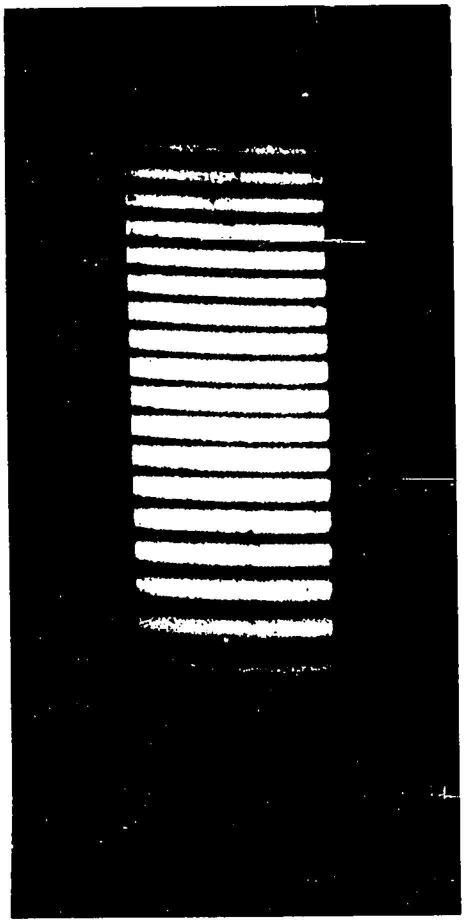

Fig. B2. Typical Static Verification Interferogram

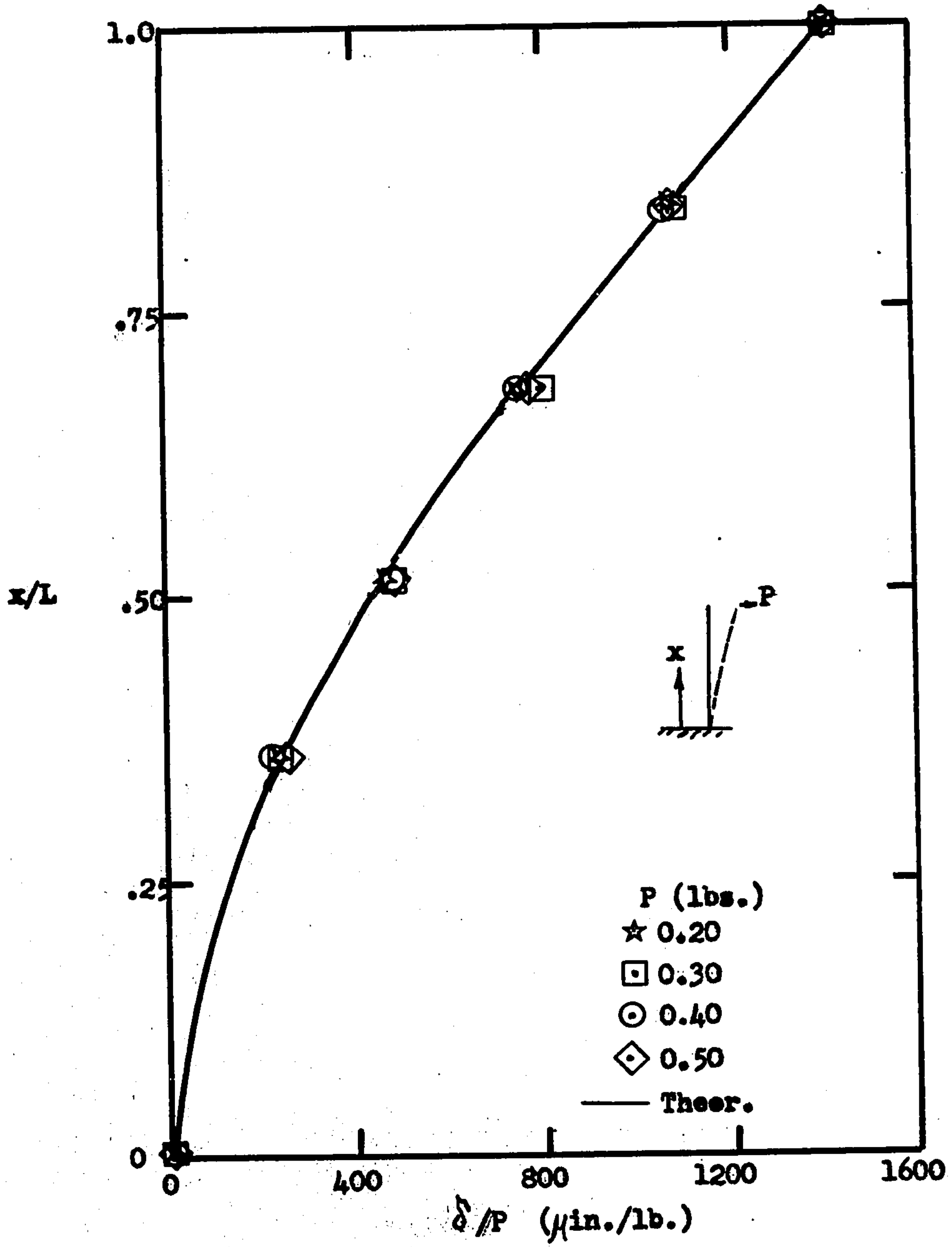

Fig. B3. Static Interferometric Verification

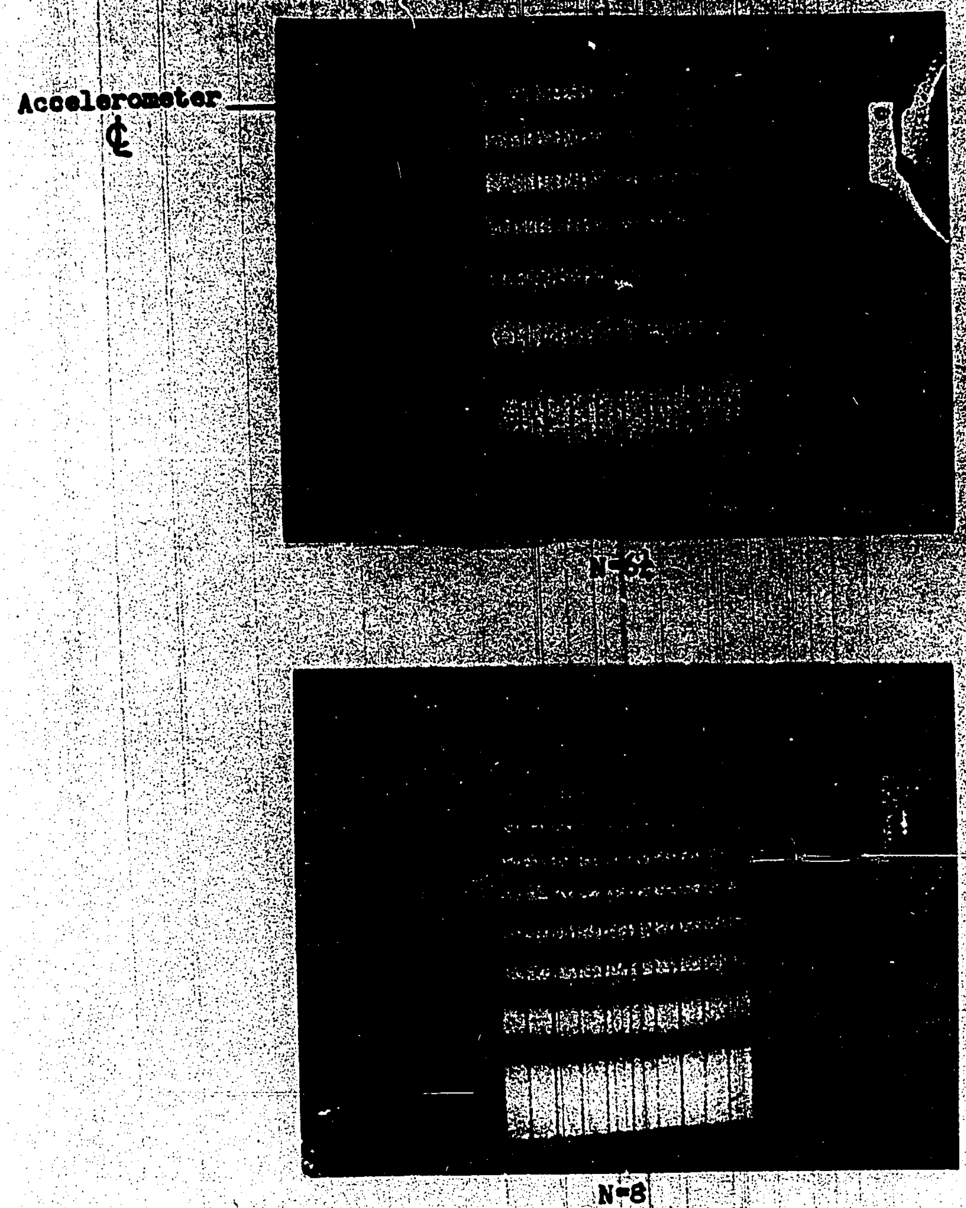

Fig. B4. Typical Dynamic Verification Interferograms

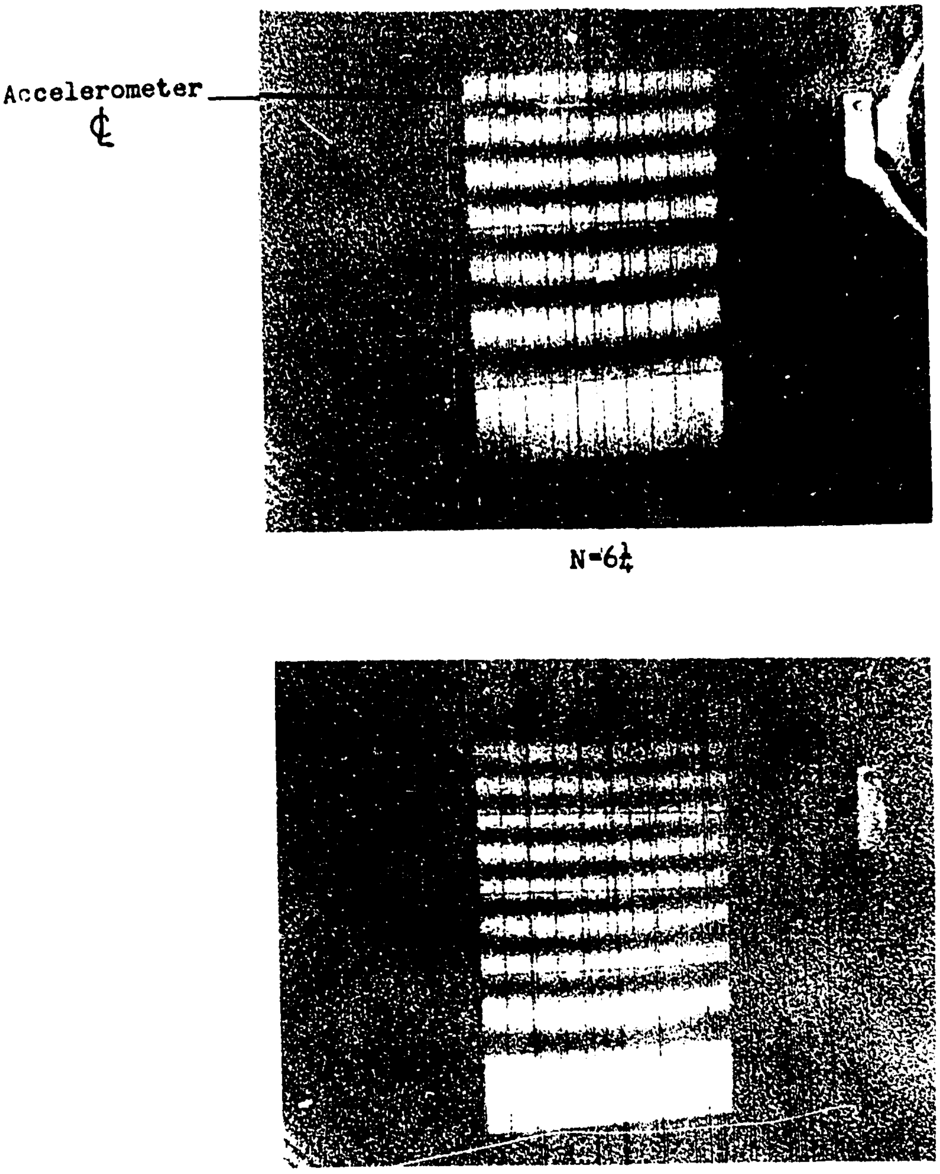

N=6¼

N=8

Fig. B4. Typical Dynamic Verification Interferograms

APPENDIX C

STROBOSCOPIC HOLOGRAPHIC INTERFEROMETRY

In order to evaluate the stroboscopic analysis of interferograms, an inexpensive stroboscopic device was constructed (92). It is basically a small 18,000 rpm. ; 1.5 in.-oz. torque motor with a stabilized power supply. The motor drives a 5.725 inch diameter strobe disc fabricated from 0.075 " thick aluminum. Thirty-six 5° slots, 0.250" deep, are cut around itsperiphery. On a 2.20" radius , 72 holes 0.040" diameter are drilled. These holes serve to strobe the laser beam.

The slots provide a modified sine wave in synchronism with the strobe pulses. This is obtained by illuminating the slots with an IR-LED and detecting the result on the other side of the disc with a phototransistor. Two strobe pulses are produced for each sine wave cycle. Since the interferogram is insensitive to direction of motion, no difficulties are created by these two pulses, which are 180° out of phase with each other. The advantage of using two pulses is that the output laser power is doubled. For 6 mw. input, 0.8 mw. results. There is a small loss of power due to diffraction by the holes. Larger holes are not acceptable since they would create a pulse too wide to stop the vibration. A photograph of the chopper is given in Fig. C1.

The output of the phototransistor is fed to the vibration excitation device by way of the appropriate power amplifier. The form of the wave may be altered to approximate a sinusoid by varying the distance from the LED to the disc and also varying the incidence angle. The phase relationship of the excitation wave to the strobe pulses is varied by moving the LED-phototransistor combination around the disc perimeter.

Due to windage losses, disc rotational speed is limited to 6000 rpm. corresponding to a frequency of 3.6 kHz. A smaller 4" diameter, 4 slot disc did run at the full 18,000 rpm., but this corresponds to 1.2 khz. A more powerful motor would increase the maximum frequency available.

The major advantage of stroboscopic work was found to lie in live fringe analysis. In this case, fringe contrast is even lower than that illustrated for equation (4). With continuous illumination, less than four fringes could normally be resolved in live analysis. With stroboscopic illumination, up to 20 fringes have been visually observed. The chopper described here is relatively inexpensive, particularly when compared to pockel's cells which have been used in many cases.

The prime advantage of stroboscopic illumination lies in extending the number of visible fringes. Figure C.2 illustrates this advantage. The figure also shows the major disadvantage - the brilliant nodal line is lost, making modal determination very difficult. If large amplitudes are to be resolved, a combination of stroboscopic and continuous illumination techniques is recommended.

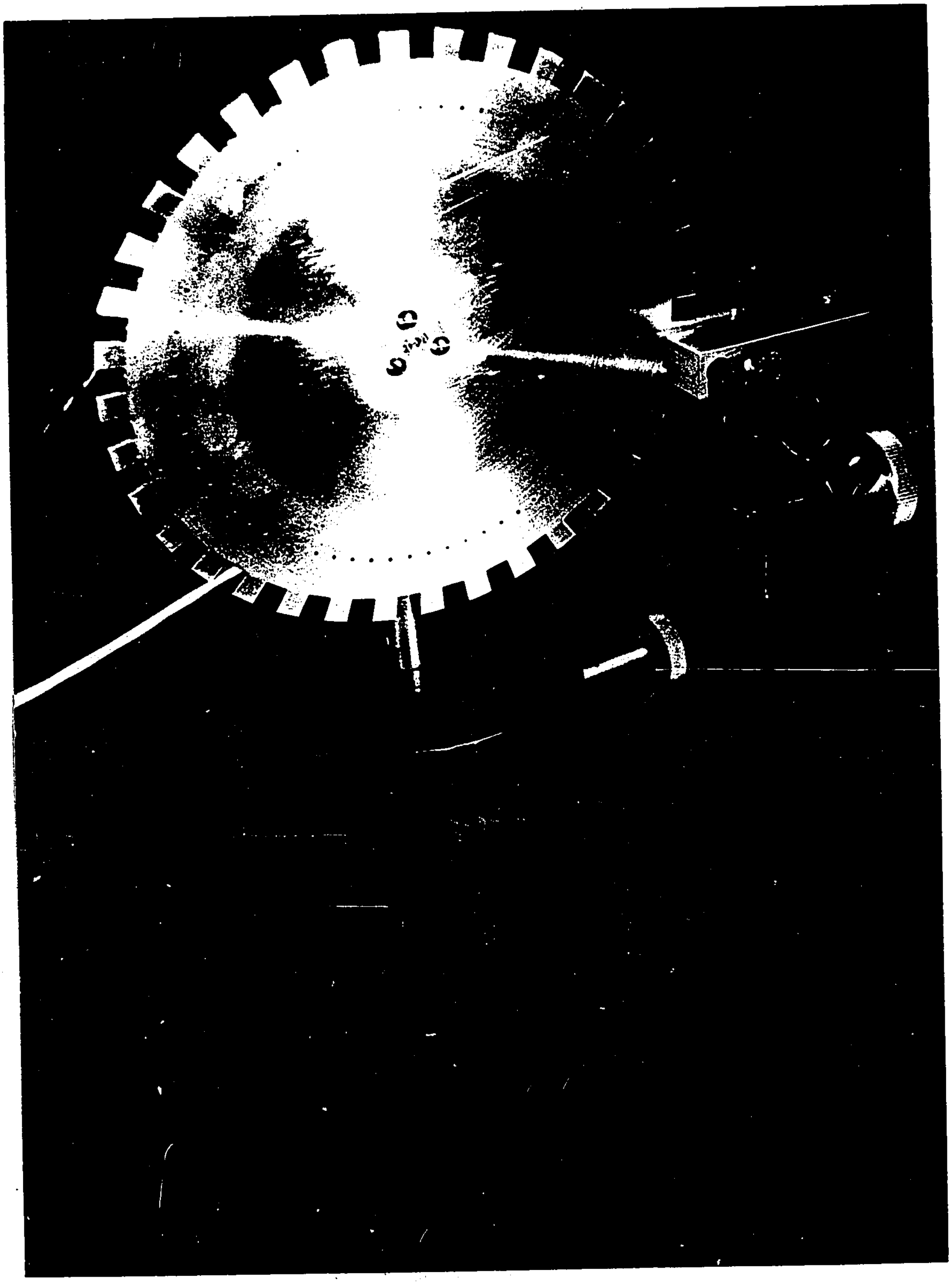

Fig. C1. Stroboscope Disc

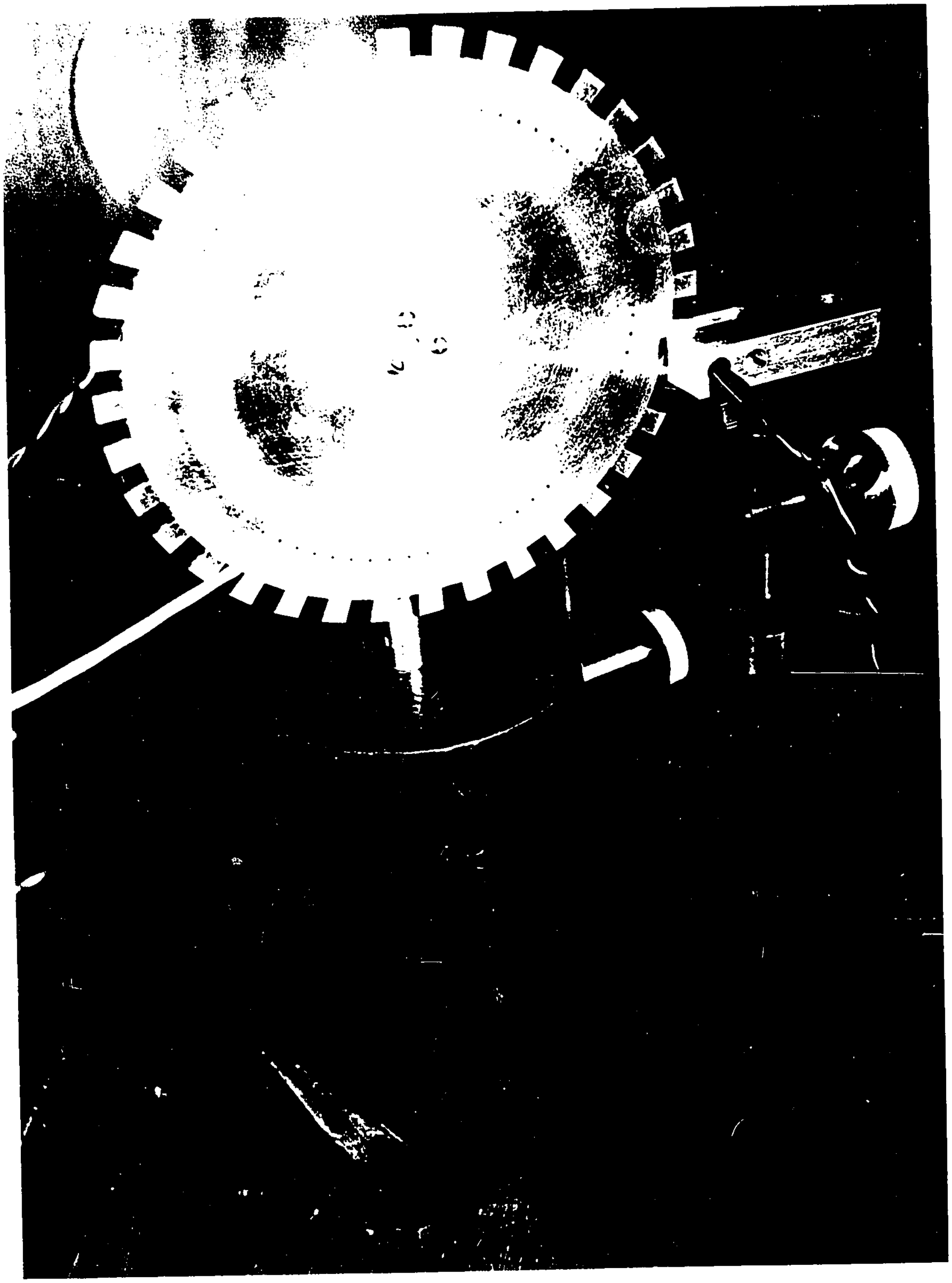

Fig. 31, Stroboscope Disc

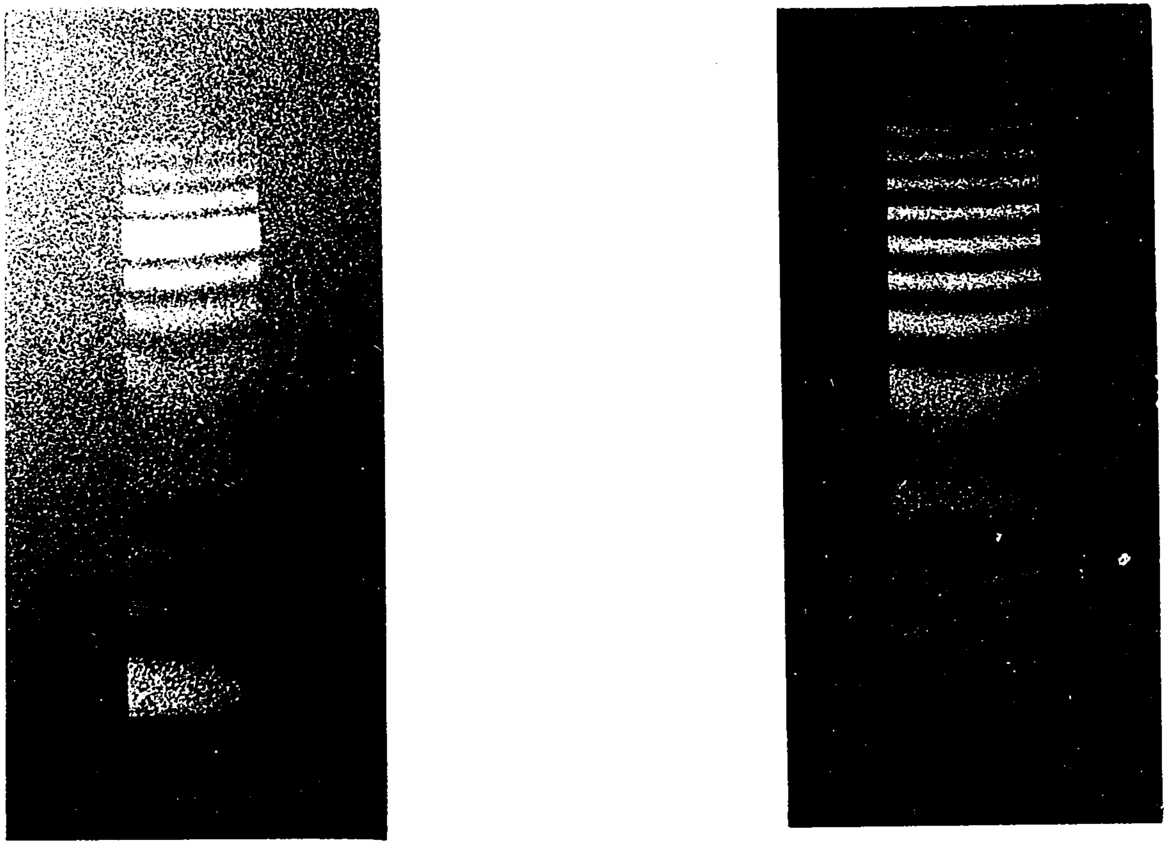

Time Average

Stroboscopically Stopped

Fig. C2. Stroboscopically Stopped Cantilever Beam

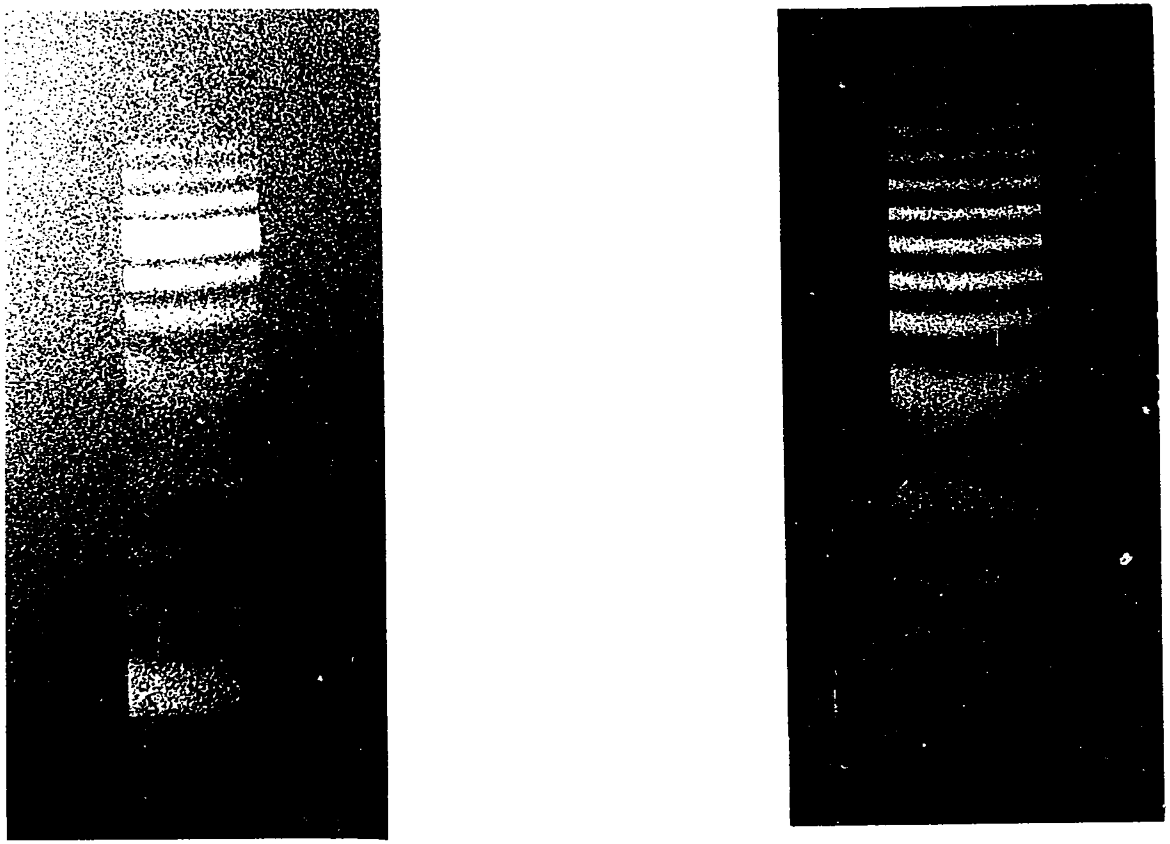

Time Average

Stroboscopically Stopped

Fig. C2. Stroboscopically Stopped Cantilever Beam

APPENDIX D

RUBY LASER INTERFEROMETRY

In the early stages of this study, the feasibility of using ruby laser illumination was investigated. A number of technical problems arise in ruby laser holography (126) (127). Coherence lengths are limited, high energy densities require special optics, alignment is difficult, and real-time analysis is not possible.

The laser used is a Korad K-1 system with water cooled head and output elaton. A Crystalab GA-7 pockels cell provides Q-switching. Output pulse width is several hundred nanoseconds.

The investigation involved a 6" X 1.5" X 0.100" cantilever beam of 6061-T6 aluminum vibrating in its fundamental mode. An initial static exposure was taken, then excitation applied to the beam. The second exposure was triggered at random. A series of interferograms were taken so that at least some would be at large amplitudes. A photograph of a typical interferogram is shown in Fig. D1. Twenty three fringes are visible and contrast is excellent. Fringes are not parallel to the base as theory predicts due to incomplete clamping at the beam root.

It was decided at this point that the disadvantages of the ruby laser outweighed the advantages. Ruby laser reliability is poor and technical problems are complex. For proper analysis, a triggering network is required to fire the laser at maximum vibratory amplitude. This trigger must also fire the flashtube approximately 500μ sec. before the laser pockels cell is fired.

The major advantage of ruby laser holography arises when a double pulse pockels cell is available. Two pulses from one firing, separated by lmsec. would stop a vibration of 250 Hz. In hostile environments, this technique could eliminate undesired path length differences between exposures due to thermal or other changes. For conventional ruby laser systems, 1 msec. is the maximum pulse separation available, making 250 Hz. the slowest vibration suitable for analysis. Again, a circuit is required to synchronize the pulses with the vibration. Also, the flashtube must be triggered in advance, and this time is very critical if equal intensity pulses are to be obtained.

As in the stroboscopic analysis, ruby laser holographic interferograms do not readily provide nodal positions.

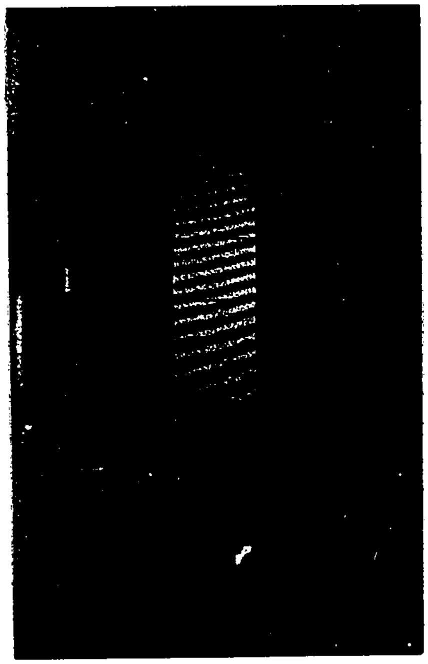

Fig. D1. Ruby Laser Interferogram

APPENDIX E

VARIABLE CORRELATION TECHNIQUE

Individual element stiffness and mass matrices must be assembled to form the total stiffness and mass matrices for the object being modelled. The total matrices may be formed for the object, then boundary conditions applied. This procedure is quite inefficient since terms are added to the overall matrices which are not required. Also, since application of boundary conditions reduces the size of matrices involved, signifigantly larger storage areas are involved than are actually required for the inversion or eigenanalysis problem.

These disadvantages are overcome by the variable correlation technique. The method is based on a correlation table for the degrees of freedom of each element. A sketch of the object (with element boundaries) is required. Each degree of freedom is numbered, using a zero for any degree of freedom which is eliminated due to boundary conditions. The numbers of the degrees of freedom associated with each element are then inserted in the correlation table. A typical correlation table for a cantilever plate modelled with four elements of twelve degrees of freedom each is shown in Fig. E1 . No symmetry has been assumed. However, if one is interested in only symmetric cases (for example, a point load at node four of element 1), then deflections on each of the sides are symmetric. Thus, degree of freedom 7 becomes 1, 16 becomes 10, etc.

The overall matrices are assembled from each element matrix by use of the table. The correlation table is scanned for each element to determine the number of the overall system degree of freedom associated with each element degree of freedom. This value is used to assemble the overall matrices. If a zero is encountered, that term is discarded since it has been nullified by the boundary conditions.

Fig. E2 shows a typical four element quadrant of a disc modelled with a 16 degree of freedom sector element. The various boundary conditions are illustrated with a correlation table given for the case of one side at a node, the other at an antinode.

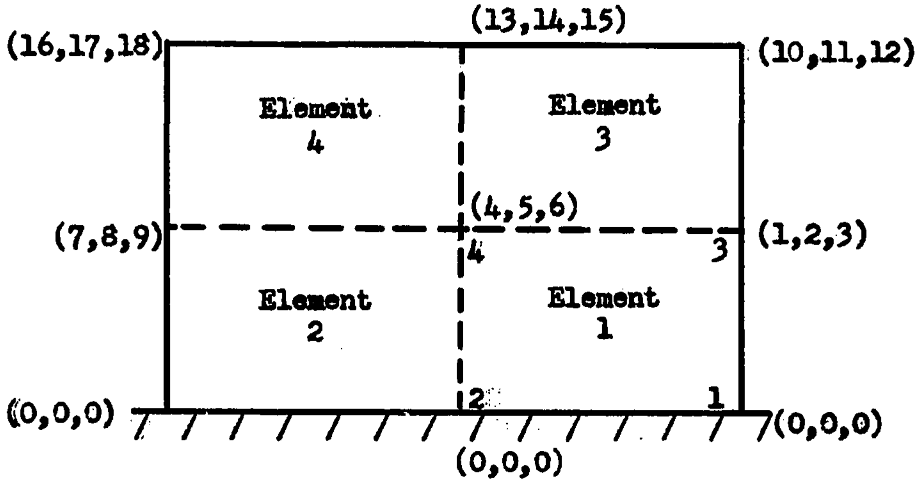

Elem. no.	w_1	w_{x1}	w_{y1}	w_2	w_{x2}	w_{y2}	w_3	w_{x3}	w_{y3}	w_4	w_{x4}	w_{y4}
1	0	0	0	0	0	0	1	2	3	4	5	6
2	0	0	0	0	0	0	4	5	6	7	8	9
3	1	2	3	4	5	6	10	11	12	13	14	15
4	4	5	6	7	8	9	13	14	15	16	17	18

Fig. E1. Variable Correlation Table - Cantilever Plate

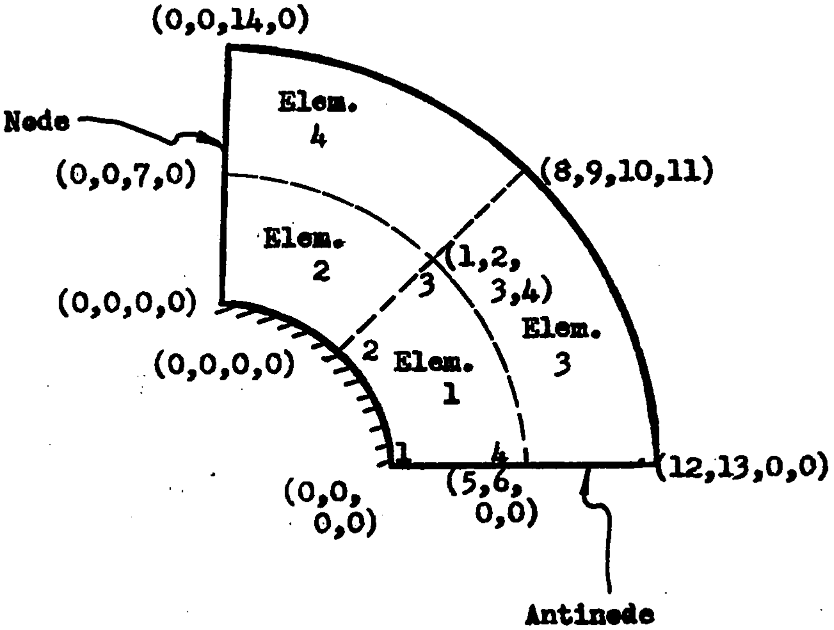

Element no.	w_1	w_{r1}	$w_{\theta 1}$	$w_{r\theta 1}$	w_2	w_{r2}	$w_{\theta 2}$	$w_{r\theta 2}$	w_3	w_{r3}	$w_{\theta 3}$	$w_{r\theta 3}$	w_4	w_{r4}	$w_{\theta 4}$	$w_{r\theta 4}$
1	0	0	0	0	0	0	0	0	1	2	3	4	5	6	0	0
2	0	0	0	0	0	0	0	0	0	0	7	0	1	2	3	4
3	5	6	0	0	1	2	3	4	8	9	10	11	12	13	0	0
4	1	2	3	4	0	0	7	0	0	0	14	0	8	9	10	11

Boundary Conditions

At a node:

$w=w_r=w_{r\theta}=0$

At an antinode:

$w_\theta=w_{r\theta}=0$

At a fixed edge:

$w=w_r=w_\theta=w_{r\theta}=0$

Fig. E2. Variable Correlation Table - Disc Sector

APPENDIX F

FINITE ELEMENT PROGRAM

```
C
C     SOLUTION OF NATURAL FREQUENCIES AND CEFLECTIONS OF
C        SIMULATED GAS TURBINE DISCS FIXED AT
C        AN INNER RADIUS
C
C     PARAMETERS
C
C     R1        HUB RADIUS
C     R2        OUTER RADIUS
C     THI       PROJECTED THICKNESS AT ZERO RACIUS
C     THO       OUTER THICKNESS
C     ANGLE     SECTOR TOTAL INCLUDED ANGLE
C     E         YOUNGS MODULUS
C     PR        POISSONS RATIO
C     RH        MATERIAL DENSITY (LB/CU. IN.)
C     NELR      NO. OF RADIAL ELEMENTS
C     NELT      NO. OF THETA ELEMENTS
C
C     TCODE INDICATES THICKNESS PROFILE
C
C          1 CONSTANT THICKNESS
C          2 LINEAR TAPER
C          3 CONSTANT STRESS
C          4 VARIABLE (ELEMENT THICKNESS READ IN)
C
C     MCODE INDICATES MODES DESIRED
C
C          1 NO DIAMETRAL NODES
C          2 ODD NO. OF DIAMETRAL NODES
C          3 EVEN NO. OF DIAMETRAL NODES
C          4 NO DIAMETRAL NODES ONLY (NELT=1)
C          5 ONE DIAMETRAL NODE PER ELEMENT (NELT=1)
C
      DIMENSION EVAL(64),EVECT(4096)
      COMMON/ONE/SM(64,64),DM(64,64),IVC(64,16)
      COMMON/TWO/GEOM(64,5)
      COMMON/THREE/Q(4,4,3),IK(16),JK(16),KK(16)
      COMMON/FOUR/SS(136),DD(136),AB(16)
      COMMON/FIVE/P(4,4,3)
      INTEGER TCODE
      PI=3.1415926
    8 READ 100,RI,RO,THI,THO,ANGLE,E,PR,RH,NELR,NELT,
     1    TCODE,MCODE
      IF (RI.EQ.0) GO TO 650
      NEL=NELR*NELT
      NDF=4*NEL-NELR*(MCODE-1)
      IF (MCODE.LT.4) GO TC 9
      NDF=2*NELR
```

```
0015             9 PRINT 22,RI,RO,THI,THO,ANGLE,E,PR,RH,NELR,NELT,
                  1   NDF,TCODE,MCODE
0016               IF (NDF.GT.64) GO TO 8
0017               RH=RH/386.0
0018               ANGLE=ANGLE*PI/180.0
0019               DO 120 I=1,64
0020               DO 120 J=1,64
0021               DM(I,J)=0
0022           120 SM(I,J)=0.0
0023               CALL GEO(RI,RO,THI,THO,ANGLE,NELR,NELT,TCODE)
0024               CALL VCT(NELR,NELT,MCODE)
0025               DO 700 K=1,NEL
0026               R1=GEOM( K,1)
0027               R2=GEOM( K,2)
0028               TH=0.5*(GEOM( K,3)+GEOM( K,4))
0029               ANGLE=GEOM( K,5)
0030               CALL SECT(R1,R2,ANGLE,TH,E,PR,RH)
0031               CALL ASSEM(K)
0032           700 CONTINUE
             C
             C     DETERMINE EIGENVALUES AND VECTORS
             C
0033               CALL ARRAYD(NDF,64,SM,SM,DM,DM)
0034               CALL NROOT(NDF,SM,DM,EVAL,EVECT)
0035               IF (NDF.LT.12) GO TO 180
0036               NDFR=12
0037               GO TO 185
0038           180 NDFR=NDF
0039           185 DO 600 II=1,NDFR
0040               I=NDF-II+1
0041               III=NDF*(I-1)+1
0042               FR=SQRT(ABS(EVAL(I)))/(2.0*PI)
0043               FND=EVAL(I)*12.*RH*RO**4*(1.-PR*PR)/(E*GEOM(1,1)**2)
0044               PRINT 620,EVAL(I),FR,FND
0045               PRINT 640
0046               DO 600 K=1,NEL
0047               DO 150 J=1,16
0048               KV=IVC(K,J)
0049               IF (KV.EQ.0) GO TO 140
0050               KVA=IABS(KV)
0051               AA=KV/KVA
0052               JJJ=III+KVA-1
0053               SS(J)=AA*EVECT(JJJ)
0054               GO TO 150
0055           140 SS(J)=0
0056           150 CONTINUE
0057               PRINT 630,K
0058               CALL DEFN( 5,K)
```

```
      PRINT 625,(SS(J),J=1,8),( DM(1,J),J=1, 5)
  160 PRINT 625,SS(13),SS(14),SS(15),SS(16),SS(9),SS(10),
     1    SS(11),SS(12),(DM(2,J),J=1,5)
      DO 600 L=3,5
      PRINT 635,( DM(L,J),J=1, 5)
  600 CONTINUE
      GO TO 8
   22 FORMAT ('1',T5,'INNER RAD=',F7.3,'  OUTER RAD=',F7.3,
     1'  INNER THICK.=',F7.4,'  OUTER THICK=',F7.4,
     2'  ANGLE=',F7.3,'DEG.',//,T10,'MOD=',E10.3,
     3'PSI  POISSONS RATIO=',F7.3,'   PRC=',F7.3,
     4'LB/CU IN',//,T10,'   NO. OF R ELEM=',I3,
     5'  NO OF THETA ELEM=',I3,'   DEG. FREEDOM=',I3,
     6'   TCODE=',I3,'   MCODE=',I3)
  100 FORMAT (2F6.2,2F6.3,F6.1,E10.3,2F6.3,4I3)
  620 FORMAT (//,' EIG. VALUE=',E10.3,'   FREQ=',E10.3,
     1   'HZ.    NON-DIM. FREQ.=',E10.3)
  625 FORMAT (T12,8(F7.4,1X) ,T80, 5(1X,F7.4))
  630 FORMAT (T8,'ELEMENT NO.',I3)
  635 FORMAT (T80, 5(1X,F7.4))
  640 FORMAT (/,T30,'DEFLECTIONS',//,T16,'W',T23,'W,R',T30,
     1  'W,T/R',T37,'W,RT/R',T48,'W',T55,'W,R',T62,
     2  'W,T/R',T69,'W,RT/R',T90,'PROFILE')
  650 STOP
      END
```

```
             BLOCK DATA
       C
       C     P(I,J,K)=COEFFICIENT ON (J-1)"TH POWER OF X IN
       C        (K-1)"TH DERIVATIVE OF I"TH INTERPOLATION
       C        FUNCTION
       C     IK(J) INDICATES WHICH OF THE 4 INTERPOLATION FUNCTIONS
       C        IN THETA MULTIPLIES DEGREES OF FREEDOM J
       C     JK(J)=SAME FOR R.
       C
             COMMON/THREE/P(4,4,3),IK(16),JK(16),KK(16)
       C
             DATA P(1,1,1),P(1,2,1),P(1,3,1),P(1,4,1)/  1.,  0., -3.,  2./
             DATA P(2,1,1),P(2,2,1),P(2,3,1),P(2,4,1)/  0.,  0.,  3., -2./
             DATA P(3,1,1),P(3,2,1),P(3,3,1),P(3,4,1)/  0.,  1., -2.,  1./
             DATA P(4,1,1),P(4,2,1),P(4,3,1),P(4,4,1)/  0.,  0., -1.,  1./
       C
             DATA P(1,1,2),P(1,2,2),P(1,3,2),P(1,4,2)/  0., -6.,  6.,  0./
             DATA P(2,1,2),P(2,2,2),P(2,3,2),P(2,4,2)/  0.,  6., -6.,  0./
             DATA P(3,1,2),P(3,2,2),P(3,3,2),P(3,4,2)/  1., -4.,  3.,  0./
             DATA P(4,1,2),P(4,2,2),P(4,3,2),P(4,4,2)/  0., -2.,  3.,  0./
       C
             DATA P(1,1,3),P(1,2,3),P(1,3,3),P(1,4,3)/ -6., 12.,  0.,  0./
             DATA P(2,1,3),P(2,2,3),P(2,3,3),P(2,4,3)/  6.,-12.,  0.,  0./
             DATA P(3,1,3),P(3,2,3),P(3,3,3),P(3,4,3)/ -4.,  6.,  0.,  0./
             DATA P(4,1,3),P(4,2,3),P(4,3,3),P(4,4,3)/ -2.,  6.,  0.,  0./
       C
             DATA IK/1,1,3,3,2,2,4,4,2,2,4,4,1,1,3,3/
       C
             DATA JK/1,3,5,7,1,3,5,7,2,4,6,8,2,4,6,8/
       C
             DATA KK/1,3,1,3,1,3,1,3,2,4,2,4,2,4,2,4/
       C
             END
```

```
0001                 SUBROUTINE ARRAYD(I,N,S1,D1,S2,D2)
            C
            C        CONVERT STORAGE MODE OF TWO MATRICES FROM MATRIX
            C                 TO VECTOR FORM
            C
0002                 DIMENSION S1(1),D1(1),S2(1),D2(1)
0003                 NI=N-I
0004                 IJ=0
0005                 NM=0
0006                 DO 130 K=1,I
0007                 DO 125 L=1,I
0008                 IJ=IJ+1
0009                 NM=NM+1
0010                 S1(IJ)=D1(NM)
0011             125 S2(IJ)=D2(NM)
0012             130 NM=NM+NI
0013                 RETURN
0014                 END
```

```
      SUBROUTINE ASSEM(K)
C
C     ASSEMBLE TOTAL S.M.
C        (FOR VARYING ELEMENT S.M. & M.M.)
C
      DIMENSION S(16,16),D(16,16)
      COMMON/ONE/SM(64,64),DM(64,64),IVC(64,16)
      COMMON/FOUR/SS(136),DD(136),AB(16)
C
C     EXPAND SM TO RECT. FORM
C
      IJ=0
      DO 50 I=1,16
      DO 50 J=1,I
      IJ=IJ+1
      D(J,I)=DD(IJ)
      S(J,I)=SS(IJ)
      D(I,J)=DD(IJ)
   50 S(I,J)=SS(IJ)
      DO 2 I=1,16
      M=IVC(K,I)
      IF (M.EQ.0)GO TO 2
      MM=IABS(M)
      A=MM/M
      DO 2 J=1,16
      N=IVC(K,J)
      IF (N.EQ.0)GO TO 2
      NN=IABS(N)
      B=NN/N
      DM(MM,NN)=DM(MM,NN)+A*B*D(I,J)
      SM(MM,NN)=SM(MM,NN)+A*B*S(I,J)
    2 CONTINUE
      RETURN
      END
```

```
      SUBROUTINE VCT(NELR,NELT,MCODE)
C
C     SET UP VARIABLE CORRELATION TABLE AS REQIRED
C        BY MCODE
      DIMENSION L(100)
      COMMON/ONE/SM(64,64),DM(64,64),IVC(64,16)
      NEL=NELR*NELT
      DO 50 I=1,64
      DO 50 J=1,16
   50 IVC(I,J)=0
      IF (MCODE.GT.3) GO TO 7000
C
C     SET UP FULL GENERAL V.C.T.
C
      NE=0
      DO 900 KR=1,NELR
      DO 900 KT=1,NELT
      NE=NE+1
      IF (KR.GT.1) GO TO 600
      IF (KT.GT.1) GO TO 300
      DO 200 J=1,16
  200 IVC(NE,J)=J
      KK=16
      GO TO 900
  300 DO 310 J=1,4
      IVC(NE,J)=IVC(NE-1,J+4)
  310 IVC(NE,J+12)=IVC(NE-1,J+8)
      DO 320 J=5,12
      KK=KK+1
  320 IVC(NE,J)=KK
      GO TO 900
  600 NNE=NE-NELT
      IF (KT.GT.1) GO TO 800
      DO 610 J=1,4
      IVC(NE,J)=IVC(NNE,J+12)
  610 IVC(NE,J+4)=IVC(NNE,J+8)
      DO 620 J=9,16
      KK=KK+1
  620 IVC(NE,J)=KK
      GO TO 900
  800 DO 810 J=1,4
      KK=KK+1
      IVC(NE,J)=IVC(NE-1,J+4)
      IVC(NE,J+4)=IVC(NNE,J+8)
      IVC(NE,J+8)=KK
  810 IVC(NE,J+12)=IVC(NE-1,J+8)
  900 CONTINUE
C
```

```
               C      APPLY APPROPRIATE B.C.'S
               C
 0042                 DO 1000 I=1,NELT
 0043                 DO 1000 J=1,8
 0044            1000 IVC(I,J)=0
 0045                 GO TO (2000,3000,3000),MCODE
 0046            2000 DO 2010 I=1,NEL,NELT
 0047                 DO 2010 J=3,4
 0048                 II=I+NELT-1
 0049                 IVC(I,J)=0
 0050                 IVC(I,J+12)=0
 0051                 IVC(II,J+4)=0
 0052            2010 IVC(II,J+8)=0
 0053                 GO TO 5000
 0054            3000 DO 3010 I=1,NEL,NELT
 0055                 II=I+NELT-1
 0056                 IVC(I,1)=0
 0057                 IVC(I,13)=0
 0058                 IVC(I,2)=0
 0059                 IVC(I,4)=0
 0060                 IVC(I,14)=0
 0061                 IVC(I,16)=0
 0062                 DO 3010 J=8,12,4
 0063            3010 IVC(II,J)=0
 0064                 IF (MCODE.EQ.3) GO TO 4000
 0065                 DO 3020 II=NELT,NEL,NELT
 0066                 DO 3020 J=7,11,4
 0067            3020 IVC(II,J)=0
 0068                 GO TO 5000
 0069            4000 DO 4010 II=NELT,NEL,NELT
 0070                 DO 4010 J=5,6
 0071                 IVC(II,J)=0
 0072            4010  IVC(II,J+4)=0
 0073            5000 CONTINUE
               C
               C      REDUCE VALUES TO LOWEST CONSECUTIVE INTEGERS
               C
 0074                 DO 6000 I=1,100
 0075            6000 L(I)=0
 0076                 LM=0
 0077                 DO 6020 I=1,NEL
 0078                 DO 6020 J=1,16
 0079                 KK=IVC(I,J)
 0080                 IF (KK.EQ.0) GO TO 6020
 0081                 IF (L(KK).GT.0) GO TO 6010
 0082                 LM=LM+1
 0083                 L(KK)=LM
 0084            6010 IVC(I,J)=L(KK)
```

```
 6020 CONTINUE
      RETURN
 7000 IF (MCODE.GT.4) GO TO 8000
      K=-3
      DO 120 I=1,NELR
      K=K+2
      DO 120 J=1,5,4
      IVC(I,J)=K
      IVC(I,J+1)=K+1
      IVC(I,J+8)=K+2
  120 IVC(I,J+9)=K+3
      IVC(1,1)=0
      IVC(1,5)=0
      RETURN
 8000 K=-1
      DO 140 I=1,NELR
      K=K+2
      IVC(I,9)=K
      IVC(I,10)=K+1
      IVC(I,13)=-K
      IVC(I,14)=-K-1
      IVC(I,6)=K-1
      IVC(I,5)=K-2
      IVC(I,2)=-K+1
  140 IVC(I,1)=-K+2
      IVC(1,1)=0
      IVC(1,5)=0
      RETURN
      END
```

```
      SUBROUTINE SECT(R1,R2,ANGLE,TH,E,PR,RH)
C
C     SET UP QUADRATIC STIFFNESS AND MASS MATRICES FOR
C        SECTOR ELEMENT (ISOTROPIC, CONSTANT THICKNESS)
C
      DIMENSION PP(8,8,3,3),QQ(4,4,3,3),RINT(22)
      COMMON/THREE/Q(4,4,3),IK(16),JK(16),LL(16)
      COMMON/FOUR/SS(136),DD(136),AB(16)
      COMMON/FIVE/P(4,4,3)
      DOUBLE PRECISION THINT2(4,4)
      DOUBLE PRECISION R1D,R2D,PPP,QQQ
      PR2=2.*(1.-PR)
      D=E*TH*TH*TH/(12.*(1.-PR*PR))
C
C     THINT2(I,J)=INTEGRAL OF X**(I+J-2) FROM ZERO TO ONE
C
      DO 10 I=1,4
        DO 10 J=1,I
          THINT2(I,J)=1.D0/DBLE(FLOAT(I+J-1))
   10     THINT2(J,I)=THINT2(I,J)
      F=ANGLE
   30 A=R2-R1
      R1D=DBLE(R1)/DBLE(A)
      R2D=DBLE(R2)/DBLE(A)
C
C     RINT(N)=INTEGRAL FROM R1D TO R2D OF R**(N-4)
C
      RINT(1)=(R2D**2-R1D**2)/(2.D0*(R1D*R2D)**2)
      RINT(2)=(R2D-R1D)/(R1D*R2D)
      RINT(3)=DLOG(R2D/R1D)
      DO 40 N=4,22
   40   RINT(N)=(R2D**(N-3)-R1D**(N-3))/DBLE(FLOAT(N-3))
      A2=A**2
      F3=F*F*F
      CALL H1R(R1,R2)
C
C     SET UP VECTOR OF A COEFFICIENTS
C
      DO 50 L=1,13,4
        AB(L)=1.
        AB(L+1)=A
        AB(L+2)=A*F
   50   AB(L+3)=A2*F
C
C     PERFORM THETA DIRECTION INTEGRATION & STORE
C            RESULTS IN QQ
C
      DO 70 J=1,4
```

```
      DO 70 K=1,J
        DO 70 N1=1,3
          DO 70 N2=1,3
            QQQ=0.
            DO 60 L=1,4
              DO 60 M=1,4
   60           QQQ=QQQ+DBLE(Q(J,L,N1))*DBLE(Q(K,M,N2))*
     1            THINT2(L,M)
            QQ(J,K,N1,N2)=QQQ
   70       QQ(K,J,N2,N1)=QQQ
C
C     PERFORM R DIRECTION INTEGRATION & STORE RESULTS IN PP
C
  300 JJ=0
      DO 330 J1=1,2
        DO 330 J=1,4
          JJ=JJ+1
          KK=0
          DO 320 K1=1,2
            DO 320 K=1,4
              KK=KK+1
              IF (KK.GT.JJ) GO TO 330
              DO 320 N1=1,3
                DO 320 N2=1,3
                  PPP=0.
                  DO 310 L=1,4
                    LM=L+J1+K1+N1+N2-5
                    DO 310 M=1,4
                      LM=LM+1
  310                 PPP=PPP+DBLE(P(J,L,N1))*
     1                  DBLE(P(K,M,N2))*RINT(LM)
                  PP(JJ,KK,N1,N2)=PPP
  320             PP(KK,JJ,N2,N1)=PPP
  330     CONTINUE
C
C     COMBINE APPROPRIATE VALUES OF PP & QQ TO FORM
C         S.M. IN SS &M.M. IN DD
C
      SMULT=D/A2
      DMULT=R1D*R1D*R2D*R2D*F*RH*TH*A2
      JKWW=0
      DO 350 J=1,16
        LX=JK(J)
        LY=IK(J)
        DO 350 K=1,J
          MX=JK(K)
          MY=IK(K)
          JKWW=JKWW+1
```

```
 0071                  ABJABK=AB(J)*AB(K)
 0072                  WRRWRR=PP(LX,MX,3,3)*QQ(LY,MY,1,1)*F
 0073                  WTTWTT=PP(LX,MX,1,1)*QQ(LY,MY,3,3)/F3
 0074                  WRWTT =PP(LX,MX,2,1)*QQ(LY,MY,1,3)/F
 0075                  WTTWR =PP(LX,MX,1,2)*QQ(LY,MY,3,1)/F
 0076                  WRWR  =PP(LX,MX,2,2)*QQ(LY,MY,1,1)*F
 0077                  WRRWTT=PP(LX,MX,3,1)*QQ(LY,MY,1,3)/F
 0078                  WTTWRR=PP(LX,MX,1,3)*QQ(LY,MY,3,1)/F
 0079                  WRWRR =PP(LX,MX,2,3)*QQ(LY,MY,1,1)*F
 0080                  WRRWR =PP(LX,MX,3,2)*QQ(LY,MY,1,1)*F
 0081                  WTWT  =PP(LX,MX,1,1)*QQ(LY,MY,2,2)/F
 0082                  WTWRT =PP(LX,MX,1,2)*QQ(LY,MY,2,2)/F
 0083                  WRTWT =PP(LX,MX,2,1)*QQ(LY,MY,2,2)/F
 0084                  WRTWRT=PP(LX,MX,2,2)*QQ(LY,MY,2,2)/F
 0085                  DD(JKWW)=PP(LX,MX,1,1)*QQ(LY,MY,1,1)*
              1                                    ABJABK*DMULT
 0086       350        SS(JKWW)=(WRRWRR+WTTWTT+WRWTT+WTTWR+WRWR
              1             +PR*(WRRWTT+WTTWRR+WRWRR+WRRWR)
              2                     +PR2*(WTWT-WTWRT-WRTWT+WRTWRT))*
              3                               ABJABK*SMULT
 0087               RETURN
 0088               END
```

```
 0001             SUBROUTINE H1R(R1,R2)
          C
          C       SET UP INTERPOLATION PCLYNOMIALS FCR ANNULAR ELEMENT
          C
          C       R1        INNER RADIUS
          C       R2        OUTER RADIUS
          C
          C       P(I,J,K)=COEFFICIENT OF (J-1) PCWER CF R IN (K-1)
          C          DERIVATIVE OF I"TH PCLYNOMIAL
          C
 0002             COMMON/FIVE/P(4,4,3)
 0003             A=R2-R1
 0004             R2A=R2/A
 0005             R1A=R1/A
 0006             P(1,4,1)=2.
 0007             P(1,3,1)=-3.*(R1A+R2A)
 0008             P(1,2,1)=6.*R1A*R2A
 0009             P(1,1,1)=R2A*R2A*(-3.*R1A+R2A)
 0010             P(2,4,1)=-2.
 0011             P(2,3,1)=3.*(R1A+R2A)
 0012             P(2,2,1)=-6.*R1A*R2A
 0013             P(2,1,1)=R1A*R1A*(3.*R2A-R1A)
 0014             P(3,4,1)=1.
 0015             P(3,3,1)=-(2.*R2A+R1A)
 0016             P(3,2,1)=R2A*(R2A+2.*R1A)
 0017             P(3,1,1)=-R1A*R2A*R2A
 0018             P(4,4,1)=1.
 0019             P(4,3,1)=-(2.*R1A+R2A)
 0020             P(4,2,1)=R1A*(R1A+2.*R2A)
 0021             P(4,1,1)=-R1A*R1A*R2A
 0022             DO 40 I=1,4
 0023                DO 20 J=2,4
 0024         20        P(I,J-1,2)=FLOAT(J-1)*P(I,J,1)
 0025                P(I,4,2)=0.
 0026                DO 30 J=2,3
 0027         30        P(I,J-1,3)=FLOAT(J-1)*P(I,J,2)
 0028                P(I,4,3)=0.
 0029                P(I,3,3)=0.
 0030         40  CONTINUE
 0031             RETURN
 0032             END
```

```
      SUBROUTINE GEO(RI,RO,THI,THO,ANGLE,NELR,NELT,TCODE)
C
C     SET UP ELEMENT GEOMETRY IN MATRIX GEOM
C
C        COL 1 INNER ELEMENT RADIUS
C        COL 2 OUTER ELEMENT RADIUS
C        COL 3 INNER ELEMENT THICKNESS
C        COL 4 OUTER ELEMENT THICKNESS
C        COL 5 ELEMENT INCLUDED ANGLE (RADIANS)
C
      COMMON/TWO/GEOM(64,5)
      INTEGER TCODE
      DO 50 I=1,64
      DO 50 J=1,5
   50 GEOM(I,J)=0
      NUMB=0
      NEL=NELR*NELT
      RINC=(RO-RI)/FLOAT(NELR)
      AINC=ANGLE/FLOAT(NELT)
      R1=RI-RINC
      R2=RI
      DO 100 I=1,NELR
      R1=R1+RINC
      R2=R2+RINC
      DO 100 J=1,NELT
      NUMB=NUMB+1
      GEOM(NUMB,5)=AINC
      GEOM(NUMB,1)=R1
  100 GEOM(NUMB,2)=R2
      GO TO(200,300,400,500),TCODE
  200 DO 210 I=1,NEL
      GEOM(I,3)=THI
  210 GEOM(I,4)=THI
      GO TO 600
  300 BETA=(THO-THI)/RO
      ALPHA=THO-BETA*RO
      DO 310 I=1,NEL
      GEOM(I,3)=ALPHA+BETA*GEOM(I,1)
  310 GEOM(I,4)=ALPHA+BETA*GEOM(I,2)
      TH=ALPHA+BETA*RI
      PRINT 800,TH
  800 FORMAT (/,T13,'THICKNESS AT INNER RADIUS=',E10.3,' IN.')
      GO TO 600
  400 FACT=ALOG(THI/THO)/(RO*RO)
      DO 410 I=1,NEL
      GEOM(I,3)=THI/(2.3026**(FACT*GEOM(I,1)*GEOM(I,1)))
  410 GEOM(I,4)=THI/(2.3026**(FACT*GECM(I,2)*GEOM(I,2)))
      TH=THI/(2.3026**(FACT*RI*RI))
```

```
                PRINT 800,TH
                GO TO 600
            500 READ 810,(GEOM(I,3),GEOM(I,4),I=1,NEL)
            810 FORMAT (2F6.3)
                TH=GEOM(1,3)
                PRINT 800,TH
            600 CONTINUE
                RETURN
                END
```

```
      SUBROUTINE DEFN(NNN,K)
C
C     CALCULATE ELEMENT DEFLECTION PROFILE
C
      DIMENSION PM(4),SN(4,10),P(4,4),Q(4,4)
      COMMON/ONE/SM(64,64),DM(64,64),IVC(64,16)
      COMMON/TWO/GEOM(64,5)
      CCMMON/THREE/Z(4,4,3),IK(16),JK(16),KK(16)
      COMMON/FOUR/SS(136),DD(136),AB(16)
      R1=GEOM(K,1)
      R2=GEOM(K,2)
      ANGLE=GEOM(K,5)
      A=R2-R1
      DO 100 I=1,4
      DO 100 J=1,4
  100 Q(I,J)=0
      Q(1,3)=-3
      Q(1,4)=2
      DO 120 J=1,4
  120 Q(2,J)=-Q(1,J)
      Q(1,1)=1
      Q(3,2)=1
      Q(3,3)=-2
      Q(3,4)=1
      Q(4,3)=-1
      Q(4,4)=1
      R1A=R1/A
      R2A=R2/A
      P(1,4)   =2.
      P(1,3)   =-3.*(R1A+R2A)
      P(1,2)   =6.*R1A*R2A
      P(1,1)   =R2A*R2A*(-3.*R1A+R2A)
      P(2,4)   =-2.
      P(2,3)   =3.*(R1A+R2A)
      P(2,2)   =-6.*R1A*R2A
      P(2,1)   =R1A*R1A*(3.*R2A-R1A)
      P(3,4)   =1.
      P(3,3)   =-(2.*R2A+R1A)
      P(3,2)   =R2A*(R2A+2.*R1A)
      P(3,1)   =-R1A*R2A*R2A
      P(4,4)   =1.
      P(4,3)   =-(2.*R1A+R2A)
      P(4,2)   =R1A*(R1A+2.*R2A)
      P(4,1)   =-R1A*R1A*R2A
      AINC=1./FLOAT(NNN-1)
      AN=-AINC
      DO 194 I=1,NNN
      AN=AN+AINC
```

```
      DO 194 JJ=1,4
  194 SN(JJ,I)=Q(JJ,1)+Q(JJ,2)*AN+Q(JJ,3)*AN*AN+
     1   Q(JJ,4)*AN*AN*AN
      DO 50 L=1,13,4
      AB(L)=1
      AB(L+1)=A
      AB(L+2)=A*ANGLE
   50 AB(L+3)=A*A*ANGLE
      DMAX=0
      RINC=(R2-R1)/FLOAT(NNN-1)
      R=R1-RINC
      DO 200 I=1,NNN
      R=R+RINC
      PP=R/A
      DO 35 II=1,4
   35 PM(II)=P(II,1)+P(II,2)*PP+P(II,3)*PP*PP+
     1      P(II,4)*PP*PP*PP
      DO 200 J=1,NNN
      WW=0
      DO 190 L=1,16
      IR=KK(L)
      IT=IK(L)
      WW=WW+SS(L)*AB(L)*PM(IR)*SN(IT,J)
  190 CONTINUE
  200 DM(I,J)=WW
      RETURN
      END
```

APPENDIX G

RECTANGULAR CANTILEVER PLATES

G.1. INTRODUCTION

An initial theoretical and experimental study of cantilever plates was undertaken for finite element and holographic technique familiarization. Both static and dynamic cases were studied.

G.2. FINITE ELEMENT ANALYSIS

The rectangular element chosen has been well-documented by Zienkiewicz (12). The element has 12 degrees of freedom: the deflections and slopes parallel to the element boundaries at each corner or node. An incomplete fourth order polynomial is used as the element deflection shape function. The mass matrix for vibration analysis is of the consistent rather than lumped mass type. A static analysis program was written in the MATLAN language, and is flowcharted in Fig. 8 . The dynamic program was written in FORTRAN and is flowcharted in Fig.9. Both programs assemble the overall matrices using the variable correlation technique (Appendix E). Both were run on an IBM 360/50 computer.

A nine degree of freedom triangular element, as described by Holland (13) was also programmed but it was found to be very inefficient. This element was therefore dropped from the study.

G.3. FINITE ELEMENT RESULTS

The static rectangular cantilever plate program was run for plates of aspect ratios (length/breadth) from 0.25 to 4.0. A point load was applied at various positions along the free edge. Results of non-dimensional maximum deflection as a function of aspect ratio are plotted in Fig. G1 for the two cases of loads at the centre and end of the free edge. Results from ref. 61 are also plotted and good agreement is seen to exist. Results become asymptotic to values predicted from cantilever theory for aspect ratios greater than 1 or 2 for centre or corner loading respectively. Good convergence was found for 36 degrees of freedom for aspect ratios greater than 0.4.

Dynamic analysis consisted of determining the natural frequencies of plates with aspect ratios 0.25 to 4.0. Results of non-dimensional frequency as a function of aspect ratio are plotted in Fig. G2 for the first several modes. Two digits are used for modal identification-- the first for the number of nodes parallel to the fixed edge, the second for the number of nodes perpendicular to the fixed edge. The results found by Barton (128) using a Ritz method are also plotted. Agreement between the two techniques is good. On the right hand side of the graph are plotted values for cantilever beams for $\nu = 0.3$. The bending modes of the finite element theory reach the cantilever values rapidly for aspect ratios greater than 0.5 . Good convergence was found for 60 degrees of freedom for aspect ratios greater than 0.4 . Deflection profiles were generated for each mode found and these were used to determine the positions of nodal lines.

G.4. EXPERIMENTAL ANALYSIS

A series of 5 cantilever plates were tested. Their properties are given in Table G1 . Material property values were determined from handbooks except for the low carbon steel for which no specifications were given. Test strips of this material were tensile tested for this purpose. Properties are given in the table and are isotropic within 2%.

The plates were drilled for the clamping fixture and painted as described in4.3.8. The plate of aspect ratio 1 was fabricated from ground flat stock to ensure that at least this sample was firmly clamped at its root.

Point static loads were applied to the plates by means of dead weights and a pulley system. Double exposure or live fringe holographic interferograms were taken for various loads and load points. Typical results are shown in Fig. G3 . Reasonable agreement with theory is shown, as plotted in Fig. G1.

The static loading frame was replaced by an appropriate vibration excitation device as described in 4.3.10. Time-average interferograms were taken of the plates at each natural frequency. Typical results for various plates are shown in Figs. G4 to G7 . The bright nodal lines are very evident. For comparison purposes, theoretical nodal lines have been added to the figures. Non-dimensional natural frequencies were calculated and added to Fig. G2 . Again reasonable agreement both with respect to frequencies and nodal lines is shown, except for frequencies of the fundamental mode. This may be attributed to the lack of good end clamping. At higher modes, clamping effects in general are less signifigant.

For purposes of illustration a fringe spoiling experiment was performed on the plate of aspect ratio 1.0 . On completion of a live fringe experiment, the holographic plate was intentionally mismatched to produce the fringe pattern of the static interferogram of Fig. G8 . Fig. G8 also shows interferograms in the first bending and first torsional modes. The nodal lines are obvious as areas where the fringes remain sharp. Fringes in antinodal areas however are washed out. This technique does not yeild information about amplitude profiles.

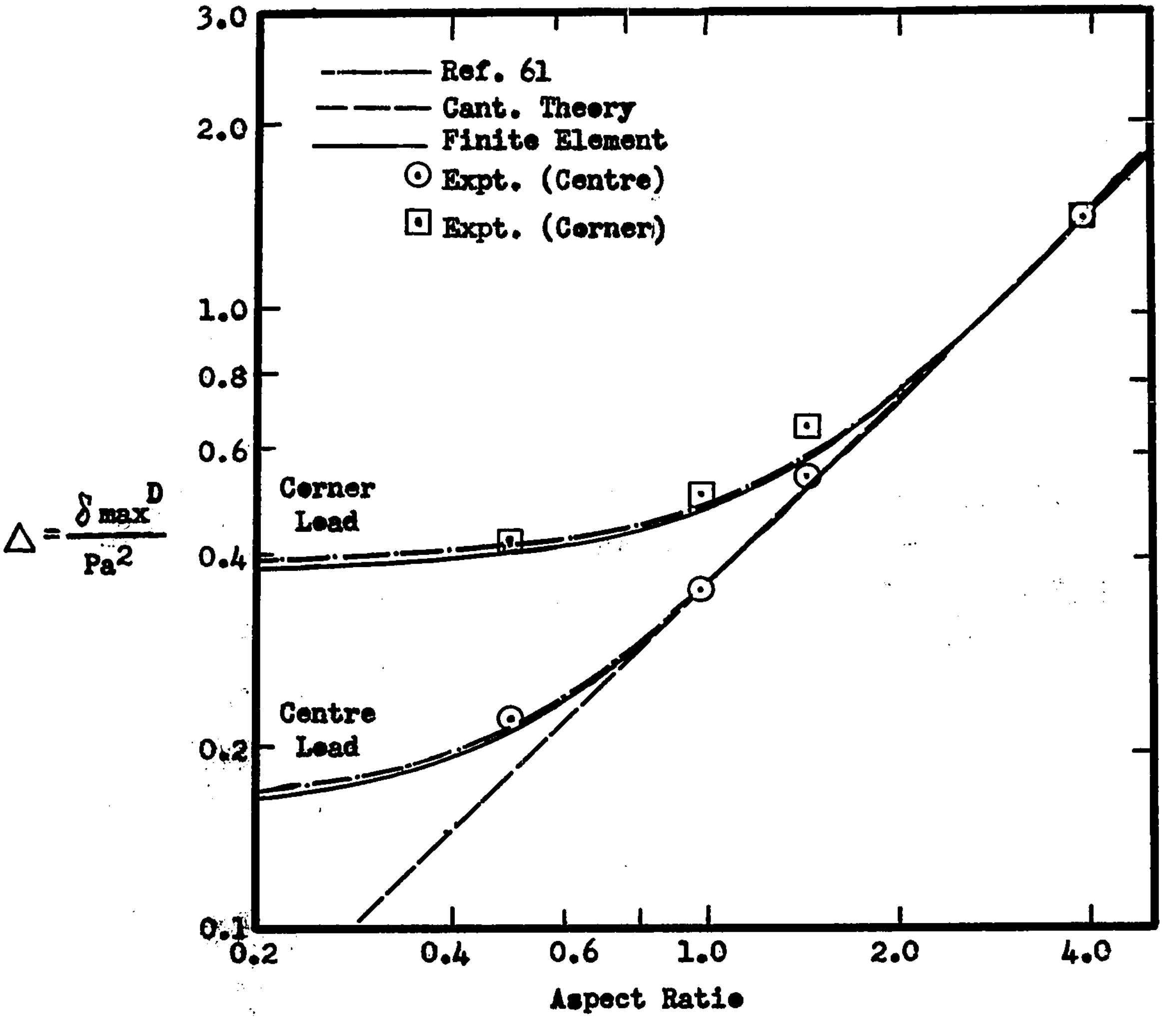

Fig. G.1. Cantilever Plate Static Deflection

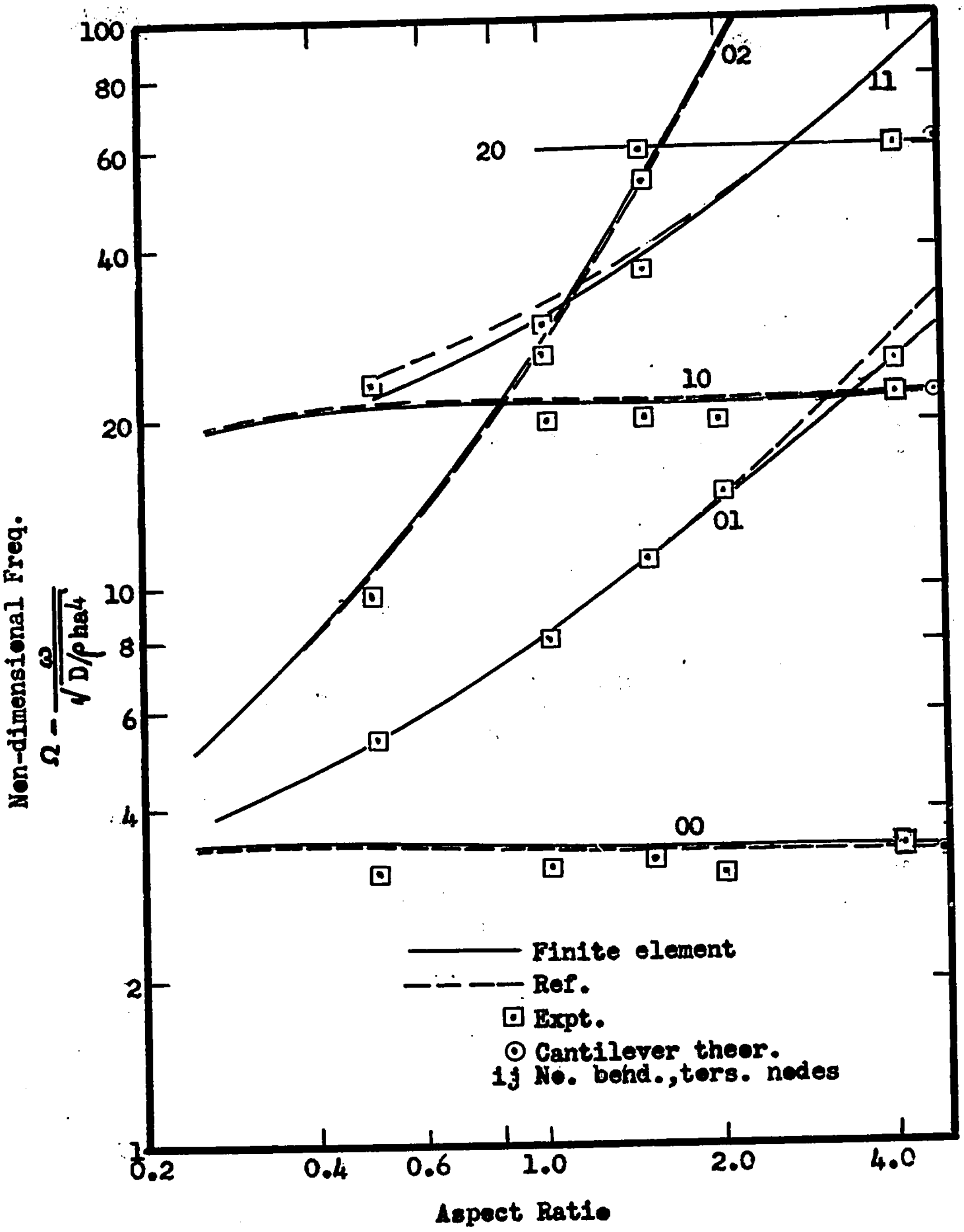

Fig. G.2. Cantilever Plate Natural Frequencies

Corner Load **Centre Load**

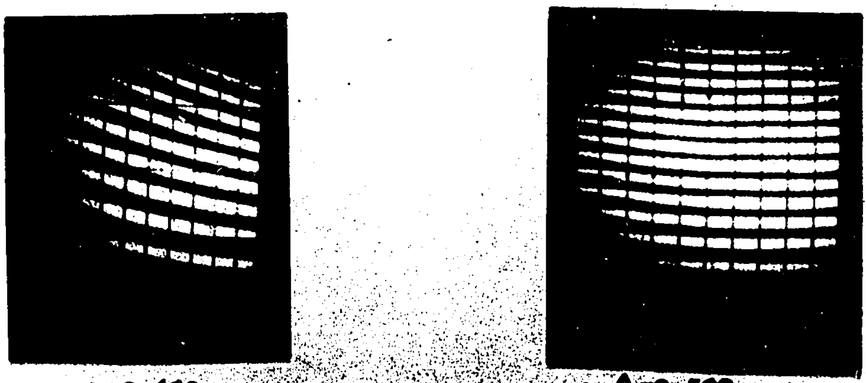

Δ =0.680 Δ =0.580

Aspect Ratio=1.5

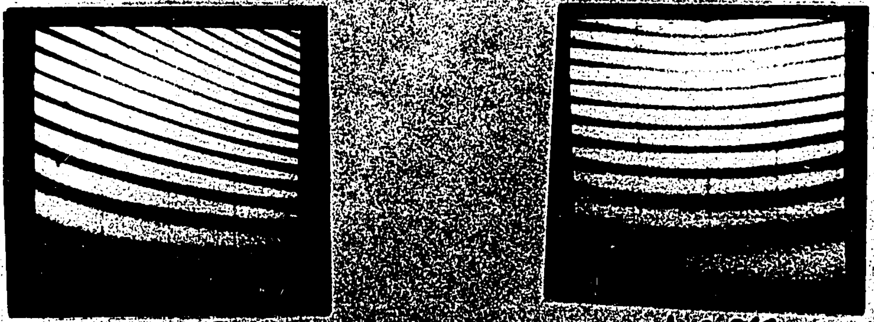

Δ =0.527 Δ =0.368

Aspect Ratio=1.0

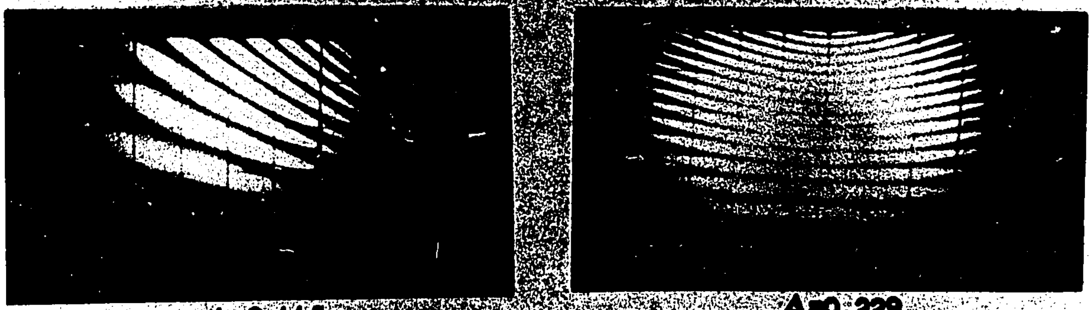

Δ =0.445 Δ =0.229

Aspect Ratio=0.5

Fig. G.3 Statically Point Loaded Cantilever Plates

Corner Load Centre Load

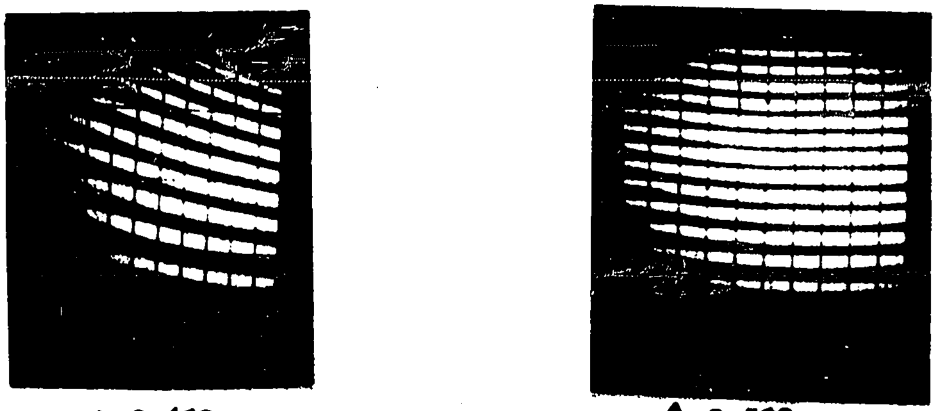

Δ =0.680 Δ =0.580

Aspect Ratio=1.5

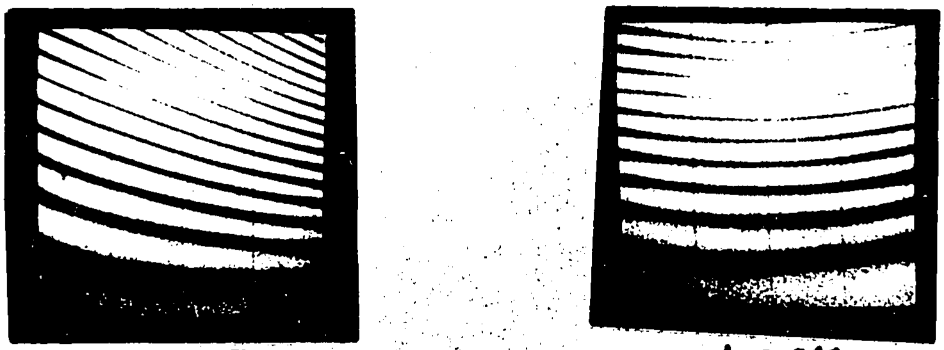

Δ =0.527 Δ =0.368

Aspect Ratio=1.0

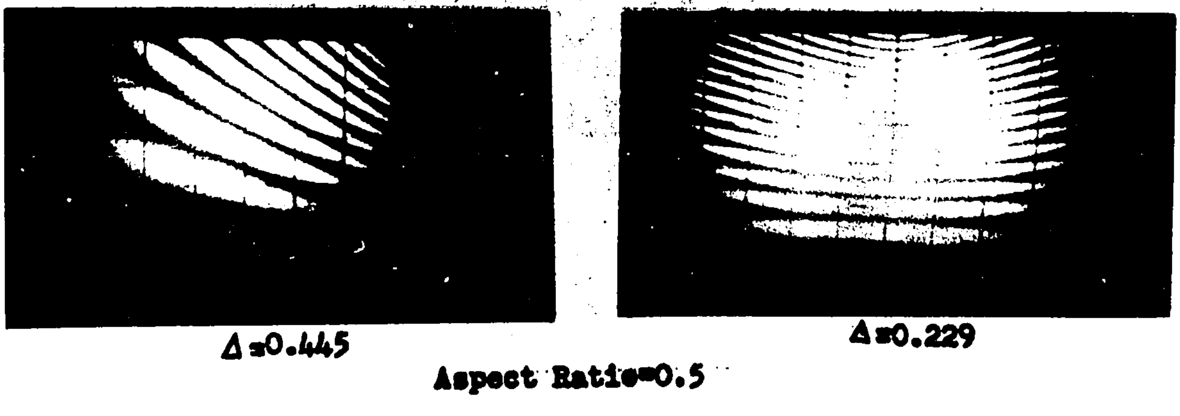

Δ =0.445 Δ =0.229

Aspect Ratio=0.5

Fig. G.3 Statically Point Loaded Cantilever Plates

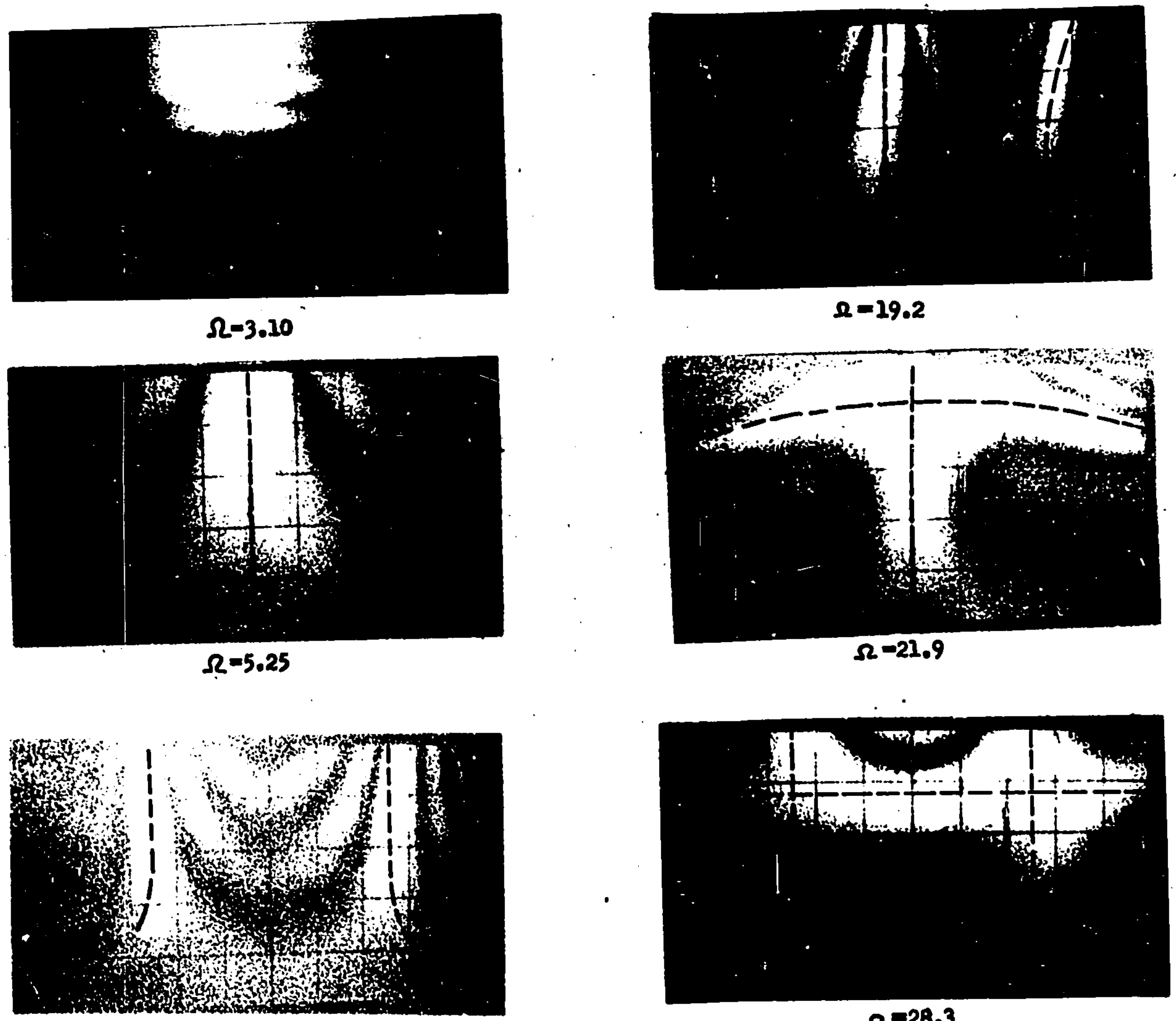

$\Omega=3.10$

$\Omega=19.2$

$\Omega=5.25$

$\Omega=21.9$

$\Omega=9.50$

$\Omega=28.3$

– – – Theor. Nodes

Fig. 44 Vibrating Cantilever Plate
(Aspect Ratio = 0.5)

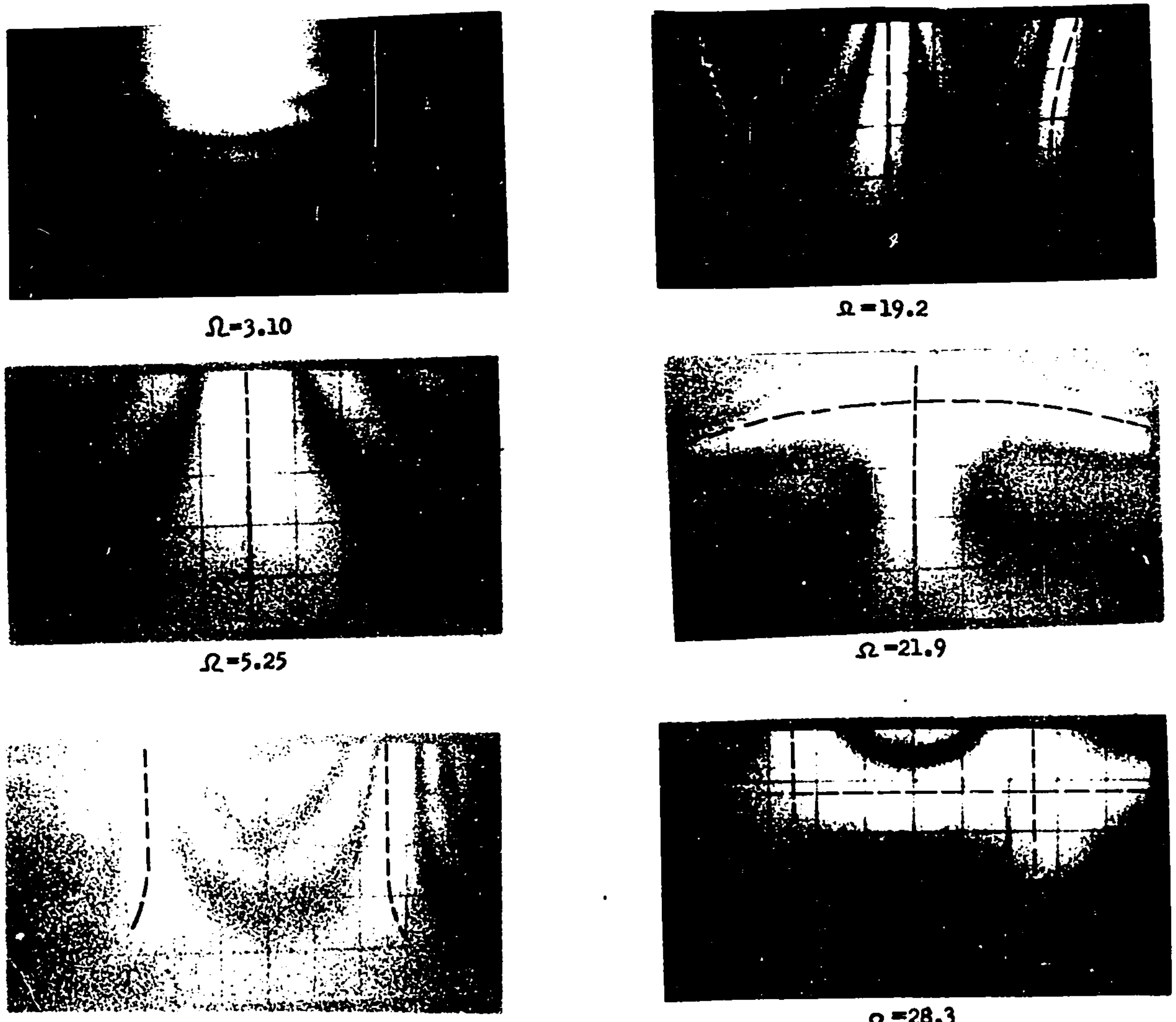

$\Omega = 3.10$

$\Omega = 19.2$

$\Omega = 5.25$

$\Omega = 21.9$

$\Omega = 9.50$

$\Omega = 28.3$

— — — Theor. Nodes

Fig. 64 Vibrating Cantilever Plate
(Aspect Ratio = 0.5)

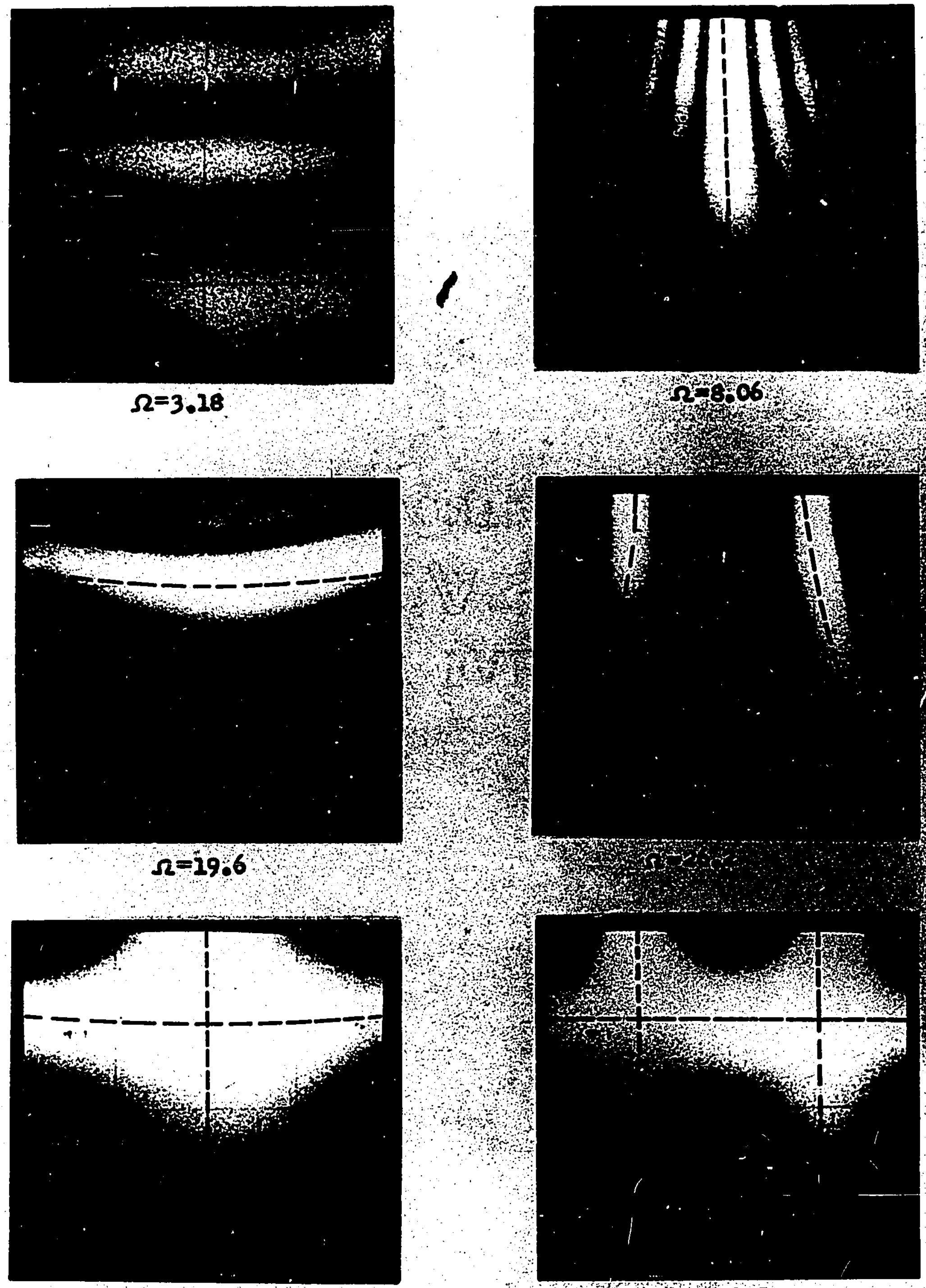

$\Omega=3.18$ $\Omega=8.06$

$\Omega=19.6$ [illegible]

$\Omega=28.8$ $\Omega=50.5$

----- Theor. Nodes

Fig G.5. Vibrating Cantilever Plate
(Aspect Ratio=1)

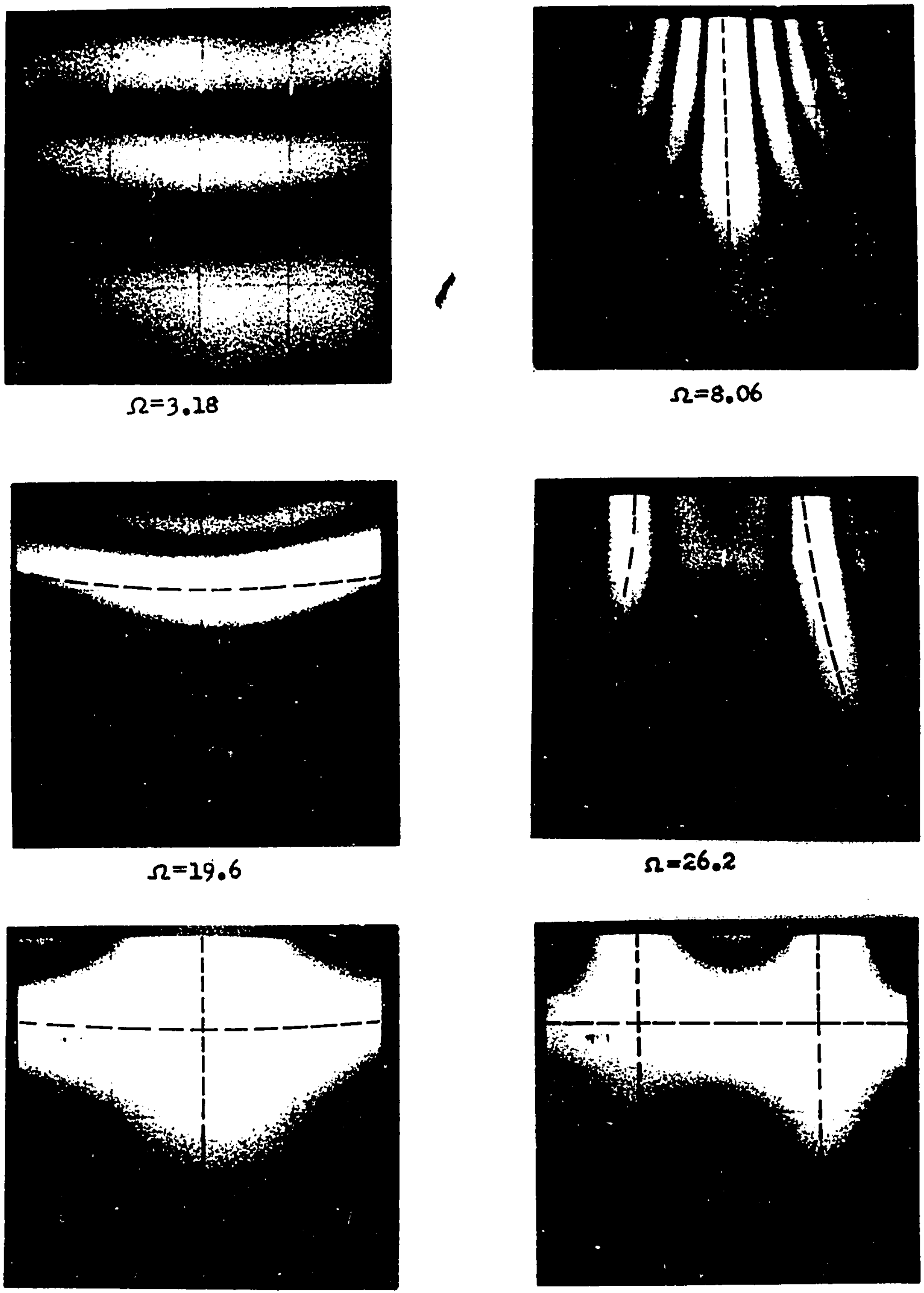

$\Omega=3.18$ $\Omega=8.06$

$\Omega=19.6$ $\Omega=26.2$

$\Omega=28.8$ $\Omega=50.5$

---- Theor. Nodes

FigG.5. Vibrating Cantilever Plate
(Aspect Ratio =1)

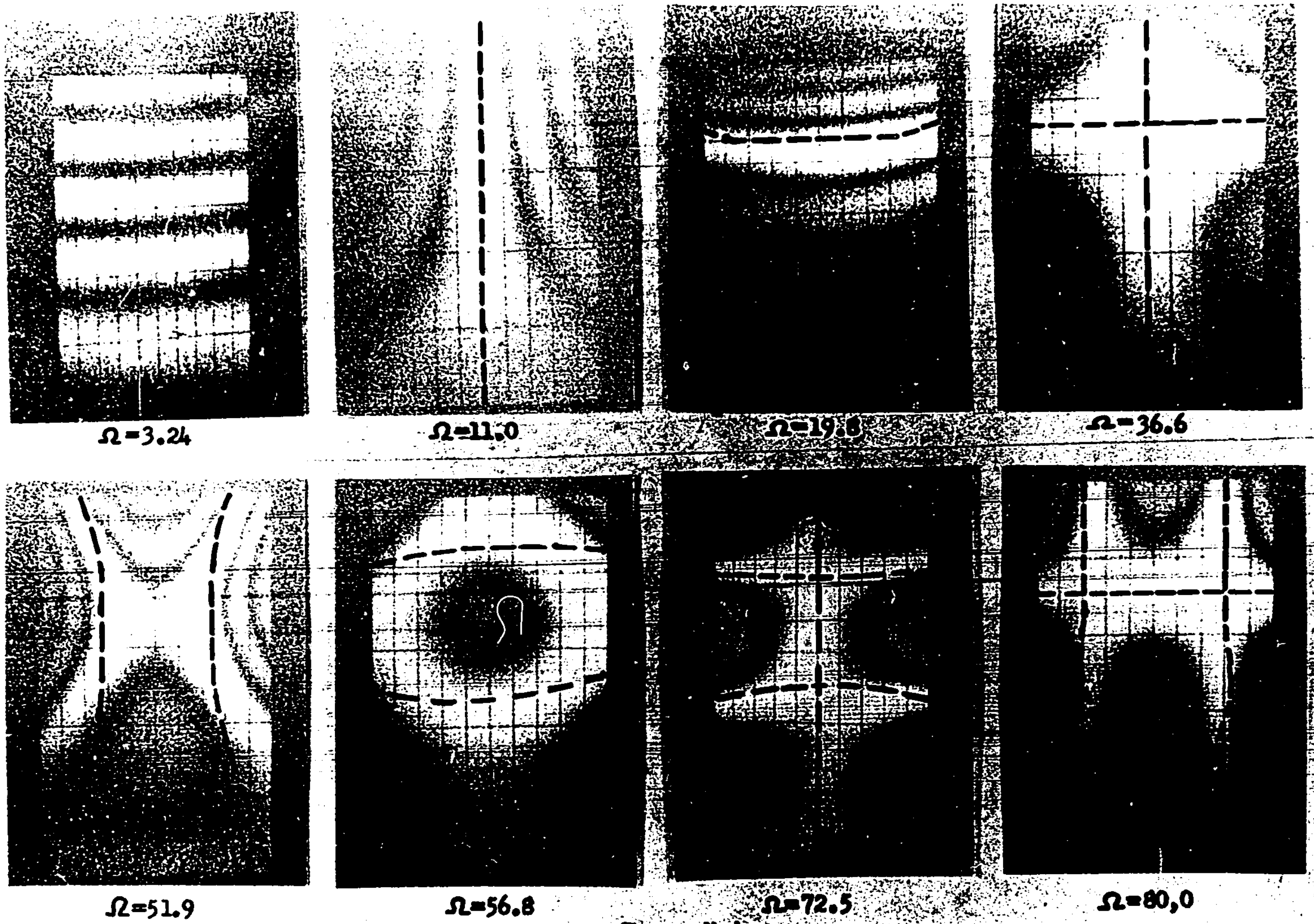

$\Omega = 3.24$ $\Omega = 11.0$ $\Omega = 19.8$ $\Omega = 36.6$

$\Omega = 51.9$ $\Omega = 56.8$ $\Omega = 72.5$ $\Omega = 80.0$

--- Theor. Nodes

Fig. G6. Vibrating Cantilever Plate
(Aspect Ratio = 1.5)

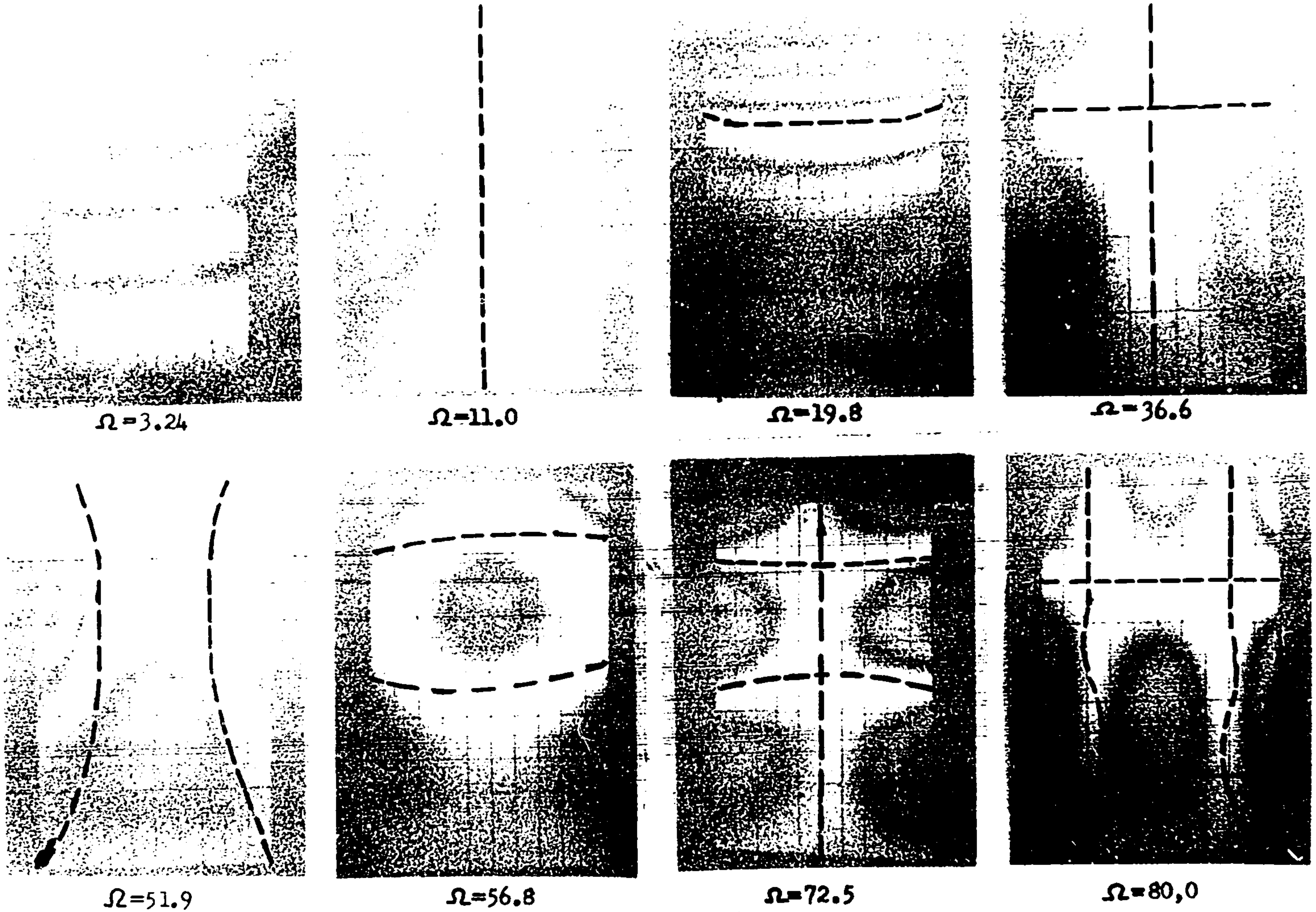

Ω=3.24

Ω=11.0

Ω=19.8

Ω=36.6

Ω=51.9

Ω=56.8

Ω=72.5

Ω=80,0

--- Theor. Nodes

Fig. G6. Vibrating Cantilever Plate
(Aspect Ratio = 1.5)

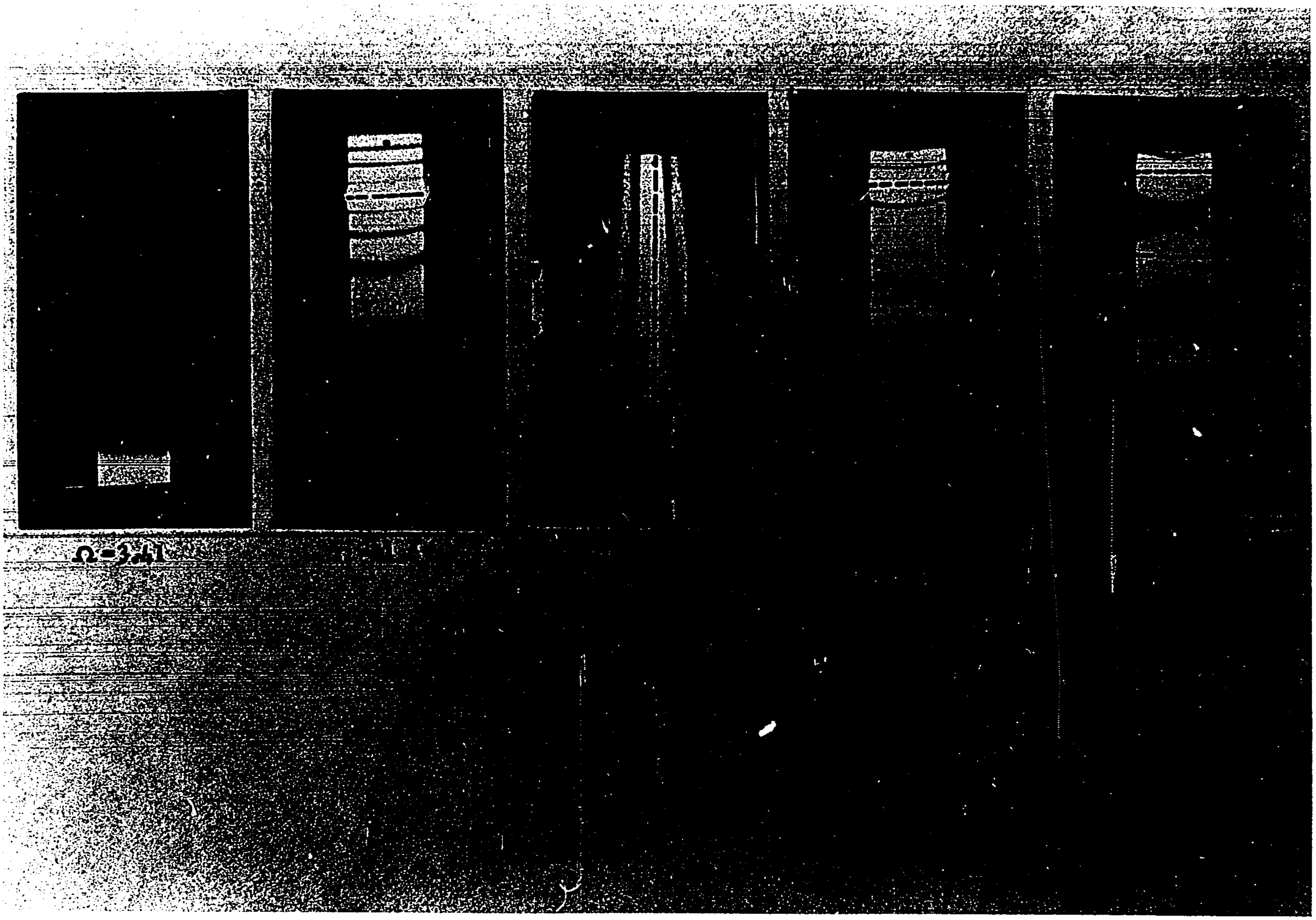
Ω-341

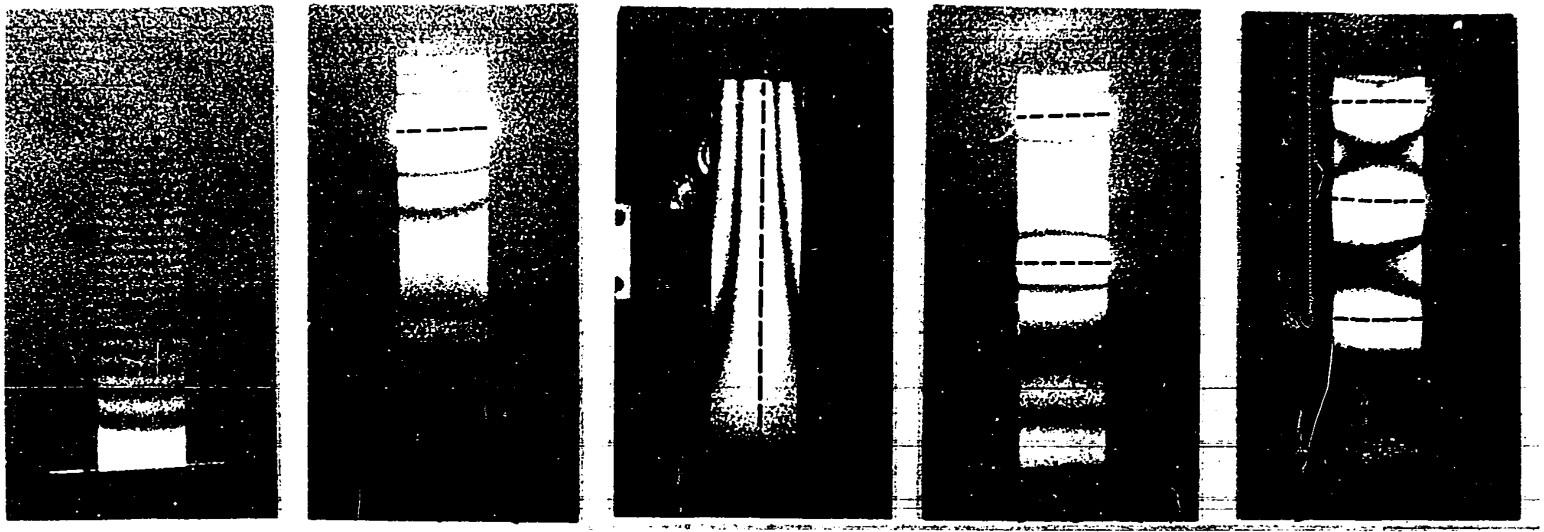

$\Omega = 3.41$ $\Omega = 21.6$ $\Omega = 27.4$ $\Omega = 60.9$ $\Omega = 119.$

---- Theoretical Nodal Lines

Fig.G7. Vibrating Cantilever Plate

(Aspect Ratio = 4.0)

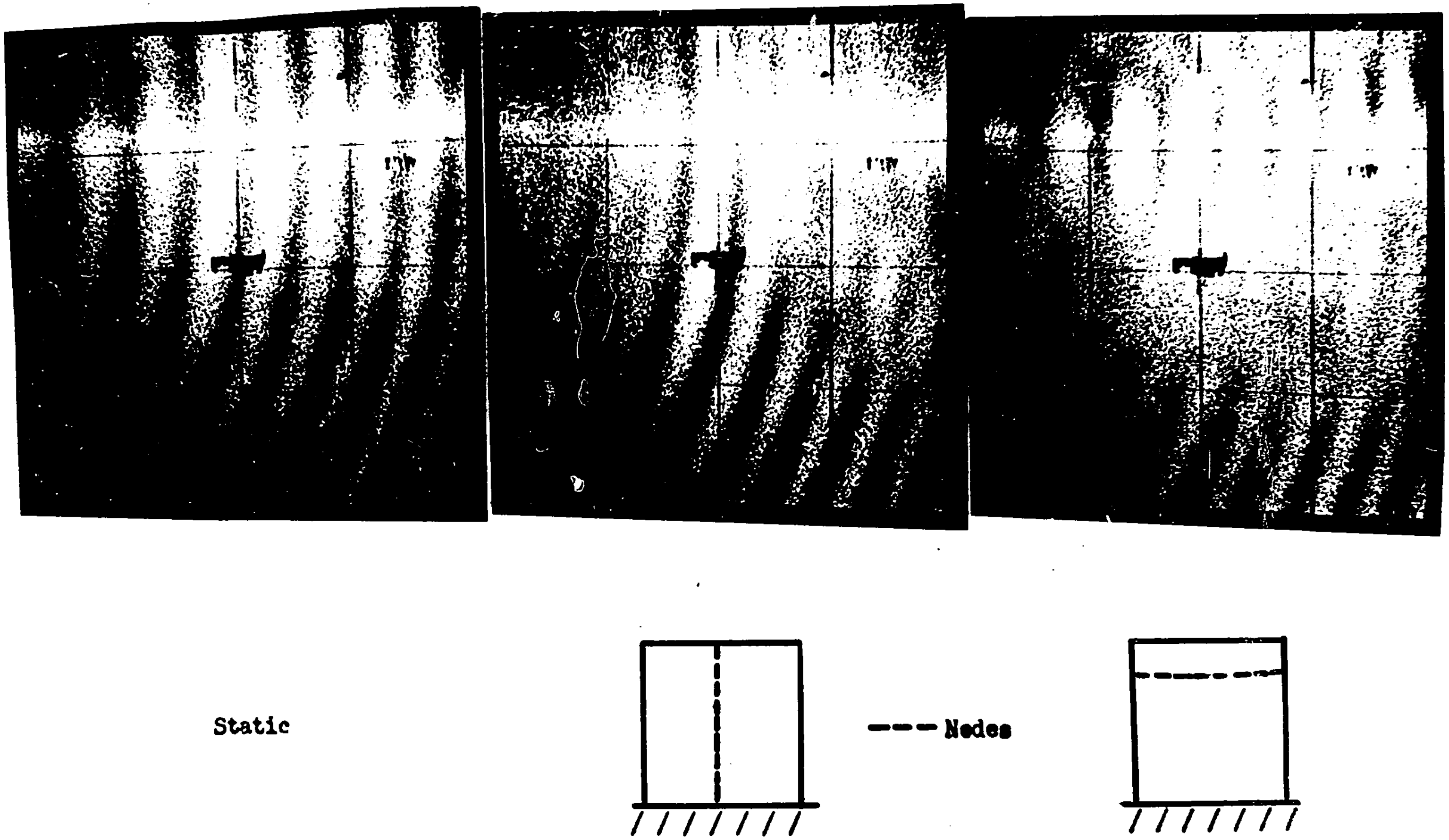

Fig.G.8.Typical Fringe Spoiled Interferograms

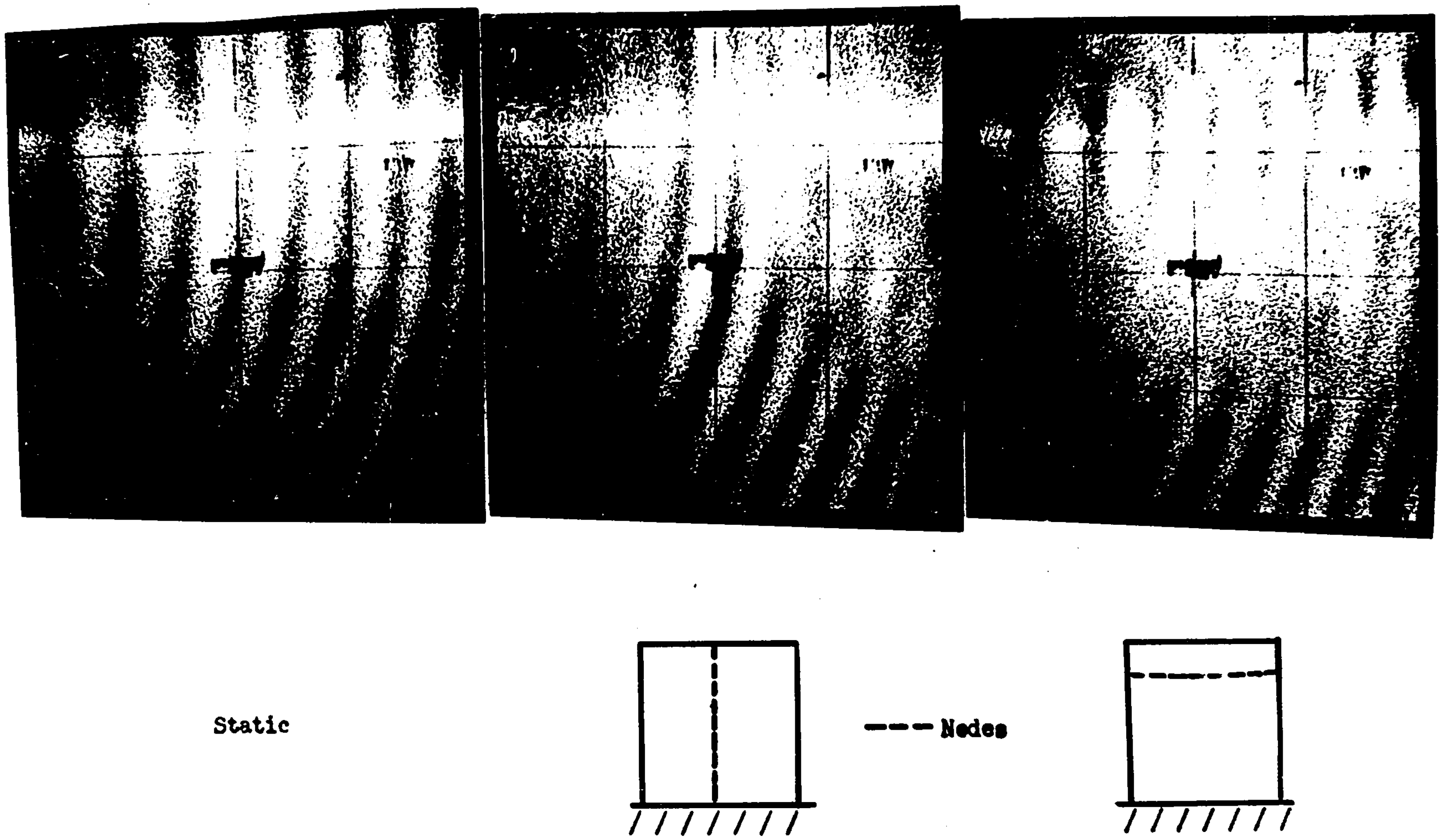

Fig.G.8.Typical Fringe Spoiled Interferograms

Aspect Ratio	0.5	1.0	1.5	2.0	4.0
Material	low carbon steel	C1018 steel	low carbon steel	low carbon steel	6061-T6 aluminum
Length (in.)	4.02	5.75	6.00	8.01	6.00
Breadth (in.)	8.00	5.75	4.00	4.00	1.50
Thickness (in.)	0.256	0.256	0.256	0.256	0.100
E (psi x 10^6)	30.1	30.0	30.1	30.1	10.0
ν	0.276	0.280	0.276	0.276	0.300

Table G.1. Cantilever Plates Tested

VITA

1945 Born in Windsor, Ontario, Canada

1967 Received the degree of Bachelor of Applied Science in Mechanical Engineering, University of Windsor, Windsor, Ontario

1969 Received the degree of Master of Applied Science in Mechanical Engineering, University of Windsor, Windsor, Ontario

1972 Presently a candidate for the degree of Doctor of Philosophy in Mechanical Engineering, University of Windsor